

**GEOMETRICAL AND ORIENTATION INVESTIGATIONS  
ON THE ELECTRONIC STRUCTURES  
OF ELEMENTS ADSORPTION ON GRAPHENE  
VIA DENSITY FUNCTIONAL THEORY**

**Geometrical and Orientation Investigations  
on the Electronic Structures  
of Elements Adsorption on Graphene  
via Density Functional Theory**

**Hantarto Widjaja**

**This thesis is presented for the degree of  
Doctor of Philosophy of  
Murdoch University  
Australia  
2016**

## **Declaration**

*I declare that this thesis is my own account of my research and contains as its main content work which has not previously been submitted for a degree at any tertiary education institution.*

*(Hantarto Widjaja)*

*To my wife, Ariani Rahardjo, and my sons, Benedict Clemence and Gregorius Lawrence.*

## ABSTRACT

Nano-sized materials have promising contemporary and novel technological applications as they possess favourable properties due to quantum effects. The nano-sized graphene material exhibits remarkable electrical, optical, thermal and mechanical characteristics. Adding impurities or doping constitutes an effective way in fine-tuning properties of graphene for specific applications. This study aims to investigate the geometrical aspects of elements adsorption on graphene to produce more accurate models of the electronic structure of graphene as a result of the doping.

Previous models investigated mainly the adsorption sites (bridge, hollow, top); however, they could not systematically explain certain phenomena, e.g. nonlinearity of band gaps to atomic ratios in oxygen-adsorbed graphene. We hypothesise that this is attributed to the positions and orientation of the adatoms (adsorbed elements) relative to one another, which is, in essence, a geometrical phenomenon.

In the present study, geometrical investigations of elemental adsorption on graphene focused on side (single-, double-sided), site (bridge, hollow, top) and orientation (the position of adatom relative to one another and graphene). The computational simulations were conducted by using the generalized gradient approximation (GGA) functional within the density functional theory (DFT) framework. The VASP (Vienna Ab initio Simulation Package) software was utilised for all simulations.

Trends in the elemental adsorption on graphene in terms of sides/sites/orientations are presented in terms of: binding energy (stability); migration (barrier) energy; adatom height; graphene distortion; Fermi energy; magnetization; charge transfer and energy band gap. The calculated results of 10 elements (Na, Mg, Al, Si, P, S, F, Cl, Br and I) adsorbed on pristine graphene indicate that the geometrical combination of side, site and orientation is vital in determining the most stable configuration of the adsorbed systems. This study reinforces the notion that the involvement of site/orientation of element (or functional group) is essential in future models of adsorption on graphene.

# TABLE OF CONTENTS

Title	i
Declaration	ii
Abstract	iv
Table of Contents	v
Acknowledgements	vii
List of Publications	viii
List of Figures	ix
List of Tables	xiv
<b>Chapter 1. Introduction</b>	1
1.1 Background	1
1.2 Objective and Scope of Study	2
<b>Chapter 2. Theoretical Background</b>	5
2.1 Electronic Structure	5
2.2 Density Functional Theory (DFT)	9
<b>Chapter 3. Review of Elemental Adsorption on Graphene</b>	17
3.1 Nano-sized Metals, Semiconductors and Insulators	17
3.2 Graphene	20
3.3 Trends on Elemental Adsorption on Graphene from Previous Studies	24
3.4 Summary	32
3.5 Supplementary Data	33
<b>Chapter 4. Computational Methods</b>	38
4.1 Computational Strategies	38
4.2 Simulation Software	39
4.3 The Geometry of Elemental Adsorption on Graphene	41
4.3.1 Bridge Cases	44
4.3.2 Adatom-adatom Interaction	46
4.4 Supplementary Data	47
<b>Chapter 5. Aluminium and Silicon Adsorption on Graphene</b>	54
5.1 Introduction	54
5.2 Methods	55
5.3 Results and Discussion	61
5.3.1 Adatom-adatom Interaction	61
5.3.2 Al- and Si-adsorbed Graphene	62
5.3.3 Electronic Analysis	65
5.4 Conclusions	67
5.5 Supplementary Data	68
<b>Chapter 6. Halogens (F-I) Adsorption on Graphene</b>	70
6.1 Introduction	70
6.2 Methods	72
6.3 Results and Discussion	76
6.3.1 Adatom-adatom Interaction	77
6.3.2 Adatom-adsorbed Graphene	78
6.3.3 Electronic Analysis	83
6.4 Conclusions	85
6.5 Supplementary Data	86

<b>Chapter 7. Double-sided Fluorine and Chlorine Adsorption on Graphene</b>	90
7.1 Introduction	90
7.2 Methods	92
7.3 Results and Discussion	94
7.4 Conclusions	103
<b>Chapter 8. Period 3 Elements (Na – Cl) Adsorption on Graphene</b>	105
8.1 Introduction	105
8.2 Methods	106
8.3 Results and Discussion	109
8.3.1 Adatom-adatom Interaction	109
8.3.2 Adatom-adsorbed Graphene	110
8.4 Conclusions	113
8.5 Supplementary Data	114
<b>Chapter 9. Concluding Remarks</b>	119
9.1 Consolidated Results	119
9.2 Conclusions	121
9.3 Future Work	123
References	124
Appendix A. Files and Parameters in VASP	132
A.1 Input and Output Files	132
A.2 INCAR Parameters	134

## ACKNOWLEDGEMENTS

I'd like to thank God for His blessings I completed this research and wrote this thesis. I'd like to thank DR. Zhong-Tao Jiang as my principal supervisor, who found me and guided me through all my research process. I'd like to thank DR. Chun-Yang Yin, Prof. Philip Jennings, DR. Mohammednoor Altarawneh and Prof. Bogdan Z. Dlugogorski as my co-supervisors, who guided me through all my research process and supported me in publishing the journal articles.

I'd like to thank my wife Ariani Rahardjo for her total and tireless support; and my sons, Benedict Clemence and Gregorius Lawrence. You are the ones I put my hope.

I also thank to my colleagues : DR. Amun Amri, DR. Bee-Min Goh, Nicholas Mondinos, DR. M. Mahbubur Rahman, DR. Shahidah Ali, DR. Ravi Brundavanam, Brian Drake, Tan Chiat Leng, Mohammedpour Ehsan, Khalil Ibrahim, Hatem Taha, Dunia Abdulsahib Hamdi, Hussein Ali Jan Miran, Zainab Najji Abdullah, Ian Wilkins and Oday Ahmed for their supports.

I also thank my parents (Harijanto Widjaja, Listyani Kartono, the late Mr. Herman Santoso Rahardjo and Endang Lukiswatiningsih), my brothers, sisters, nephews and niece (Agus Muliadi, Marta Widjaja, Tonny Rustandi, Silvia Widjaja, Winarto Widjaja, Olivia Yunita, William Muliadi, Wilona Muliadi, Dionisius Rustandi), Niko and Maureen Litic, DR. Juniati Gunawan, Grace Kurniawan, and the Mother Mary Holy Trinity Community Perth who always pray for me during my study.

I'm grateful to the Australian Government for providing financial support under Australian Postgraduate Awards (APA) via Murdoch University. This study has been supported by a grant of computing time from the National Computational Infrastructure (NCI) in Canberra and the Pawsey Supercomputing Centre (iVEC) in Perth.

Murdoch, Western Australia, June 2016

Hantarto Widjaja



## LIST OF PUBLICATIONS

- [1] H. Widjaja, M. Altarawneh, Z.-T. Jiang, C.-Y. Yin, B.-M. M. Goh, N. Mondinos, and B. Z. Dlugogorski, “Geometrical and orientational investigations on the electronic structure of graphene with adsorbed aluminium or silicon,” *Mater. Des.*, vol. 89, pp. 27–35, 2016.
- [2] H. Widjaja, Z.-T. Jiang, M. Altarawneh, C.-Y. Yin, B.-M. Goh, N. Mondinos, and B. Z. Dlugogorski, “Towards a better understanding of the geometrical and orientational aspects of the electronic structure of halogens (F–I) adsorption on graphene,” *Appl. Surf. Sci.*, vol. 356, pp. 370–377, 2015.
- [3] H. Widjaja, Z.-T. Jiang, M. Altarawneh, C.-Y. Yin, B.-M. Goh, N. Mondinos, A. Amri, and B. Z. Dlugogorski, “Double-sided F and Cl adsorptions on graphene at various atomic ratios: Geometric, orientation and electronic structure aspects,” *Appl. Surf. Sci.*, vol. 373, pp. 65–72, 2016.
- [4] H. Widjaja, Z.-T. Jiang, and M. Altarawneh, “Trends on elemental adsorption on graphene,” *Can. J. Phys.*, vol. 94, no. 5, pp. 437–447, 2016.
- [5] M. M. Rahman, Z. Jiang, Z. Xie, X. Duan, Z. Zhou, P. C. Wo, C. Yin, N. Mondinos, Q. Gu, H. Widjaja, K. Jack, A. Yago, and A. Amri, “Understanding Local Bonding Structures of Ni-Doped Chromium Nitride Coatings through Synchrotron Radiation NEXAFS Spectroscopy,” *J. Phys. Chem. C*, vol. 118, pp. 18573–9, 2014.
- [6] A. Amri, Z.-T. Jiang, P. A. Bahri, C.-Y. Yin, X. Zhao, Z. Xie, X. Duan, H. Widjaja, M. M. Rahman, and T. Pryor, “Surface Electronic Structure and Mechanical Characteristics of Copper–Cobalt Oxide Thin Film Coatings: Soft X-ray Synchrotron Radiation Spectroscopic Analyses and Modeling,” *J. Phys. Chem. C*, vol. 117, no. 32, pp. 16457–16467, Aug. 2013.
- [7] P. Jennings, Z.-T. Jiang, N. W. M. W. Wyatt, D. Parlevliet, C. Creagh, C.-Y. Yin, H. Widjaja, and N. Mondinos, “Characterization of silicon nanowires grown on silicon, stainless steel and indium tin oxide substrates,” *Appl. Phys. A*, vol. 113, no. 3, pp. 723–728, 2013.

## LIST OF FIGURES

1.1	Schematic diagram of elemental adsorption on graphene, grey spheres are carbon, red spheres are adatom, B=bridge, H=hollow, T=top, (a) zigzag orientation (subscript z), (b) armchair orientation (subscript a).	3
2.1	Electronic excitation process that is not covered in pure DFT.	13
2.2	Computational simulation flowchart using DFT.	16
3.1	Zigzag and armchair terminated graphene nanoribbon. Grey is carbon atom. Black circles are added to mark the edges of the nanoribbon.	20
3.2	Some trends in the periodic table of elements. Properties are written at the corners with the largest value.	24
3.3	Binding energies (eV) of element-adsorbed on zigzag $3 \times 3$ graphene supercell. Colours indicate the most stable site, with green, red, yellow are bridge, hollow, top sites.	26
3.4	Adatom heights (Å) of element-adsorbed on zigzag $3 \times 3$ graphene supercell. Red is less than 2.00 Å and yellow is more than 2.00 Å.	26
3.5	Migration energies (eV) of element-adsorbed on zigzag $3 \times 3$ graphene supercell. Grey, light green and green are less than 0.10 eV, between 0.10 and 0.50 eV, and more than 0.50 eV.	26
3.6	Charge transfer from adatom to graphene (number of electrons) of element-adsorbed on zigzag $3 \times 3$ graphene supercell. Yellow, light green and green are less than 0.00 electron, between 0.00 and 0.50 electron, and more than 0.50 electron. Yellow has negative Fermi energy shift from pristine graphene, while light green and green have positive Fermi energy shift. Fermi energy trend might be proportional to charge transfer trend.	27
3.7	Comparison of Chan <i>et al.</i> and Nakada and Ishii's calculations, dotted lines are added as a guidance.	28
3.8	Magnetizations ( $\mu_B$ ) of elemental adsorbed/doped on graphene from previous studies. Light green are positive (at < 50 at.%), light yellow are zero (at < 50 at.%), grey is element with no data.	29
3.9	Band gaps at Fermi energy (eV) of elemental adsorbed/doped on graphene from previous studies. Light green is positive (at < 50 at.%), green is positive (at $\geq$ 50 at.%), light yellow is zero (at < 50 at.%), yellow is zero (at $\geq$ 50 at.%), grey is element with no data.	30
3.10	Some trends and <i>indicators</i> on elemental adsorption on graphene in the periodic table of elements. Properties are written at the corners with the largest value. <i>Indicators</i> need further verifications/investigations.	33
3.S1	Pauling's electronegativities. Light blue, green, yellow and pink are less than 1.5, between 1.5 and 1.9, between 2.0 and 2.9, and more than 2.9.	36
3.S2	First ionization energies (eV). Light blue, yellow and pink are less than 7.00 eV, between 0.70 and 10.00 eV, and more than 10.00 eV.	36
3.S3	Metallic characters. Orange, blue and green are metals, metalloids and nonmetals.	36

3.S4	Atomic radii (Å). Pink, yellow and red are less than 1 Å, between 1 and 1.5 Å, and more than 1.5 Å.	37
3.S5	Number of unpaired valence electrons, green is anomalous electron configuration.	37
4.1	Typical density of states (DOS) curve of (a) metals, (b) semiconductors/insulators. $E_F$ is Fermi energy. Yellow is filled states.	41
4.2	(a) Original density of states (DOS), difficult to integrate numerically, (b) smearing is applied at $E_F$ , easy to integrate numerically. $E_F$ is Fermi energy. Yellow is filled states.	41
4.3	Graphene cell/supercells (number of C atoms in a unit cell, maximum adatom radius):(a) zigzag $1 \times 1$ (2, $\approx 1.23$ Å), (b) zigzag $2 \times 1$ (4, $\approx 1.23$ Å), (c) zigzag $\sqrt{3} \times \sqrt{3}$ (6, $\approx 2.13$ Å), (d) zigzag $3 \times 1$ (6, $\approx 1.23$ Å), (e) zigzag $2 \times 2$ (8, $\approx 2.46$ Å), (f) armchair $2 \times \sqrt{3}$ (8, $\approx 2.13$ Å), (g) zigzag $4 \times 1$ (8, $\approx 1.23$ Å).	42
4.4	Most stable configuration of single-sided fluorinated graphene of 25 at.%, red spheres are F atoms, grey spheres are C atoms, and big red circles are added to guide the eyes.	43
4.5	Schematic diagrams of adsorption on the graphene supercells for 1:8 atomic ratio, (a) zigzag $2 \times 2$ and (b) armchair $2 \times \sqrt{3}$ . O(0,0) is origin. B, H, T, z, a are bridge, hollow, top, zigzag and armchair.	43
4.6	Equivalency of graphene supercells, (a) armchair $1 \times \sqrt{3}$ (red) is equivalent to zigzag $2 \times 2$ (blue), (b) slant $3 \times \sqrt{7}$ (red) is equivalent to zigzag $9 \times 9$ (blue).	44
4.7	$B_{a1}$ and $B_{a3}$ adsorption position on graphene are mirror images of each other. Shading is to guide the eyes.	44
4.8	Bridge cases on zigzag $2 \times 2$ ( $B_z$ ) and armchair $2 \times \sqrt{3}$ ( $B_{a1}$ , $B_{a2}$ ) (3 unique positions).	45
4.9	Bridge cases on zigzag $3 \times 3$ ( $B_z$ ), slant $3 \times \sqrt{7}$ ( $B_{s1}$ , $B_{s2}$ , $B_{s3}$ ) and mirror of slant $3 \times \sqrt{7}$ (4 unique positions).	45
4.10	Bridge cases on zigzag $4 \times 4$ ( $B_z$ ), slant $4 \times \sqrt{13}$ ( $B_{s1}$ , $B_{s2}$ , $B_{s3}$ ) and armchair $4 \times 2\sqrt{3}$ ( $B_{a1}$ , $B_{a2}$ ) (6 unique positions).	45
4.11	Bridge cases on zigzag $5 \times 5$ ( $B_z$ ), slant <sub>1</sub> $5 \times \sqrt{21}$ ( $B_{s1-1}$ , $B_{s1-2}$ , $B_{s1-3}$ ), slant <sub>2</sub> $5 \times \sqrt{19}$ ( $B_{s2-1}$ , $B_{s2-2}$ , $B_{s2-3}$ ) and mirror of slant <sub>2</sub> (7 unique positions).	46
4.12	Adatom's nearest neighbours, (a) zigzag $2 \times 2$ and (b) armchair $2 \times \sqrt{3}$ , $r = 4.936$ Å.	46
4.13	Elements-adsorbed graphene inspected in this thesis. Light blue is at 5.6 at.%, green is between 5.6 and 12.5 at.%, and pink is between 5.6 and 100 at.%.	47
4.S1	S1 Binding energies (eV) of element-adsorbed on zigzag $3 \times 3$ graphene supercell. Colours indicate the most stable site, with green, red, yellow are bridge, hollow, top sites. Cyan is site-independent adsorption. Blue elements are unstable adsorption.	49
4.S2	Adatom heights (Å) of element-adsorbed on zigzag $3 \times 3$ graphene supercell. Red is less than 2.00 Å and yellow is more than 2.00 Å. Blue elements are unstable adsorption.	49

4.S3	Migration energies (eV) of element-adsorbed on zigzag $3 \times 3$ graphene supercell. Grey, light green and green are less than 0.10 eV, between 0.10 and 0.50 eV, and more than 0.50 eV. Blue elements are unstable adsorption.	50
4.S4	Charge transfer from adatom to graphene (number of electrons) of element-adsorbed on zigzag $3 \times 3$ graphene supercell. Yellow, light green and green are less than 0.00 electron, between 0.00 and 0.50 electron, and more than 0.50 electron. Blue elements are unstable adsorption.	50
4.S5	Graphene distortions ( $\text{\AA}$ ). Light green is less than 0.40 $\text{\AA}$ and green is more than 0.40 $\text{\AA}$ . Blue elements are unstable adsorption.	50
4.S6	Fermi energy shifts from pristine graphene (eV). Yellow, light green and green are less than 0.00 eV, between 0.00 and 0.50 eV, and more than 0.50 eV. Blue elements are unstable adsorption.	51
4.S7	Magnetizations ( $\mu_B$ ) of elemental adsorbed/doped on graphene. Light green is positive (at $< 50$ at.%), light yellow is zero (at $< 50$ at.%). Blue elements are unstable adsorption.	51
4.S8	Our calculation on density of states (DOS) (total spin) from H- to Cl-adsorbed graphene. 0.0 eV is Fermi energy. The blue area denotes zero DOS.	52
4.S9	Some trends on elemental adsorption on graphene in the periodic table of elements. Properties are written at the corners with the largest value.	52
5.1	Graphene cell/supercells (adsorption atomic ratio, maximum adatom radius): (a) zigzag $1 \times 1$ (50%, $\approx 1.23 \text{\AA}$ ), (b) zigzag $2 \times 1$ (25%, $\approx 1.23 \text{\AA}$ ), (c) zigzag $\sqrt{3} \times \sqrt{3}$ (16.7%, $\approx 2.13 \text{\AA}$ ), (d) zigzag $3 \times 1$ (16.7%, $\approx 1.23 \text{\AA}$ ), (e) zigzag $2 \times 2$ (12.5%, $\approx 2.46 \text{\AA}$ ), (f) armchair $2 \times \sqrt{3}$ (12.5%, $\approx 2.13 \text{\AA}$ ), (g) zigzag $4 \times 1$ (12.5%, $\approx 1.23 \text{\AA}$ ).	56
5.2	The $2 \times 2$ and $2 \times \sqrt{3}$ graphene supercells, with 3 sites (8 adatom positions, see table 5.1): bridge ( $B_z, B_{a1}, B_{a2}, B_{a3}$ ), hollow ( $H_z, H_a$ ) and top ( $T_z, T_a$ ).	58
5.3	Schematic diagrams of adsorption on the graphene supercells for 1:8 atomic ratio, (a) zigzag $2 \times 2$ and (b) armchair $2 \times \sqrt{3}$ . O(0, 0) is origin. $4 \times 1$ graphene supercell is excluded.	59
5.4	Adatom-adatom binding energies for : (a) $n \times n$ zigzag supercells, (b) $2 \times \sqrt{3}$ armchair and $2 \times 2$ zigzag supercells.	62
5.5	DOS and Fermi energy (0 eV) of (a) Al-adsorbed graphene at its most stable position ( $H_z$ ), spin up and spin down are degenerate, (b) Si-adsorbed graphene at its most stable position ( $B_{a2}$ ).	65
5.6	Charge density difference of Al-adsorbed graphene, $H_z$ case, (a) is isometric view, (b) is front view. Brown spheres are C, grey spheres are Al. Yellow surfaces enclose the charge density greater than 0.015 electron/ $\text{\AA}^3$ (electron surplus), while cyan surfaces enclose the charge density less than -0.015 electron/ $\text{\AA}^3$ (electron deficit).	67
5.7	Charge density difference of Si-adsorbed graphene, $B_{a2}$ case, (a) is isometric view, (b) is side 1 view, (c) is side 2 view. Brown spheres are C, blue spheres are Si. Yellow surfaces enclose the charge density greater than 0.015 electron/ $\text{\AA}^3$ (electron surplus), while cyan surfaces enclose the charge density less than -0.015 electron/ $\text{\AA}^3$ (electron deficit).	67

6.1	Most stable configuration of single-sided fluorinated graphene of 25 at.%, red spheres are F atoms, grey spheres are C atoms, and big red circles are added to guide the eyes. This figure was adopted from figure 4.4.	71
6.2	Graphene supercells, (a) zigzag $2 \times 2$ , (b) armchair $2 \times \sqrt{3}$ , (c) zigzag $4 \times 1$ .	73
6.3	Schematic diagrams of adsorption on the graphene supercells for (a) 1:6, (a) 1:8 zigzag $2 \times 2$ , (c) 1:8 armchair $2 \times \sqrt{3}$ and (d) 1:18 atomic ratios.	74
6.4	Adatom-adatom binding energies for (a) various zigzag $n \times n$ supercells, (b) $2 \times \sqrt{3}$ and $2 \times 2$ supercells.	78
6.5	Some trends for halogen adsorption on graphene at 1:6, 1:8 and 1:18 atomic ratios.	82
6.6	DOS (total spin) and Fermi energy (0 eV) of halogen-adsorbed graphene at 3 different atomic ratios (1:6, 1:8 and 1:18). F is top ( <i>T</i> ) cases, Cl/Br/I are the average values of zigzag ( <i>Z</i> ) and armchair ( <i>A</i> ) cases.	84
6.7	Charge density difference of F-adsorbed graphene at 1:8 atomic ratio, $T_z$ case, (a) is isometric view, (b) is side view. Brown spheres are C, grey spheres are F. Yellow surfaces enclose the charge density greater than 0.01 electron/ $\text{\AA}^3$ (electron surplus), while cyan surfaces enclose the charge density less than -0.01 electron/ $\text{\AA}^3$ (electron deficit).	85
6.8	Charge density difference of Br-adsorbed graphene at 1:8 atomic ratio, $T_z$ case, (a) is isometric view, (b) is side view. Brown spheres are C, blue spheres are Br. Yellow surfaces enclose the charge density greater than 0.01 electron/ $\text{\AA}^3$ (electron surplus), while cyan surfaces enclose the charge density less than -0.01 electron/ $\text{\AA}^3$ (electron deficit).	85
6.S1	Equivalency of graphene supercells, (a) armchair $1 \times \sqrt{3}$ (red) is equivalent to zigzag $2 \times 2$ (blue), (b) slant $3 \times \sqrt{7}$ (red) is equivalent to zigzag $9 \times 9$ (blue). This figure was adopted from figure 4.6.	87
6.S2	DOS (total spin) and Fermi energy (0 eV) of graphene and the elements at 3 atomic ratios. Average values of zigzag ( <i>Z</i> ) and armchair ( <i>A</i> ) cases are used.	88
6.S3	DOS (total spin) and Fermi energy (0 eV) of fluorographene, band gap $\approx 2.99$ eV.	88
7.1	Side, site and orientation in elemental adsorption on graphene.	91
7.2	Most stable configuration of single-sided fluorinated graphene of 25 at.%, red spheres are F atoms, grey spheres are C atoms. This figure was adopted from figure 6.1.	91
7.3	Graphene cells/supercells, all are zigzag orientation, except $2 \times \sqrt{3}$ is armchair and $3 \times \sqrt{7}$ is slant.	92
7.4	Most stable $C_2X_2$ cluster ( $X=F/Cl$ ), grey is C, red is F/Cl.	96
7.5	Two-adatom adsorbed on graphene, big red circle is adatom at the upper side of graphene, small red circle is adatom at the lower side of graphene (a) is represented using a triangle (b).	96
7.6	All possible initial configurations for F/Cl-adsorbed graphene based on the used atomic ratios, red triangle is a pair of F/Cl adsorbed on the upper and lower side of the graphene ( $X=F/Cl$ ).	97

7.7	Initial configurations that produce the most stable configurations for F/Cl-adsorbed graphene based on the used atomic ratios, red triangle is a pair of identical adatoms adsorbed on upper and lower side of the graphene, from left to right (X=F/Cl) : CX <sub>0.111</sub> (18:2), CX <sub>0.250</sub> (8:2), CX <sub>0.333</sub> (6:2), CX <sub>0.500</sub> (8:4), CX <sub>0.667</sub> (6:4), CX <sub>0.750</sub> (8:6), CX <sub>0.889</sub> (18:16), CX (2:2).	98
7.8	DOS (total spin) and Fermi energy (0.0 eV) of (a) CF <sub>a</sub> - GGA, (b) CF <sub>a</sub> - HSE06, (c) CCl <sub>a</sub> - GGA, (d) CCl <sub>a</sub> - HSE06. The blue areas are zero DOS.	99
7.9	Calculated trends for CF <sub>a</sub> and CCl <sub>a</sub> , none creates magnetization. Dotted lines are added as guides and do not imply continuity.	101
7.10	Calculated trends for CF <sub>a</sub> compared to Liu <i>et al.</i> 's work. Dotted lines are added as guides and do not imply continuity.	102
8.1	Schematic diagrams of adsorption on the graphene supercells for (a) 1:6 zigzag $\sqrt{3} \times \sqrt{3}$ , (a) 1:8 zigzag $2 \times 2$ , (c) 1:8 armchair $2 \times \sqrt{3}$ , (d) 1:18 zigzag $3 \times 3$ , and (e) 1:18 slant $3 \times \sqrt{7}$ . (e) is not used.	107
8.2	Adatom-adatom binding energies for (a) various zigzag $n \times n$ supercells, (b) $2 \times \sqrt{3}$ and $2 \times 2$ supercells. Connecting lines have been added as guidance.	110
8.3	Calculation results for period-3 elements adsorbed on graphene, lines are added as a guidance. $E_1$ is binding energy with respect to adatom, $E_2$ is binding energy with respect to adatom-adatom interaction.	112
8.4	Binding energies for period-3 elements adsorbed on graphene, lines are added as a guidance. $E_1$ is binding energy with respect to adatom, $E_2$ is binding energy with respect to adatom-adatom interaction.	113
8.S1	DOS (total spin) and Fermi energy (0 eV) of element-adsorbed graphene at 3 atomic ratios, $z$ is zigzag, $a$ is armchair.	116

## LIST OF TABLES

2.1	Examples of materials' properties.	6
3.1	Overall trends/indicators on elemental adsorption on graphene based on previous studies.	25
3.S1	Magnetizations and band gaps of elemental adsorbed/doped on graphene from previous studies. Atomic ratios are printed in parenthesis.	33
5.1	Sites and orientations for elemental adsorbed graphene for $2 \times 2$ and $2 \times \sqrt{3}$ supercells.	57
5.2	Calculation results for Al-adsorbed graphene (Al:C = 1:8). Spin up and spin down are degenerate. Literature results (at zigzag orientation) are included for $4 \times 4$ graphene supercell and $3 \times 3$ graphene supercell.	63
5.3	Calculation results for Si-adsorbed on graphene (Si:C = 1:8). Spin up and spin down are not degenerate. Literature results (at bridge site) are included: armchair orientation on $4 \times 4$ graphene supercell and zigzag orientation on $3 \times 3$ graphene supercell.	64
5.S1	Initial atomic positions for each case in figure 5.3 (in fractional coordinate).	68
5.S2	Converged $k$ -points and supercell sizes used in each stage.	69
6.1	Halogen-adsorbed graphene. Bold numbers are the values at the most stable position for F cases. Value in brackets are calculation results from previous studies, with its reference number in the square bracket. $B, H, T, Z, A$ are bridge, hollow, top, zigzag and armchair. All cases do not open the band gap.	80
6.2	Difference between calculations with and without van der Waals and dipole corrections in halogen-adsorbed graphene. All values are in %. $B, H, T, Z, A$ are bridge, hollow, top, zigzag and armchair.	83
6.S1	Converged $k$ -points and supercell sizes used in each stage.	86
6.S2	Atomic/ionic radius and Pauling's electronegativity.	86
6.S3	Calculation results of graphene and the elements.	87
7.1	Configurations and binding energies for F- and Cl-adsorbed graphene.	95
8.1	Adatom-adsorbed/doped graphene results from previous studies, atomic ratios are printed in parenthesis.	106
8.2	Results for period 3-elements adsorbed graphene at three atomic ratios. $B, H, T, Z, A, +, -$ are bridge, hollow, top, zigzag, armchair, positive and negative. Atomic ratios printed in parenthesis override the atomic ratio column.	111
8.S1	Atomic/ionic radius and Pauling's electronegativity.	114
8.S2	Calculation results of graphene and the elements.	114
8.S3	Period 3-elements adsorbed graphene. Bold numbers are the values at the most stable position. $B, H, T, Z, A$ are bridge, hollow, top, zigzag and armchair.	115
9.1	Results from previous studies for period 3-elements and halogens adsorbed/doped graphene. $B, H, T, +, -$ are bridge, hollow, top, positive and negative. Grey is cell with no data. Atomic ratios printed in parenthesis override the atomic ratio column.	119

9.2 Results from our calculations for period 3-elements and halogens adsorbed 120  
graphene. *B, H, T, Z, A*, +, - are bridge, hollow, top, zigzag, armchair, positive  
and negative. Atomic ratios printed in parenthesis override the atomic ratio  
column.



# CHAPTER ONE

## INTRODUCTION

---

### 1.1 Background

Materials reduced to the nanoscale can show different properties compared to what they exhibit on a macro scale, enabling the creation of new and unique applications. This is due to the quantum effects, such as quantization of certain physical properties, wave-particle duality, Heisenberg uncertainty principle, quantum superposition and entanglement, and significant amount of surface energy compared to the bulk energy. One example is the semiconducting nano-sized materials, which open up novel opportunities for production of nanoscale electronic and photonic devices such as transistors, biosensors, light sources and detectors [1]. In order to realise the full potential of nano-sized materials with specific properties, it is desirable to fully investigate the electronic structure of nano-sized materials as this determines their electrical, optical, magnetic, thermal, mechanical and chemical properties.

This study is performed using computational simulations, as this is one of the effective methods to investigate the electronic structure of nano-sized materials. Computational simulations are done with density functional theory (DFT) framework[2], which is presently one of the most promising approaches for computation of the electronic structure of matter.

The main material for this investigation is graphene. Graphene is a two-dimensional hexagonal lattice made of carbon atoms. The nearest distance between carbon atoms in graphene is  $\approx 1.42 \text{ \AA}$ . Graphene is currently popular research theme amongst the researchers in the world after the seminal paper of Novoselov and Geim in 2004 [3]. Novoselov *et al.* successfully highlighted the remarkable electronic, mechanical and optical properties of graphene. Thus graphene facilitates the development of novel applications, such as solar cells, display screens, high frequency transistors, hydrogen storage and chemical sensors.

Besides its remarkable properties, graphene is well known as a semimetal material, which has zero electronic band gap at Fermi energy; thus absorbs any incident energy. This is unattractive for solar energy materials or electronic devices applications, which require band gap threshold. Adding impurities or doping is a solution to this problem. As doping is a vast subject, the investigation was limited in subjects of elemental adsorption on graphene.

## 1.2 Objective and Scope of Study

The scope of this study is divided into two parts. The first part is to investigate the electronic structure of nano-sized metallic, semiconducting and insulating materials using DFT via appropriate software and compare the theoretical results with experimental findings. However, the second part is to apply the findings in the first part for the selected materials.

In the first part, the following topics were studied in depth : (1.1) the electronic properties of materials; (1.2) nano-sized metallic, semiconducting and insulating materials; (1.3) the electronic properties of nano-sized metallic, semiconducting and insulating materials; (1.4) DFT; (1.5) how DFT calculation produces results that can be directly compared to the experiment results, *e.g.* Raman/infrared spectra, electron density distribution, band structure; (1.6) the suitable computational methods within DFT for calculating the properties of nano-sized metallic, semiconducting and insulating materials; and (1.7) the suitable simulation software to perform these calculations.

Subsequent to understanding the aforementioned topics, some DFT strategies and customisations were created and applied successfully to verify the structures of some materials. These materials were prepared and characterized by Surface Analysis and Materials Engineering Research Group (SAMERG) at Murdoch University: Raman spectra of Si and SiO<sub>2</sub> [4], material structure verification (lattice constants and atomic positions) for Cu<sub>x</sub>Co<sub>3-x</sub>O<sub>4</sub>

(spinel) [5], and  $Ni_xCr_{1-x}N$  [6]. However, these verifications are not discussed further in this thesis.

In the second part, having been confident with DFT, graphene was chosen as the base material for this thesis. For this selected material, the results from the previous studies were consulted and analysed: (2.1) the recent progresses of its fabrications and characterizations; (2.2) the recent progresses of its simulation studies; and (2.3) the potential problems that can be tackled within the time frame of this Ph.D. period.

After intensive literature review, geometrical and orientation aspects of elemental adsorption on graphene was selected as the main research topic. Currently, many researchers studied the effects of sites (bridge, hollow, top) on elemental adsorption on graphene (see figure 1.1a). Upon inspecting this matter carefully, it was found that orientation (zigzag and armchair) is also important in adsorption (see figure 1.1). Orientation is the position of adatom (adsorbed elements) relative to one another and also relative to graphene. Surprisingly, this orientation is often overlooked in the previous studies.

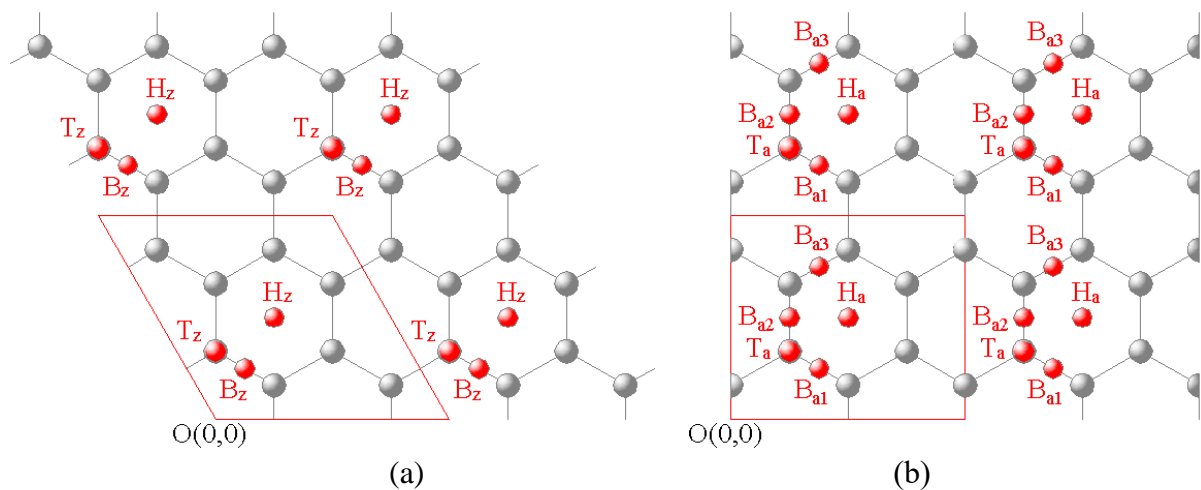


Figure 1.1 Schematic diagram of elemental adsorption on graphene, grey spheres are carbon, red spheres are adatom, B=bridge, H=hollow, T=top, (a) zigzag orientation (subscript z), (b) armchair orientation (subscript a).

So three objectives are targeted for this thesis, *i.e.* (1) to report the suitable computational methods within DFT for the investigation of the electronic structure of nano-sized metallic, semiconducting and insulating materials; (2) to report novel insights of the geometrical and orientations aspects of elemental adsorption on graphene, which is the primary objective of this thesis; and (3) to give recommendations for the future work on elemental adsorption on graphene. Finally, the main goal of this study is to enable us to make better predictions of the characteristics of elemental adsorption on graphene.

This thesis is organised in nine chapters. Chapter one introduces the background, objective and scope of the study. Chapter two discusses the theoretical background, which includes two sections: electronic structure and DFT. This chapter answers topics 1.1, 1.4 and 1.5 and objective 1. Chapter three discusses nano-sized metals, semiconductors and insulators; introduces the graphene and reviews the literatures of elemental adsorption on graphene. This chapter answers topics 1.2, 1.3 and 2.1 to 2.3. Chapter four explains the computational strategies, simulation software and the details of the geometry of the elemental adsorption on graphene. This chapter answers topics 1.6 and 1.7. Chapters five to eight summarize the main results of this thesis, which include the orientation aspects of adatom-adsorption on graphene. The inspected atoms belong to group 3 of the periodic table (Na, Mg, Al, Si, P, S, Cl) and the halogens (F, Cl, Br, I). These chapters address objective 2. Finally, chapter nine consolidates the overall results in this study, gives conclusions and potential future work, which addresses objective 3.

# CHAPTER TWO

## THEORETICAL BACKGROUND

---

This chapter highlights two things, *i.e.* the electronic structure and the Density Functional Theory (DFT).

### 2.1 Electronic Structure

Electrons are one of the fundamental particles, which together with protons and neutrons form atoms. Due to their small size, electrons are studied using quantum mechanics at low velocity and quantum field theory at high velocity[7, p. 2]. This thesis emphasises the low velocity realm, therefore quantum mechanics is used. Quantum mechanics has the main formula to work with, *i.e.* Schrödinger equation :

$$-\frac{\hbar^2}{2m}(\nabla^2 + V(\mathbf{r}, t))\psi(\mathbf{r}, t) = -i\hbar \frac{\partial}{\partial t}\psi(\mathbf{r}, t) \quad (2.1)$$

where  $\hbar$  is reduced Planck's constant ( $1.05457 \times 10^{-34}$  Joule second);  $m$  is the mass of the particle;  $\nabla^2$  is Laplacian (kinetic energy of the system);  $V(\mathbf{r}, t)$  is the potential energy of the system;  $\psi(\mathbf{r}, t)$  is the wave function of the system;  $i$  is imaginary number;  $-i\hbar \frac{\partial}{\partial t}$  is the energy operator;  $\mathbf{r}$  is position vector;  $t$  is time. Equation (2.1) is an eigenvalue problem, with two unknowns,  $\psi(\mathbf{r}, t)$  and its time derivative  $-i\hbar \frac{\partial}{\partial t}\psi(\mathbf{r}, t)$ . These two unknowns must be computed to simultaneously satisfy equation (2.1). Planck's constant is a quantised angular momentum. Its appearance in an equation indicates that quantum effect is in use. Unfortunately, Schrödinger equation can be solved exactly only for the simplest cases, *i.e.* hydrogen (H) and hydrogen-like atoms ( $\text{He}^+$ ,  $\text{Li}^{2+}$ ,  $\text{Be}^{3+}$ , ...). For other cases, approximations or numerical calculations must be used.

The systems observed in this thesis were time-independent. Equation (2.1) in time-independent form is

$$-\frac{\hbar^2}{2m}(\nabla^2 + V(\mathbf{r}))\psi(\mathbf{r}) = E\psi(\mathbf{r}) \quad (2.2)$$

where  $-i\hbar \frac{\partial}{\partial t}$  becomes a number called the energy of the system ( $E$ ). Solving equation (2.2) results multivalued  $\psi(\mathbf{r})$  and  $E$ , so it is introduced the first three quantum numbers, *i.e.*  $n$  (principal),  $l$  (orbital),  $m_l$  (orbital magnetic) to label  $\psi(\mathbf{r})$  and  $E$ . They become  $\psi_{n,l,m_l}(\mathbf{r})$  and  $E_{n,l,m_l}$ . Sometimes, different  $\psi_{n,l,m_l}(\mathbf{r})$  gives identical  $E_{n,l,m_l}$ , this is called energy level degeneracy.  $\psi_{n,l,m_l,m_s}(\mathbf{r})$  determines the electronic structure/configuration of the materials, and the electronic structure of materials determines the materials' properties. Some of materials' properties are listed in table 2.1.

Table 2.1 Examples of materials' properties.

Properties of materials	Examples
electrical	electrical conductivity (superconductor, metal, semiconductor, insulator), capacitance, inductance, impedance, permittivity
optical	index of refraction, damping constant, absorbance, reflectivity, transmittance, optical spectra, diffraction, polarization, interference, penetration depth
magnetic	dia-, para-, ferro-, antiferro-, ferri-magnetism, permeability, magnetic moment, hysteresis, spin
thermal	heat capacity, thermal conductivity, melting point, boiling point, thermal expansion
mechanical	density, hardness, Young's/bulk/shear modulus, elasticity, plasticity, viscosity, compressibility
chemical	electronegativity, bond type & polarity (ionic, covalent, polar, non-polar, hydrogen bond, van der Waals), ionization, affinity, adsorption, dipole moment

However, to explain spin, one result from the quantum field theory, *i.e.* Pauli exclusion principle must be considered even at low velocity[8, p. 180]. To accommodate this, the last

quantum number is introduced, *i.e.*  $m_s$  (spin magnetic)[9, p. 1223]. For electron case, Pauli exclusion principle states that no two or more electrons, in an atom, can occupy the same four quantum numbers ( $n, l, m_l, m_s$ ) simultaneously. Spin is also a quantised angular momentum, with certain magnitudes ( $0\hbar, \frac{1}{2}\hbar, 1\hbar, \frac{3}{2}\hbar, 2\hbar, \dots$ ). Electrons have spin of magnitude  $\frac{1}{2}\hbar$ .

Electrons have orbital angular momentum as it orbits around the nucleus. This orbital angular momentum interacts with spin angular momentum (spin-orbit coupling), suggests a useful quantity for spectroscopy, that is total angular momentum ( $j$ ). This  $j$  breaks the degeneracy of energy levels with the same  $n$  and  $l$  quantum numbers, which introduces the famous Hund's rule. The Hund's rule states that for degenerate orbitals, the lowest energy is achieved when the electrons have the same spin. For carbon atom ( $1s^2 2s^2 2p^2$ ), the degenerate  $2p$  orbital has 2-spin-up electrons, instead of a pair of spin-up/down electrons. This unbalance spin creates spin magnetic dipole moment, with one unpaired spin creates spin magnetic dipole moment at about  $1\mu_B$  (Bohr magneton or  $9.274 \times 10^{-24}$  Joule/Tesla). This slight difference from  $1\mu_B$  is explained using theory of quantum electrodynamics (QED). Magnetization is defined as the density of spin magnetic dipole moment, *e.g.*  $\mu_B$  per unit cell. So, while the total charge is the sum of total spin up and spin down, magnetization is the difference between total spin up and spin down.

For atoms, electronic structure is called atomic orbital. For example, the atomic orbital of carbon atom is  $1s^2 2s^2 2p^2$ . When atoms interact with other atoms to form molecules, its energy levels split. For molecules, electronic structure is called molecular orbital. The well known examples of molecular orbital are  $sp^3$  hybridization of methane ( $\text{CH}_4$ ) and  $sp^2$  hybridization of graphene. For methane, one carbon atom is connected to four hydrogen atoms, so the  $2s^2 2p^2$  changes to four identical  $sp^3$ . For graphene, one carbon atom is connected to three other carbon atoms, so the  $2s^2 2p^2$  changes to three identical  $sp^2$  plus one  $2p$ .

When many atoms interact with other atoms to form condensed matter, its energy levels split further. This creates a set of macroscopically continuous allowed and forbidden energy levels, that is called energy bands. Electrons are only possible to occupy the allowed energy bands. An energy band between two allowed energy levels is called band gap.

For the condensed matter, the concept of density of states (DOS) is very useful to describe the electronic structure. DOS ( $n(E)$ ) is number of states available for electrons ( $n$ ) as a function of energy of the system ( $E$ ). This concept holds generally for crystallines, amorphous, liquids, organic materials, small systems (quantum dots, molecules), strongly correlated materials (superconductors, Mott insulators), inhomogeneous materials (local defects, impurities, materials' interfaces).

At ground state, electrons in a system occupy fully the lower part of the DOS. The highest energy level that is occupied by electrons is called Fermi energy. The DOS for the energy above the Fermi level is quite important. It controls the flow of electrons upon excitations, and explains three categories of materials, *i.e.* metals (and also semimetals), semiconductors and insulators. These three categories are based on the band gap above the Fermi level. For the rest of this thesis, band gap is defined as the band gap above the Fermi level. Metals have no band gap, semimetals have zero band gap, semiconductors have small band gap, and insulators have large band gap. The band gap threshold for semiconductors and insulators is set by convention, usually the blue light ( $\approx 3.1$  eV). This thesis uses eV unit ( $1$  eV =  $1.602 \times 10^{-19}$  Joules).

Modifying the band gap is desirable to create materials that suit our needs. There are many ways to modify the band gap, *e.g.* adding impurities (doping), changing its crystal structure, applying pressure, operating at different temperature, creating defects, interfacing two surfaces, and deforming its shape. There is another approach, that is designing materials



that suppresses the quantum effects, thus extending a little bit longer the existing technology[10]. This might be a cheaper and more useful approach.

With the rise of nanotechnology, there is one more way to modify the band gap, *i.e.* reducing the material size to nanoscale. Nanoscale is a scale of nanometre length (about the size of atoms).

## 2.2 Density Functional Theory (DFT)

Nano-sized material research is very vast subject. The demand of this technology is growing at ever increasing rate. To achieve the desired properties, unlimited numbers of permutation of elements must be inspected. It sounds like daunting tasks, but computational simulation offers solutions in an effective way. Some of the computational simulation advantages are :

1. able to suggest only the prospective cases for the experiments
2. able to verify / confirm the experimental results
3. able to predict the properties of materials where experiments are impossible to perform
4. the cost per case might be lower than the experiments
5. the time per case might be lower than the experiments.

Hartree-Fock method is a natural approach to solve the Schrödinger equation numerically. For  $N$ -electron system, the ground state wave function is approximated by a Slater determinant.  $\psi(\mathbf{r}_1, \mathbf{r}_2, \dots, \mathbf{r}_N)$  in equation (2.2) is decomposed into combination of orthonormal orbitals  $\phi_i$ . Orthonormal means

$$\int_{all\ space} \phi_i \phi_j d\tau = \delta_{ij} \quad (2.3)$$

with  $\delta_{ij}$  is Kronecker delta :

$$\delta_{ij} = \begin{cases} 1 & \text{if } i = j \\ 0 & \text{if } i \neq j \end{cases} \quad (2.4)$$

The decomposition that satisfies antisymmetric (Pauli exclusion principle) of  $\psi(\mathbf{r}_1, \mathbf{r}_2, \dots, \mathbf{r}_N)$  is Slater determinant with spin:

$$\begin{aligned} & \psi(\mathbf{r}_1, \mathbf{r}_2, \dots, \mathbf{r}_N) \\ &= \frac{1}{\sqrt{N!}} \text{Det} \begin{bmatrix} \phi_1(\mathbf{r}_1) \uparrow_1 & \phi_1(\mathbf{r}_1) \downarrow_1 & \phi_2(\mathbf{r}_1) \uparrow_1 & \phi_2(\mathbf{r}_1) \downarrow_1 & \dots & \phi_{N/2}(\mathbf{r}_1) \uparrow_1 & \phi_{N/2}(\mathbf{r}_1) \downarrow_1 \\ \phi_1(\mathbf{r}_2) \uparrow_2 & \phi_1(\mathbf{r}_2) \downarrow_2 & \phi_2(\mathbf{r}_2) \uparrow_2 & \phi_2(\mathbf{r}_2) \downarrow_2 & \dots & \phi_{N/2}(\mathbf{r}_2) \uparrow_2 & \phi_{N/2}(\mathbf{r}_2) \downarrow_2 \\ \vdots & \vdots & \vdots & \vdots & \ddots & \vdots & \vdots \\ \phi_1(\mathbf{r}_N) \uparrow_N & \phi_1(\mathbf{r}_N) \downarrow_N & \phi_2(\mathbf{r}_N) \uparrow_N & \phi_2(\mathbf{r}_N) \downarrow_N & \dots & \phi_{N/2}(\mathbf{r}_N) \uparrow_N & \phi_{N/2}(\mathbf{r}_N) \downarrow_N \end{bmatrix} \end{aligned} \quad (2.5)$$

where  $\uparrow$  is spin up and  $\downarrow$  is spin down. The transpose of this matrix results the same Slater determinant.

But this Hartree-Fock calculation is rather time consuming. However, DFT has the capacity to overcome this problem. DFT replaces the complicated  $\psi(\mathbf{r}_1, \mathbf{r}_2, \dots, \mathbf{r}_N)$  into simple  $\rho(\mathbf{r})$ , where  $\rho$  is electron density and  $\mathbf{r}$  is spatial coordinate.

DFT is a computational method using quantum mechanical theory to investigate the electronic structure of materials[2]. It is presently one of the most promising approaches for computation of the electronic structure of matter. DFT is not a semi-empirical method but is derived from the first principles of quantum mechanics (*ab initio* method). Semi-empirical method is a method that uses adjustable parameters to match the experimental data or *ab initio* results. In contrast, *ab initio* method uses only fundamental constants, such as Planck constant ( $6.626 \times 10^{-23}$  Joule second), speed of light in vacuum (299,792,458 metre/second), electron charge magnitude ( $1.602 \times 10^{-19}$  Coulomb), mass of electron ( $9.109 \times 10^{-31}$  kilograms), and masses of nuclei. Foresman and Frisch noted that there is still controversy whether DFT is an *ab initio* method or not [18, p. 6], but this philosophical question is not discussed in this thesis.

DFT rests on Kohn-Hohenberg theorems[2], which state :

1. the ground-state energy from Schrödinger equation is a unique functional of the electron density  $\rho$ ,
2. the electron density that minimizes the energy of the overall functional is the true electron density corresponding to the full solution of the Schrödinger equation.

Thus, DFT uses functional of electron density as the input, and total energy of the system as the output. Functional is a function of another function, for example in DFT :

$$E_{XC}[\rho(\mathbf{r})] \quad (2.6)$$

where  $E_{XC}$  is exchange-correlation energy,  $\rho$  is electron density, and  $\mathbf{r}$  is spatial coordinate.

DFT uses Kohn-Sham equation, that is computed self-consistently :

$$E[\rho(\mathbf{r})] = E_K[\rho(\mathbf{r})] + E_{N-N} + E_{N-e}[\rho(\mathbf{r})] + E_{e-e}[\rho(\mathbf{r})] + E_{XC}[\rho(\mathbf{r})] \quad (2.7)$$

where  $E$  is total energy of the system,  $E_K$  is total kinetic energy,  $E_{N-N}$  is nuclear-nuclear interaction energy,  $E_{N-e}$  is nuclei-electron interaction energy,  $E_{e-e}$  is electron-electron interaction energy,  $E_{XC}$  is exchange-correlation energy. Only  $E_{N-N}$  that doesn't depend on electron density.

$$E_{XC}[\rho(\mathbf{r})] = E_X[\rho(\mathbf{r})] + E_C[\rho(\mathbf{r})] \quad (2.8)$$

where  $E_X$  is exchange energy that comes from the anti-symmetrisation of wave functions, and  $E_C$  is correlation energy that comes from the dynamic correlation of electrons due to the electrons' constant motion relative to one another. Although  $E_K$ ,  $E_{N-e}$  and  $E_{e-e}$  are known exactly,  $E_{XC}$  is not. Approximations have to be made to calculate  $E_{XC}$ . There are some approximation methods to calculate  $E_{XC}$  :

1. Local density approximation (LDA)  $E_{XC} = E_{XC}[\rho(\mathbf{r})]$
2. Generalized gradient approximation (GGA)  $E_{XC} = E_{XC}[\rho(\mathbf{r}), \nabla\rho(\mathbf{r})]$
3. Meta-GGA  $E_{XC} = E_{XC}[\rho(\mathbf{r}), \nabla\rho(\mathbf{r}), \nabla^2\rho(\mathbf{r})]$
4. Hybrid exchange functional (hyper-GGA)  $E_{XC} = E_{XC}[\rho(\mathbf{r}), \nabla\rho(\mathbf{r}), E_X^{HF}]$

where  $\nabla$  is gradient of a function,  $\nabla^2$  is Laplacian and  $E_X^{HF}$  is Hartree-Fock (HF) exact exchange functional. LDA approximates this  $E_{XC}$  as homogeneous electron gas. However, as the electron density is usually not homogeneous, the GGA, meta-GGA and hyper-GGA approximations are developed. By incorporating the derivative of electron density ( $\nabla\rho(\mathbf{r})$ ) or its higher derivative ( $\nabla^2\rho(\mathbf{r})$ ), mathematically, there is more room to improve the accuracy.

The main advantage of DFT is the balance between accuracy and cost, so it is very desirable for nanomaterial computations. However, DFT has some limitations :

1. in calculating electronic excited states
2. exact functional is not known
3. underestimate the band gap calculations for semiconducting and insulating materials
4. inaccurate in van der Waals interaction calculations
5. like all *ab initio* methods, DFT is not feasible for large cluster of atoms or very long time reactions.

For the first limitation, as DFT rests on Kohn-Hohenberg theorems which apply only to ground state, it has limited accuracy to calculate excited states. Electronic excitation processes happen in three stages: photoemission, inverse-photoemission, and the formation of exciton, as illustrated in figure 2.2. Some methods beyond DFT, *e.g.* Time-dependent DFT (TDDFT), GW approximation and Bethe-Salpeter equation try to address this limitation.

To overcome the second limitation, many approximations within LDA/GGA/meta-GGA/hyper-GGA are continuously developed.

The third limitation is probably the most well known, *i.e.* DFT band gap underestimation. HSE06 functional [19] and GW approximation are some of the methods that address this limitation. Both methods are computationally expensive. GW approximation is the most expensive, but theoretically more accurate than HSE06.

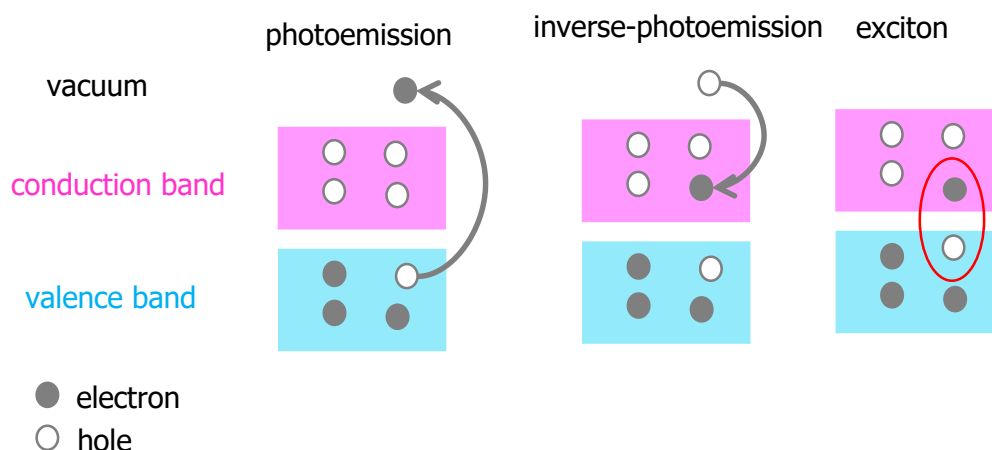


Figure 2.1 Electronic excitation process that is not covered in pure DFT.

In the fourth limitation, DFT does not include van der Waals forces [20]. Van der Waals forces are two phenomena in the intermolecular electrical attractions between electrically neutral molecules, *i.e.* dispersion forces (caused by instantaneous dipole moment in nonpolar molecules) and dipole-dipole attractions (caused by permanent dipole moment in polar molecules) [21, p. 428]. A pair of particles separated by distance  $r$  exhibits weak short-range Van der Waals interaction proportional to  $r^{-6}$  [22, p. 345].

Addressing the last limitation of DFT, for the larger clusters and longer time reactions, semi-empirical method is more appropriate in both cost and time. Some examples of semi-empirical methods include AM1, PM3, MNDO and PM6 [18, p. 111]

Basis set is a set of functions used to create atomic orbitals (see Eq. 2.5). This is a kind of signature of atom. There are two approaches in basis set, *i.e.* all electron and valence electron. All electron basis sets use functions of all electron to describe atoms, while valence electrons basis sets use functions of only valence electrons to describe atoms. Calculations with all electron basis sets are slower than the valence electrons ones, but can describe the core electrons. A function that is useful for basis set is Gaussian function, that is  $G(\alpha, \mathbf{r}) \propto e^{-\alpha|\mathbf{r}|^2}$ , where  $\alpha$  is a constant and  $\mathbf{r}$  is spatial coordinate. An advantage of using Gaussian function is that multiplication of two Gaussian functions results another Gaussian function :

$$e^{-\alpha|r-\mathbf{R}_A|^2} e^{-\beta|r-\mathbf{R}_B|^2} = K e^{-\gamma|r-\mathbf{R}_C|^2} \quad (2.9)$$

where  $K = e^{-\frac{\alpha\beta}{\alpha+\beta}|\mathbf{R}_A-\mathbf{R}_B|^2}$ ;  $\gamma = \alpha + \beta$ ;  $\mathbf{R}_C = \frac{\alpha\mathbf{R}_A+\beta\mathbf{R}_B}{\alpha+\beta}$ .

In accordance with valence electrons calculation, it is known *pseudopotential* term. In pseudopotential, the details of the electronic wave function  $\psi(r)$  near the nucleus (inside cut off radius  $r_c$ ) is smoothed and matched against all electron wave function at radius greater than  $r_c$ . This strategy reduces the number of the plane-waves, thus speeds up the calculation, but introduces new parameter  $r_c$  that must be tuned to obtain convergence result. The greater  $r_c$  the faster the calculation, but the less the accuracy. It is discussed very briefly two types of pseudopotential here, *i.e.* ultrasoft pseudopotential and projector-augmented wave (PAW). These two pseudopotentials do not conserve the norm of the all electron wave function. Norm of a wave function  $\psi(r)$  is defined as

$$\|\psi(r)\| \equiv \sqrt{\langle\psi(r)|\psi(r)\rangle} = \sqrt{\int_{-\infty}^{\infty} \psi^*(r)\psi(r)dr} \quad (2.10)$$

So the total energy calculated using these pseudopotentials is different from the one calculated using all-electrons potential. This suggests that calculations using these pseudopotentials are only meaningful in terms of total energy difference, such as binding energies. Ultrasoft pseudopotential uses larger  $r_c$  than PAW.

Only time-independent DFT with valence electron basis set that is used in this thesis. Nuclei are fixed in space (Born-Oppenheimer approximation). These simplify the calculations significantly. However, spin polarization is not ignored in this thesis, as spin is essential to obtain the true ground state energy and reveal magnetic properties of the materials.

Figure 2.2 shows the computational simulation flowchart using DFT. The computational simulation is started by defining the atoms and their initial positions. There are two types of defining these, *i.e.* molecular cluster and periodic lattice. Molecular cluster is suitable for defining localised clusters of atoms or molecules, while periodic lattice is suitable

for defining crystal structures. However, molecular cluster can be defined using periodic lattice, and vice versa, but this creates inefficiency in the subsequent calculations. In periodic lattice, there are two types of coordinates, *i.e.* absolute coordinate and relative coordinate. Absolute coordinate is the coordinate relative to the absolute space, while relative coordinate is the coordinate relative to the lattice parameters in a unit cell. This thesis always uses periodic lattice and relative coordinate. Calculations on atomic clusters were done using large periodic lattice.

The second step is to select the suitable basis sets, based on the desired accuracy and cost. Mixing basis set in a calculation is possible, for example in inspecting the interaction of two atomic clusters in water solution. Using cheap and less accurate basis sets for the background atoms (water solution), and using more expensive and more accurate basis sets for the inspected/focused atomic clusters.

These two initial sets of information (atoms' positions and basis sets) are inserted into DFT, and the results are the energy and atomic forces of the system. In the normal time-independent systems, calculations are valid if all the atoms are fully relaxed, as this is the most probable configuration. An atom is fully relaxed if there is no force working on that atom. Force is the derivative of energy against position, or the gradient of energy. So to achieve valid calculation, energy and forces must be minimised simultaneously. Note that, this criteria doesn't apply for calculating systems under stress.

If the energy and forces are not minimum, atomic positions must be modified using various molecular dynamics algorithms, and DFT recalculation must be performed. For numerical calculations or calculations using approximation, the criteria of minimum are :

1. the energy difference of two consecutive calculations below a threshold (eV)
2. the forces of all atoms below a threshold (eV/Å).

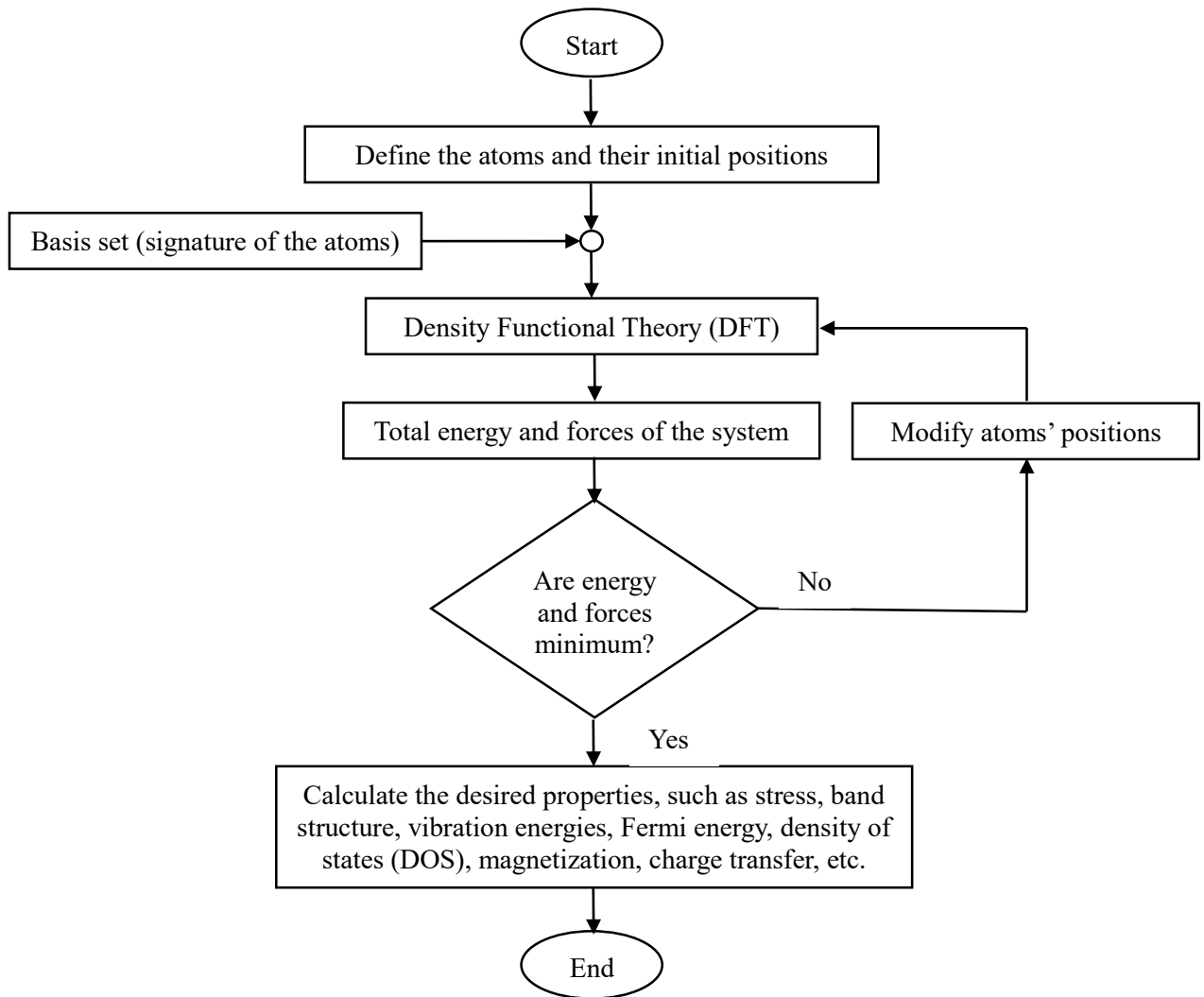


Figure 2.2 Computational simulation flowchart using DFT.

If the minimum energy and forces are achieved, the final step is to calculate the desired properties, such as stress, band structure, vibration energies, Fermi energy, density of states (DOS), magnetization, binding energy, charge transfer, etc.



## CHAPTER THREE

### REVIEW OF ELEMENTAL ADSORPTION ON GRAPHENE

---

Ideally, introducing foreign materials into/onto the graphene should give the desired properties without degrading the properties of graphene. In reality, this certainly is a trade off. One of the most important goals of a study is its ability to predict, and one key aspect of prediction is trend. Related to the predictions on elements, it is natural to know the trends in the periodic table of elements. So this chapter presents a literature study that reviews the trends in elemental adsorption on graphene in terms of various properties *e.g.* binding energy/stability, the most stable site (bridge, hollow, top), migration (barrier) energy, adatom height, graphene distortion, Fermi energy, magnetization, charge transfer and band gap at Fermi energy. Some of these trends are compared to our calculation results in chapters 4 to 8 in this thesis. This chapter consists of four sections: nano-sized materials, graphene, trends on the elemental adsorption on graphene from previous studies, and the summary that can be brought to chapters 4 to 8.

#### 3.1 Nano-sized Metals, Semiconductors and Insulators

Nano-sized materials are materials with at least one dimension in the order of up to 100 nanometre. A nanometre ( $10^{-9}$  metre) is the typical size of atoms/molecules. Materials reduced to the nanoscale can show different properties compared to what they exhibit on a macro scale, enabling the creation of new and unique applications. This is due to the quantum effects, such as quantization of certain physical properties, wave-particle duality, Heisenberg uncertainty principle, quantum tunnelling, superposition and entanglement, and significant amount of surface energy compared to the bulk energy. The investigations of nano-sized materials are inevitable as driven by the needs for faster computations/communications, denser data storages,

more efficient energy converters, better flexible display screens, lighter yet stronger and more durable materials. However, further reduction of the material size is sometimes not possible or not desirable, so other routes are applied, such as doping or modifying its structures.

The development of this type of material has been stimulated by the availability of:

1. various nano material synthesis methods *e.g.* nanolithography, mechanical exfoliation, self-assembly, molecular beam epitaxy (MBE), chemical vapour deposition (CVD);
2. nanoscopy, *e.g.* scanning tunnelling microscopy, field emission scanning electron microscopy and atomic force microscopy;
3. nanoparticle modelling and simulations, *e.g.* the Hartree-Fock method and DFT;
4. faster computers (or supercomputers) for doing the simulations;
5. rapid flow on research collaboration and research information exchange via internet, as this nanotechnology enterprise is highly collaborative and multidiscipline.

There are two approaches in nanofabrication, *i.e.* top-down and bottom-up. Top-down method is to slice down a larger material to form a nanomaterial. While bottom-up method is to assemble atom-by-atom to form a nanomaterial. Some examples of top-down method include nanolithography and mechanical exfoliation. Nanolithography is carving at nanoscale. This method is ideal to extend the current integrated circuit fabrication to the nanoscale. Mechanical exfoliation is a well known method to produce graphene from graphite[11].

Some examples of bottom-up method include self-assembly, molecular beam epitaxy (MBE) and chemical vapour deposition (CVD). Self-assembly is a method to assemble atoms by utilising their own mutual interactions, *e.g.* fabrication of bio-nanomaterials. MBE is a method of depositing atoms (in its molecular beams form) onto a surface. MBE is able to deposit as low as 1 atomic layer. CVD is a method of depositing atoms (in its vapour state) onto a surface, *e.g.* fabrication of carbon nanotubes. Although CVD is less accurate than MBE,

but it is more economical. In regard to Surface Analysis and Materials Engineering Research Group (SAMERG), sol-gel dip-coating method is one of the favoured methods in fabricating nano-sized materials [12]. This method is facile, environmentally friendly and cost-effective.

Nanoscopy is a tool for materials characterization at nanoscale, which is the natural extension of microscopy. Scanning tunnelling microscope (STM), field emission scanning electron microscope (FESEM), atomic force microscope (AFM), transmission electron microscope (TEM), high resolution transmission electron microscope (HRTEM) are some of modern tools of nanoscopy [13]. STM and FESEM function like microscope at nanometre. While AFM is a more advance technology, which is able to probe and also manipulate materials at atomic level. Besides nanoscopy, common spectroscopy techniques are also powerful tools to characterize nano-materials, *e.g.* Raman spectroscopy, ultraviolet-visible near infrared (UV-Vis-NIR) spectroscopy, Fourier transform infrared (FTIR) spectroscopy, X-ray diffraction (XRD), wide angle XRD, synchrotron XRD, X-ray photoelectron spectroscopy (XPS), near-edge absorption fine structure (NEXAFS) spectroscopy, energy dispersive X-ray (EDX) spectroscopy [14]. Lastly, to characterize the mechanical properties of the materials, nanoindentation test is widely used. This nanoindentation test in the experimental side can be with complemented with finite element modelling (FEM) in the theoretical side. The characterization techniques above are routinely used in Surface Analysis and Materials Engineering Research Group (SAMERG).

The grouping of materials based on its band gap (metal, semiconductor and insulator) is still important at nanoscale. Besides, nanoscale offers richer options, such as topological insulators, which two different band gaps coexist in the same material. Based on the dimensionality (D), nano materials are categorized into nanocrystal and nanoparticle (3D), nanosheet and nanoribbon (2D), nanotube, nanowire and nanorod (1D), and nanodot (0D). It is reported that band gap of nano-sized semiconductors increases with the decrease of

dimensionality[15], [16]. Band gap can also change dramatically from metal to insulator by simply applying mechanical tension in 1D nanomaterials[17].

It is well known that zigzag or armchair termination of graphene nanoribbon determines its band gap (see figure 3.1). Zigzag orientation creates metal, while armchair orientation (depending on its width) creates metal/semiconductor. This highlights the importance of a geometric aspect, *i.e.* orientation, to the properties of materials. Orientation is an interacting many body effect. Thus it does not have any meaning on a single entity, or on non-interacting many bodies.

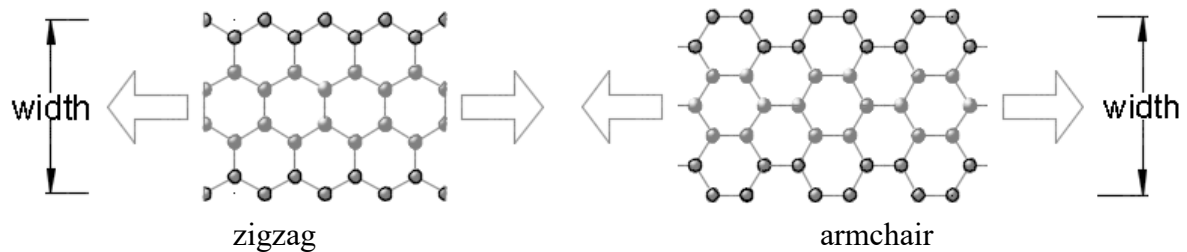


Figure 3.1 Zigzag and armchair terminated graphene nanoribbon. Grey is carbon atom. Black circles are added to mark the edges of the nanoribbon.

### 3.2 Graphene

Graphene is a two-dimensional hexagonal lattice made of carbon atoms with the nearest distance between carbon atoms in graphene is about 1.42 Å. The seminal paper of Novoselov and Geim and their collaborators in 2004 successfully prepared graphene via mechanical exfoliation and highlighted its remarkable electronic, mechanical and optical properties [23]. Graphene has ambipolar field effect; very high Young's modulus (1.0 TPa); exhibits ballistic transport; high electron mobility (200,000 cm<sup>2</sup>/V.s); high thermal conductivity (5 kW/m.K); high optical transparency (97.7%); super hydrophobicity; low resistivity (10<sup>-6</sup> Ω.cm); chemical inertness[24], [25]. With these properties, graphene is very promising in facilitating the development of novel applications, which includes solar cells, display screens, high frequency transistors, hydrogen storage, chemical and biosensors.

Dresselhaus [26] and Geim [27] have elaborated the history of graphene. On the theoretical side, as early as 1947, Phil Wallace calculated the band structure of graphene. On the experimental side, researchers started studying graphite in 1960s, graphite intercalation compounds in 1970s, buckyballs in 1980s and carbon nanotubes in 1990s, before graphene took over in 2000s. Graphite intercalation compound is single or a few layers of graphene sandwiched with one or a few layers of other compounds called intercalate layer. Graphite is weakly interacting graphene layers, which is three-dimensional. Buckyball is carbon atoms that form a sphere/ellipsoid, which is quasi-zero-dimensional. Carbon nanotube is carbon atoms that form a tube, which is quasi-one-dimensional. Moreover, graphene has a two-dimensional carbon structure. The research of graphene that started half a century ago is now at peak and will continue to rise.

Since then, graphene has been synthesized around the world using various methods, including mechanical exfoliation, chemical synthesis, unzipping nanotubes, chemical vapour deposition (CVD), reducing graphene oxide and epitaxial growth on metals/carbides. As an example, in 2012, Sony Corporation produced a 100-m-long by 210-mm-width graphene using CVD[28]. Another example is graphene grown epitaxially on silicon carbide (SiC). SiC is a wide band gap semiconductor suitable for high temperature, high electric field and high speed devices, superior to silicon[29]. The most interested structures are hexagonal 4H and 6H with band gap of 3.2 eV and 3.0 eV. Graphene grown epitaxially on SiC is found to be promising for commercial wafer-scale production [30], large-scale patterning[31] and also for the integration with the current silicon technology in electronic industries[32]. It induces n-type doping on graphene naturally[33]. The third example, was presented recently by Lin *et al.* [34] fabricated graphene from commercial polymer films using laser, which offers rapid production of graphene.

Besides its remarkable properties, graphene is well known as a semimetal (zero band gap) material. This makes graphene unattractive for solar energy materials or electronic devices applications that require band gap threshold. Adding impurities (doping), introducing defects, modifying its geometry/size, applying external constraints (*e.g.* electric field, strain, temperature), or its combinations are some potential solutions to this problem. These functionalizations tailor the properties of graphene and also open wider applications.

The first strategy is doping. There are two types of doping on graphene, *i.e.* adsorption and substitution. Adsorption is adding adatoms on the graphene surface, while substitution is replacing carbon atoms in graphene with substituents. Atomic ratio is the ratio of the number of adatom to the number of carbon atoms in a graphene cell/supercell. For substitution case, it is recommended that substituents' size (atomic radius) is comparable to carbon atomic radius, so the substituents do not disrupt the graphene sheet. Disrupting graphene sheet reduces the mechanical properties and electrical conductivity of graphene significantly.

The second strategy is introducing defects. Defects can be introduced by: (1) removing carbon atoms from the graphene; or (2) modifying hexagonal carbon networks into non-hexagonal ones (*e.g.* Stone-Wales defects [35]).

The third strategy is modifying its geometry/size (*e.g.* graphene nanoribbons, buckyballs, carbon nanotubes/nanorods/nanoscrolls) [36, p. 4]. A well-known example is that zigzag termination nanoribbons create metallic materials, while armchair termination (depending on its width) creates metallic/semiconductor materials [25, p. 5].

To wrap up this overview on graphene and its functionalizations, there have been excellent reviews on graphene (*e.g.* a 214-page review [37], a roadmap of graphene [11], 270-page book [38], graphene as a super material [39]); functionalizations on graphene (*e.g.* 59-page[40] and a 44-page review [41]); and graphene and family of 2D materials [42].

As doping on graphene is a vast subject, the investigation was limited to elemental adsorption only. The main reasons are listed as follows :

1. The elemental adsorption is relatively simpler to simulate than molecular adsorption
2. The elemental adsorption gives hints to study more complex structures, however there might be some subtleties that are overlooked despite its simplicity.

In chemistry, elements are substances that cannot be decomposed into simpler substances[21, p. 7]. These elements are summarized in the periodic table of elements. Adsorption is adhesion or binding of atoms, ions or molecules (adsorbates) to a surface[21, p. 590]. It is a Fermi energy matching between the adsorbates and the surface. There are two types of adsorption, i.e. physisorption and chemisorption. Physisorption is a weak adsorption due to dispersive force, while chemisorption is a strong adsorption that modifies the electronic bonding between the adsorbates and the surface significantly (creates new types of electronic bonds). Van der Waals force is weak interactions between two atoms/molecules which is proportional to  $\approx r^{-6}$ , where  $r$  is the distance between these two atoms/molecules[22, p. 345]. A well-known example of chemisorption is the change of  $sp^2$  into  $sp^3$  hybridization in graphene (fully hydrogenated graphene)[43]. The binding energy for physisorption can be said up to 100 meV/adsorbate, while energy of chemisorption is in order of eV/adsorbate. As a comparison, room temperature is around 26 meV, which is important for the elements with either low adsorption or low barrier (migration) energy. Barrier energy is the energy needed for the adatom to move/roam on the graphene surface. A well known method in finding barrier energy is nudged elastic band (NEB) method[44]. As NEB method is computationally expensive, this thesis uses simpler approach to find barrier energy, which is by comparing two energy minima in the adatom-graphene system (explained in detail in section 4.4).

### 3.3 Trends on Elemental Adsorption on Graphene from Previous Studies

The capability of making predictions on the trends in elemental adsorption on graphene is very useful in building our understanding towards the more complex cases in adsorption on graphene. It also provides useful guidelines for fabricating graphene-based materials with novel properties. The most logical way to provide these trends is by following the periodic table of elements. Before seeing the previous journal articles, the results from the general chemistry (figures 3.S1 – 3.S5 in the supplementary data) are summarized in figure 3.2 [21].

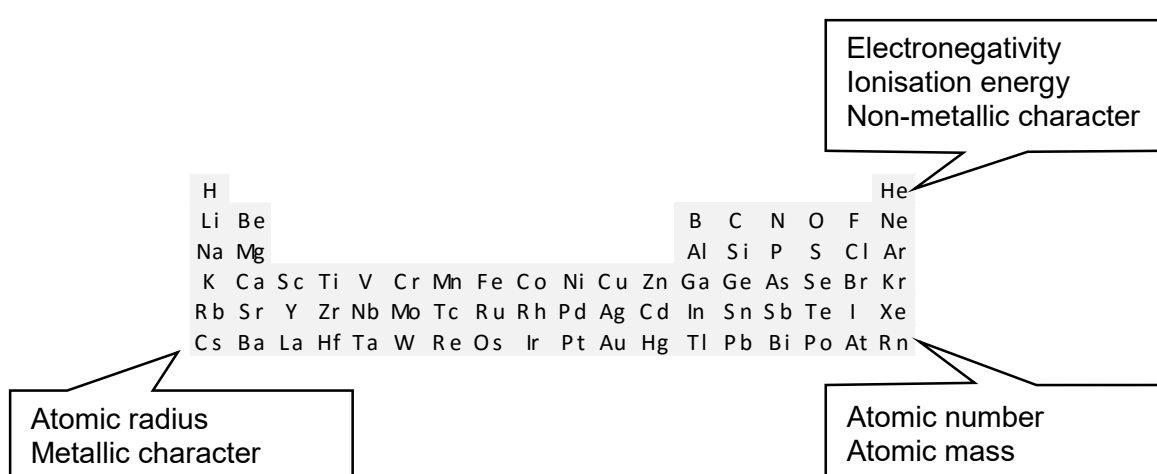


Figure 3.2 Some trends in the periodic table of elements. Properties are written at the corners with the largest value.

This section is intended to show : (1) some trends of elemental adsorption on graphene following the periodic table of elements, (2) the effects of adsorption atomic ratios, based on previous experimental and theoretical studies. However, the effects of adsorption atomic ratios will be discussed in brief.

The collected properties include stability (binding energy), the most stable site (bridge, hollow, top), adatom height, migration energy (barrier energy for adatom to roam on graphene), Fermi energy shift (from pristine graphene), graphene deformation/distortion, magnetization, charge transfer (from adatom to graphene) and electronic energy band gap at Fermi energy ( $E_g$ ) (see table 3.1).  $E_g$  classifies materials into metals, semiconductors or insulators. The  $E_g$



threshold for semiconductors and insulators is set by convention, usually the blue light ( $\approx 3.1$  eV).

Table 3.1 Overall trends/indicators on elemental adsorption on graphene based on previous studies.

Property	Figure	trend/indicator
Binding energy	3.3	trend
Most stable site	3.3	trend
Adatom height	3.4	trend
Migration energy	3.5	trend
Charge transfer	3.6	trend
Graphene distortion/deformation	3.3	indicator
Fermi energy shift from pristine graphene	3.8	indicator
Magnetization	3.9	indicator
Band gap at Fermi energy	3.10	indicator

The base template used is based on Nakada and Ishii's work (figures 3.3 – 3.6) [45], [46]. Nakada and Ishii calculated adsorption energy, migration (barrier) energy and most stable site of the absorbed element on zigzag  $3 \times 3$  graphene supercell (adatom:C = 1:18) using DFT, for all elements in the periodic table from hydrogen (H) to bismuth (Bi), except noble gases and lanthanides. Although the calculations were done non-magnetically and without corrections (*e.g.* van der Waals and dipole corrections), but it is still valuable to provide the landscape of elemental adsorption on graphene. The thresholds in figures 3.3- 3.6, 3.8, 3.9, 3.S1, 3.S2 and 3.S4 (*e.g.* 2.00 Å in figure 3.4, 0.10 and 0.50 eV in figure 3.5, 0.00 and 0.50 electron in figure 3.6) were set arbitrarily to enhance the visualisation.



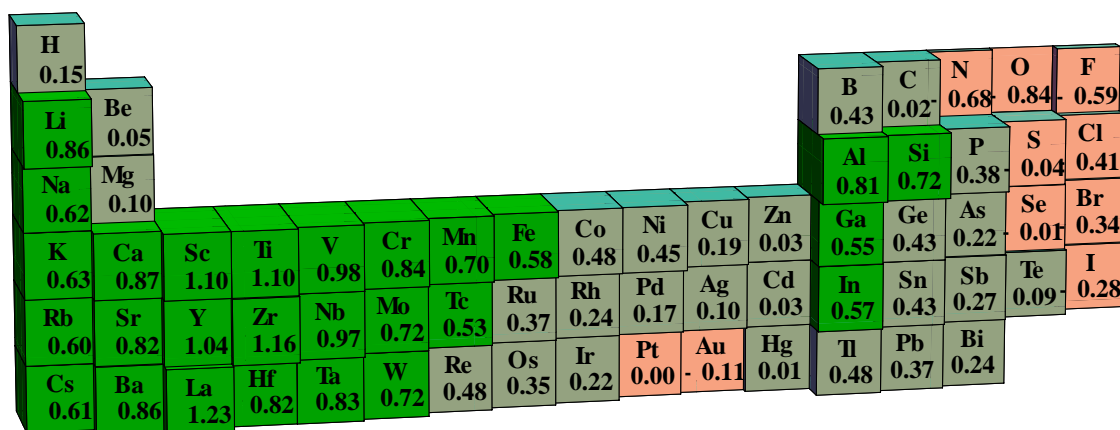


Figure 3.6 Charge transfer from adatom to graphene (number of electrons) of element-adsorbed on zigzag  $3 \times 3$  graphene supercell. Yellow, light green and green are less than 0.00 electron, between 0.00 and 0.50 electron, and more than 0.50 electron [46]. Yellow has negative Fermi energy shift from pristine graphene, while light green and green have positive Fermi energy shift [33]. Fermi energy trend might be proportional to charge transfer trend.

Binding energies (figure 3.3) are qualitatively inversely proportional to adatom heights (figure 3.4), proportional to migration energies (figure 3.5), and proportional to the number of unpaired valence electrons (figure 3.S5). Charge transfers (figure 3.6) are qualitatively inversely proportional to Pauling's electronegativities with carbon as the reference atom (figure 3.S1). Positive charge transfer from adatom to graphene signifies n-type doping, and thus increases the Fermi energy from the Fermi energy of pristine graphene (positive Fermi energy shift) [33]. Despite of not having quantitative data of Fermi energy shifts, charge transfer trend is a good indicator of Fermi energy shift trend, *i.e.* charge transfer might be qualitatively proportional to Fermi energy shift, or at least they have the same sign (positive/negative).

Graphene distortion is an indicator of the adatom's presence, which is the average displacement of the carbon atoms in the graphene supercell (in Å/carbon atom). Using an argument that the stronger binding energy the larger graphene distortion, it can be stated that graphene distortion might be qualitatively proportional to binding energy (figure 3.3). But this argument demands further verifications/investigations.

Most metals (figure 3.S3) are stable at hollow site, most metalloids and nonmetals are stable at bridge site, while H and halogens are stable at top site. Anomaly in most stable site for Cu, Ag, Pd and Pt (figure 3.3) might be related to the anomaly of electron configurations (figure 3.S5).

Chan *et al.*[20] calculated some metals (Li, Na, K, Ca, Al, Ga, In, Sn, Ti, Fe, Pd, Au) adsorbed on zigzag  $4 \times 4$  graphene supercell (adatom:C = 1:32) using DFT. They included spin polarization, van der Waals and dipole corrections. These more accurate calculations supports Nakada and Ishii's results in terms of most stable site, binding energy, adatom height and migration energy; but not quite match for charge transfer (figure 3.7). This suggests that calculation with spin polarization is important to give the more correct charge transfer.

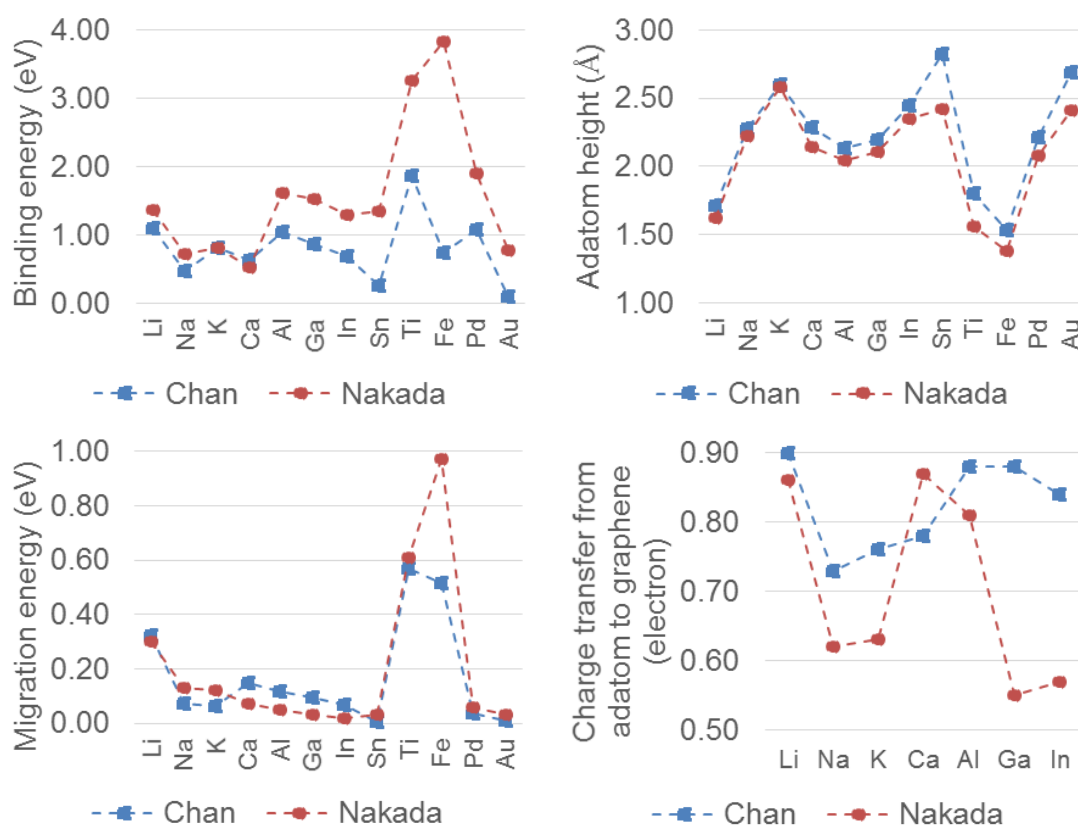


Figure 3.7. Comparison of Chan *et al.* [20] and Nakada and Ishii's [45], [46] calculations, dotted lines are added as a guidance.

Since there is no single study that covers the last two properties (magnetizations and band gaps) comprehensively across the periodic table of elements, these properties were collected from many papers, as tabulated in table 3.S1 in the supplementary data. Both elemental adsorption (adatom on graphene) and substitution/doping (adatom on graphene with C atom vacancy(ies)) cases were included.

Vienna Ab initio Simulation Package (VASP) [47] was used in about half of the data, as seen in table 3.S1. This indicates that VASP is one of the popular simulation software. Figures 3.8 and 3.9 summarize the data in table 3.S1. These figures, together with table 3.S1, do not reflect to the popularity of elements in accordance with adsorption/substitution on graphene. These figures are shown as indicators only (not trends), because of the uniqueness of experimental conditions, assumptions or theoretical methods in each paper. The farthest values from pristine graphene were selected, and the significant figures were set to two. With such a limited data, it is seen in figures 3.8 – 3.9, that there is no pattern on magnetizations and band gaps. This might mean nonlinearity of elemental adsorbed/doped on graphene on these two properties. To see the trends of these three properties and also graphene distortion reliably, unified experiments or simulations across the elements are needed.

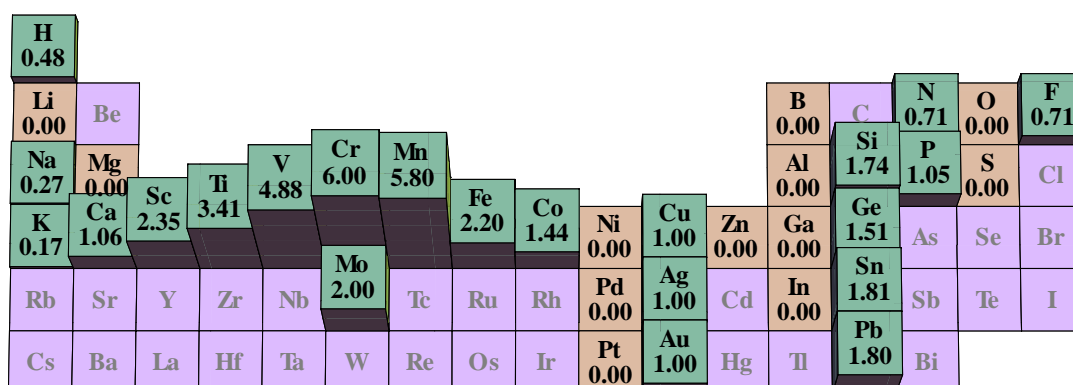


Figure 3.8 Magnetizations ( $\mu_B$ ) of elemental adsorbed/doped on graphene from previous studies. Light green is positive (at < 50 at.%), light yellow is zero (at < 50 at.%), grey is element with no data.



adatom interaction and migration energy. Migration energy has big role in this dynamic domain, as it determines the fluidity of the adatoms to arrange themselves to obtain the lowest energy. So depositing and removing adatoms may follow different route. This might even lead to irreversible process. But this is also a prospect for further investigation.

In the experimental side, Pi *et al.* reported that Pt doping on graphene can produce n-type or weakly p-type doping at high coverage [51]. While at low coverage, it is expected that Pt exhibits n-type doping. This shows the complexity of the effects of atomic ratio, where dopant-dopant interaction is strong.

The elemental adsorption on graphene looks like the simplest problem among the simulation studies in adsorption on graphene. However, not much data can be collected (see greyed elements in figures 3.8 and 3.9). Firstly, this is due to prominent challenge in the experimental side, as advance techniques (*e.g.* scanning tunnelling microscopy (STM)) must be used. Secondly, although elemental adsorption can give hints to study more complex structures, however, information on elemental adsorption might not reflect the molecular counterpart due to some nonlinearities (*e.g.* adatom-adatom interaction). Thirdly, despite its simplicity, there might be some subtleties that are overlooked in the study of elemental adsorption on graphene. As mentioned above, during this review, a problem was noticed, *i.e.* adsorption orientation. Adsorption orientation is the position of adatom relative to one another and also relative to graphene.

Finally, adatom-graphene systems likely have more applications, if they attain :

1. large binding energy (stronger adatom-graphene interaction),
2. smaller adatom height, as adatom height is inversely proportional to binding energy,
3. large migration energy (adatom does not roam easily on graphene),
4. similar/smaller/lighter adatom size/mass compared to C size/mass, as this reduces the graphene deformation,

5. small graphene deformation, as this may retain the remarkable properties of pristine graphene,
6. non zero band gap at Fermi energy (for semiconductor or insulator applications),
7. easily tuned properties (*e.g.* by varying its atomic ratio).

### 3.4 Summary

In summary, many studies predominately examine three (high symmetry) sites, *i.e.* bridge, hollow, top. The most used simulation software in this literature review is Vienna Ab initio Simulation Package (VASP)[47], as discussed in sections 4.2 and 4.3 in this thesis. Adatom height is inversely proportional to binding energy. Pauling's electronegativity gives good indicator for charge transfer. Spin polarization is important for charge transfer calculation. Beside adatom's electron valence, adatom size/mass compared to carbon atom size/mass affect the properties of the adsorption. Finally, the trends on elemental adsorption on graphene based on previous studies, especially for lower atomic ratios, are summarized in figure 3.10.

It is clearly seen that there are still many challenges and opportunities to investigate the electronic structures of this elemental adsorption on graphene (*e.g.* increasing the accuracy and predictability, adding the trends of some other properties) across the periodic table of elements in three dimensions, *i.e.* by : period, group and atomic ratio. Investigations were started by performing spin-polarized calculations, and then quantifying Fermi energy shift, graphene distortion, magnetization, and band gap, to convert these indicators into trends. The subsequent chapters in this thesis address some of those challenges and opportunities.



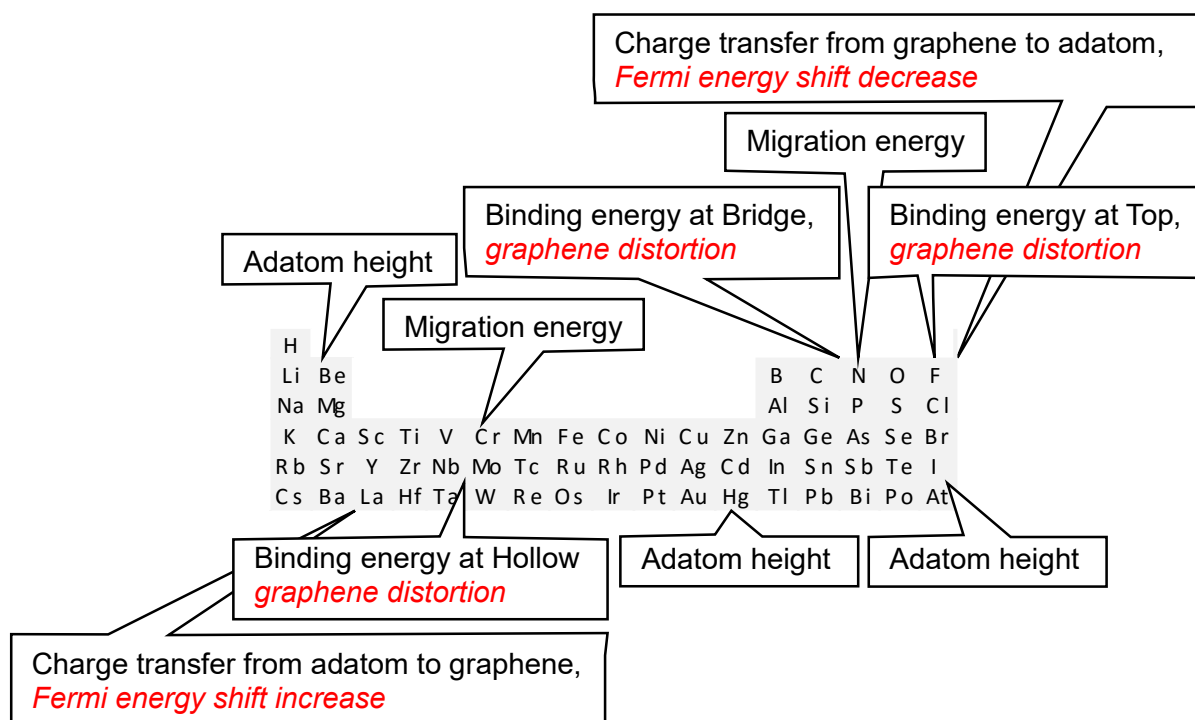


Figure 3.10 Some trends and *indicators* on elemental adsorption on graphene in the periodic table of elements. Properties are written at the corners with the largest value. *Indicators* need further verifications/investigations.

### 3.5 Supplementary Data

Table 3.S1 Magnetizations and band gaps of elemental adsorbed/doped on graphene from previous studies. Atomic ratios are printed in parenthesis.

	Magnetization ( $\mu_B$ )	Band gap# (eV)
H	0 (2:2)~ [52]	3.42 (2:2)~ [54]
	0.48 (1:98)~ [53]	
Li	0.00 (1:32)~ [20]	0.41 (1:6) [56]
	0.0 (1:72)~ [55]	
Be		
B	0.00 (1:49)~ [57]	0.14 (1:49)~ [57]
	0.00 (1:71) [58]	0.14 (1:49) – 0.72 (6:44)~ [59]
		0.54 (14 at.%)* [60]
C		
N	0.00 (1:49)~ [57]	0.14 (1:49)~ [57]
	0.00 (1:71) [58]	0.14 (1:49) – 0.72 (6:44)~ [59]
	0.71 (1:98)~ [53]	0.2 (0.4 at.%) [61]
O		3.004 (2:4)~ [49]
	0.00 (1:49)~ [57]	0.52 (1:31) [62]
		0.5 (1:49)~ [57]
		3.39 (1:2) [63]
F	0.71 (1:49)~ [57]	2.96 (2:2)~ [54]

		2.93 (2:8) [48]
Na	0.27 (1:32)~ [20] 0.0 (1:72)~ [55]	
Mg	0.0 (1:72)~ [55]	
Al	0.00 (1:32)~ [20] 0.0 (1:72)~ [55] 0.00 (1:71) [58]	metallic (1:31 to 1:127) [64]
Si	0.27 (1:8)~ [65] 1.02 (1:32)~ [65] 1.74 (1:72)~ [66] 0 (1:32)~ [67] 0.00 (1:71) [58]	0.00 (1:31) [64] 0.08 (1:71) [64] 2.02 (1:1) [68] 2.13 (1:1) [69]
P	1 (1:31 to 1:127) [64] 1 (1:31 to 1:241) [70] 1.05 (1:71) [58] 0.20 (1:98)~ [53]	0.67 (1:31) [64] 0.14 (1:71) [64] 0.50 (1:127) [70]
S	0 (1:31 to 1:241) [70]	0.57 (1:31) [64] 0.01 (1:71) [64] 0.80 (1:31) [70]
Cl		1.21 (2:2) bonding~ [54] 0.00 (2:2) non-bonding~ [71]
K	0.17 (1:32)~ [20] 0.0 (1:72)~ [55]	
Ca	1.04 (1:32)~ [20] 0.0 (1:72)~ [55] 1.06 (1:32)~ [72]	
Sc	2.35 (1:24) [73]	
Ti	3.41 (1:32)~ [20] 3.18 (1:24) [73]	
V	4.5 (1:72)~ [55] 4.88 (1:24) [73]	
Cr	5.6 (1:72)~ [55] 6 (1:24) [73] 2.00 (1:71) [58]	
Mn	5.8 (1:72)~ [55] 5.62 (1:32) [74] 5 (1:24) [73] 3.00 (1:71) [58]	
Fe	2.03 (1:32)~ [20] 2.0 (1:72)~ [55] 2.20 (1:32) [74] 2 (1:24) [73]	0.54 (1:31) [62]
Co	1.0 (1:72)~ [55] 1.10 (1:32) [74] 1.44 (1:24) [73]	
Ni	0.0 (1:72)~ [55] 0 (1:24) [73]	
Cu	1.0 (1:72)~ [55] 0.89 (1:50)~ [75] 1 (1:24) [73]	metallic (1:50)~ [75]

Zn	0 (1:24) [73]	0.03 (1:31) [62]
Ga	0.0 (1:32)~ [20]	
Ge	0.63 (1:8)~ [65]	
	1.51 (1:32)~ [65]	1.86 (1:1) [69]
	1.25 (1:32), 0 (1:31)~ [76]	
As		0.62 (1:31) [62]
Se		0.54 (1:31) [62]
Br		0.00 (2:2) non-bonding~ [71]
Rb, Sr, Y, Zr, Nb		
Mo	2 (1:31)~ [77]	
	0 (1:24) [73]	
Tc, Ru, Rh		
Pd	0.00 (1:32)~ [20]	
	0.0 (1:72)~ [55]	
	0 (1:24) [73]	
Ag	1.0 (1:72)~ [55]	
	1 (1:24) [73]	
Cd		0.11 (1:31) [62]
In	0.00 (1:32)~ [20]	0.49 (1:31) [62]
	0.0 (1:72)~ [55]	
Sn	1.81 (1:32)~ [20]	0.60 (1:31) [62]
		0.82 (1:1) [69]
Sb		0.49 (1:31) [62]
Te		
I		0.46 (1:31) [62]
		0.00 (2:2) non-bonding~ [71]
Cs, Ba, La, Hf, Ta, W, Re, Os, Ir		
Pt	0.0 (1:72)~ [55]	
	0 (1:24) [73]	
Au	0.96 (1:32)~ [20]	
	1.0 (1:72)~ [55]	
	1 (1:24) [73]	
Hg		0.03 (1:31) [62]
Tl		
Pb	1.8 (1:72)~ [55]	0.30 (1:31) [62]
Bi, Po, At		

# Electronic energy band gap at Fermi energy.

\* Experimental study.

~ Calculation software used was Vienna Ab initio Simulation Package (VASP).



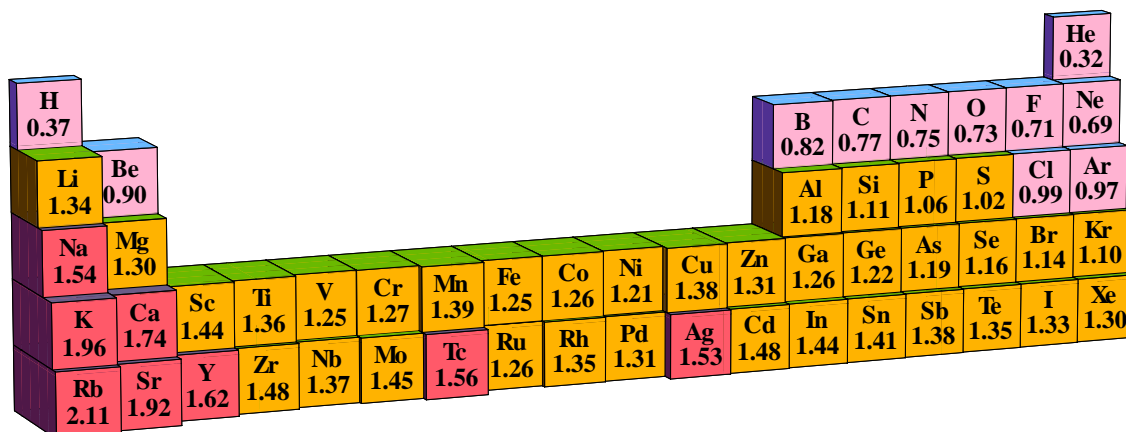


Figure 3.S4 Atomic radii (Å). Pink, yellow and red are less than 1 Å, between 1 and 1.5 Å, and more than 1.5 Å [21, p. 255].

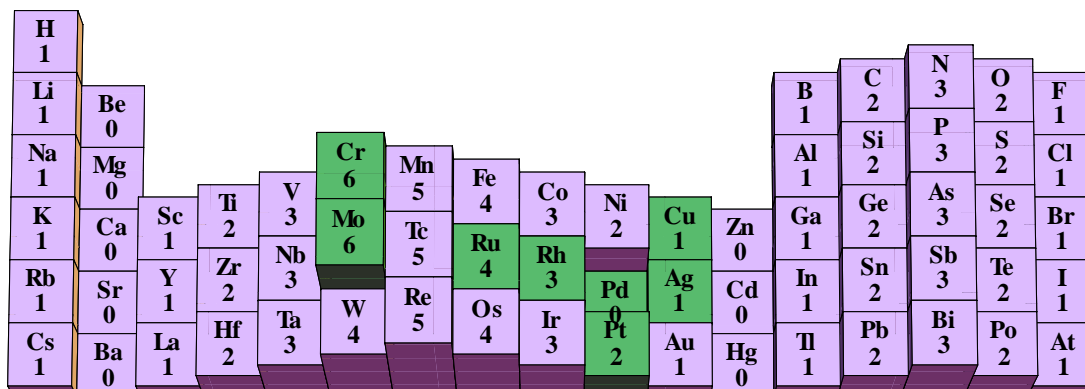


Figure 3.S5. Number of unpaired valence electrons, green is anomalous electron configuration [21, p. 236].

---

A manuscript based on the major research outcomes of this chapter was submitted in :

H. Widjaja, Z.-T. Jiang, and M. Altarawneh, “Trends on elemental adsorption on graphene,” *Can. J. Phys.*, vol. 94, no. 5, pp. 437-447, 2016. (*This is publication [4] in the List of Publications*)

---

# CHAPTER FOUR

## COMPUTATIONAL METHODS

---

Computational method is a method of solving problems using computers. Computers are general computational machines that are programmed and configured to do algorithmic and repetitive tasks. Computers are essential for this thesis, as the numerical problems in this thesis are highly algorithmic and repetitive. This chapter discusses about :

1. The computational strategies of elemental adsorbed on graphene using DFT method,
2. The description of the simulation software, and
3. The geometry of elemental adsorption on graphene.

### 4.1 Computational Strategies

The computational strategies used in this thesis are to: (1) minimize the number of cases to calculate, (2) utilise parallel computation, (3) optimise the calculations within DFT, (4) do convergence tests, and (5) conduct calculations in stages.

The first strategy is to minimize the number of cases to calculate. This is done using geometrical analysis of elemental adsorption on graphene, which is elaborated in section 4.3.

The second strategy is to utilise parallel computation. Researchers in computational chemistry favours time efficiency over hardware/infrastructure expenses, so parallel computation is highly desirable. Parallel computations transform calculations from time domain into space domain. Adding hardware, optimising parallel architecture and multithreading are some of the parallel computation strategies. Adding hardware includes adding computers, processors/computer, cores/processor, RAM (Random Access Memory), solid state drives and networks. Optimising parallel architecture is the strategy to interconnect

hardware to deliver the best performances. While multithreading is managing multiple tasks running on a single hardware simultaneously.

The third strategy is to optimise the calculations within DFT itself. This includes the selection of the simulation software, basis set, pseudopotential, exchange-correlation potential and various corrections (*e.g.* van der Waals, dipole corrections). This matter is discussed in section 4.2.

The fourth strategy is to do convergence tests. Every calculations that involve approximations must have some parameters. These parameters must be tuned against the convergence of the results. As an example is the calculation of single isolated atom in a periodic potential. This atom must be put in a relatively large empty cube such that the potential at the sides of the cube is very small, thus there is no interaction between atoms in the adjacent unit cells. For this case, tuning must be done to obtain the smallest cube sides and the convergence of energy simultaneously. This matter is discussed in appendix A.1 (POSCAR and KPOINTS) and appendix A.2.

The fifth strategy is, to increase the productivity and the effectiveness of this research, the calculations are conducted in stages. In the initial stage, the least expensive method is used, which is fast but less accurate. The result of the initial stage is fed to the next stage, where a more expensive and slower, but more accurate method is used. This process is iterated until the desired accuracy is reached. This matter is discussed in appendix A.1 (KPOINTS).

## **4.2 Simulation Software**

There are many computational simulation software that are based on DFT. Some examples include Abinit[78], Amsterdam Density Functional (ADF)[79], Gaussian[80] with GaussView[81], NWChem[82], Orca[83], Quantum Espresso[84], SIESTA[85] and Vienna Ab initio Simulation Package (VASP)[47].

Subsequent to comprehensive literature review (see table 3.S1) and trials on these simulation software, in relation to the elemental adsorption on graphene, and the availability (in the supercomputer), VASP was selected. VASP supports all features needed in this thesis, and is in conjunction with the Surface Analysis and Materials Engineering Research Group (SAMERG) direction.

Kresse *et al.* [47, p. 1] defined “VASP is a complex package for performing *ab initio* quantum mechanical molecular dynamics (MD) simulations using pseudopotentials or the projector-augmented wave method and a plane wave basis set.” This thesis relies heavily on this software at version 5.3.3. The details of files and parameters in VASP are discussed in appendix A. In regard to pseudopotential, as VASP development team has stopped maintaining ultrasoft pseudopotential [86], and strongly recommends projector-augmented wave (PAW) [87], we have used PAW throughout all our calculations.

Also in conjunction with the Surface Analysis and Materials Engineering Research Group (SAMERG) direction, GGA approximation was selected and successfully tested on the materials prepared and characterized by SAMERG: *i.e.* Si and SiO<sub>2</sub> [4], Cu<sub>x</sub>Co<sub>3-x</sub>O<sub>4</sub> (spinel) [5], and Ni<sub>x</sub>Cr<sub>1-x</sub>N [6], as mentioned in section 1.2.

Furthermore, specific to our case (adsorption on graphene), two corrections were applied to improve the accuracy, *i.e.* van der Waals and dipole correction. Grimme D2 method [88] has been used for van der Waals correction, as this method is available in VASP version 5.3.3 and computationally cheap. This helps improving the results of weak adsorption (physisorp) cases [58]. For Van der Waals corrections in our calculations, default parameters and default atomic parameters are used. The default parameters are pair interaction cut off radius (30 Å), global scaling factor  $S_6$  (0.75 Å) and damping length (20 Å). While the default atomic parameters are  $C_6$  (Joule.nanometer<sup>6</sup>/mol) and  $R_0$  (Å) from Grimme. This method covers elements from hydrogen to iodine only.



The second correction is dipole correction along the  $Z$ -direction. Adatom-graphene systems create dipole along the  $z$ -direction, and these dipoles interact with one another in the repeating unit cells (which is also in  $z$ -direction). As this is unwanted interaction, so dipole correction is applied.

The last strategy that is used in this thesis is smearing. Smearing is needed to simplify the difficulty (inefficiency) in integrating discontinuous function numerically. There is discontinuity at Fermi energy in typical DOS curve of metals (figure 4.1a). Smearing smoothens this abrupt change in the DOS curve (figure 4.2b). Gaussian smearing with the default broadening of 0.2 eV is used in this thesis.

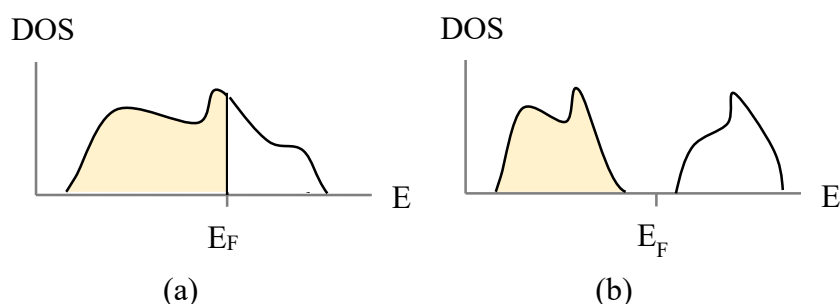


Figure 4.1 Typical density of states (DOS) curve of (a) metals, (b) semiconductors/insulators.  $E_F$  is Fermi energy. Yellow is filled states.

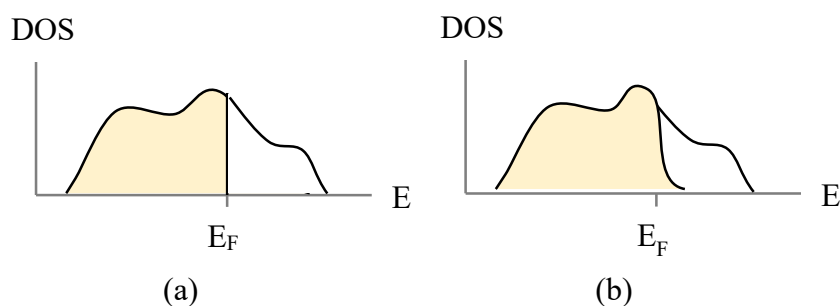


Figure 4.2 (a) Original density of states (DOS), difficult to integrate numerically, (b) smearing is applied at  $E_F$ , easy to integrate numerically.  $E_F$  is Fermi energy. Yellow is filled states.

### 4.3 The Geometry of Elemental Adsorption on Graphene

Chapters 5 to 8 share common geometrical analysis that is unified in this section. Firstly, Figure 4.3 shows graphene various cell/supercells. Before calculating the electronic properties of graphene with adsorbed elements (adatoms), it is essential to determine the most

stable adatom position correctly. To find the most stable configuration, it is necessary to examine all possible positions. But unfortunately, this is not practical to do, as the number of cases will be unlimited. In this regard, two factors appear to play an important role, namely, atomic percent (at.%) and atomic ratio, *e.g.* a 50 at.% has multiple atomic ratios (1:2, 2:4, 3:6, 4:8, ...). A famous example is fluorinated (F-adsorbed) graphene at 25 at.% cannot be explained using the simplest atomic ratio (1:4), but rather 2:8 (see Figure 4.4) [48]. In this thesis, adatoms are assumed to be uniformly distributed throughout the graphene.

We are interested in zigzag  $2 \times 2$  and armchair  $2 \times \sqrt{3}$  supercells (Figure 4.5), as they give identical atomic ratio, but with totally different adsorption configuration. Many studies predominately examine three sites, *i.e.*, bridge, hollow and top (see figure 4.5a). Actually, the orientation (*i.e.* zigzag or armchair) of the adsorbed element needs to be considered as well, as the combination of sites and orientations gives distinct structural information. We define orientation as the position of adatom relative to one another and also relative to graphene. This aspect is surprisingly overlooked (or very marginally discussed) by many previous studies and, as such, it is vital that this facet should be explored to cover the remaining knowledge gaps pertaining to adatom-adsorbed graphene systems.

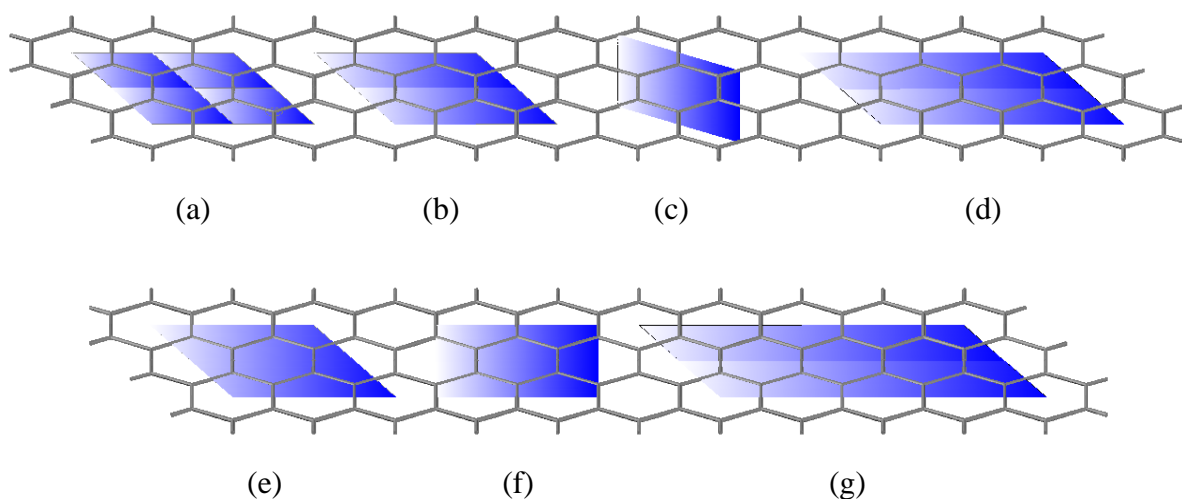


Figure 4.3 Graphene cell/supercells (number of C atoms in a unit cell, maximum adatom radius):(a) zigzag  $1 \times 1$  (2,  $\approx 1.23$  Å), (b) zigzag  $2 \times 1$  (4,  $\approx 1.23$  Å), (c) zigzag  $\sqrt{3} \times \sqrt{3}$  (6,  $\approx 2.13$  Å), (d) zigzag  $3 \times 1$  (6,  $\approx 1.23$  Å), (e) zigzag  $2 \times 2$  (8,  $\approx 2.46$  Å), (f) armchair  $2 \times \sqrt{3}$  (8,  $\approx 2.13$  Å), (g) zigzag  $4 \times 1$  (8,  $\approx 1.23$  Å).

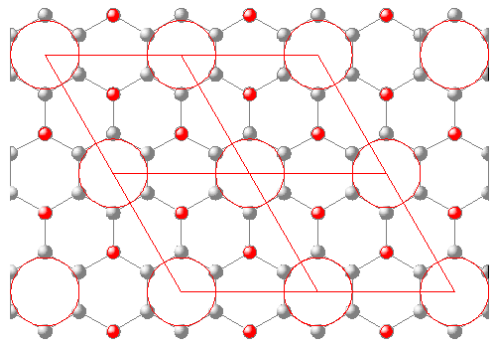


Figure 4.4 Most stable configuration of single-sided fluorinated graphene of 25 at.%, red spheres are F atoms, grey spheres are C atoms, and big red circles are added to guide the eyes[48].

It's understood that any non-zigzag graphene supercells (armchairs/slants) can be represented by larger zigzag graphene supercells with the origin  $O(0,0)$  translated/rotated (see figure 4.6) and vice versa. However, in this study, we use armchair graphene supercell, as it is the simplest case to track the effects of the orientation. This section highlights two things, *i.e.* bridge cases and adatom-adatom interaction.

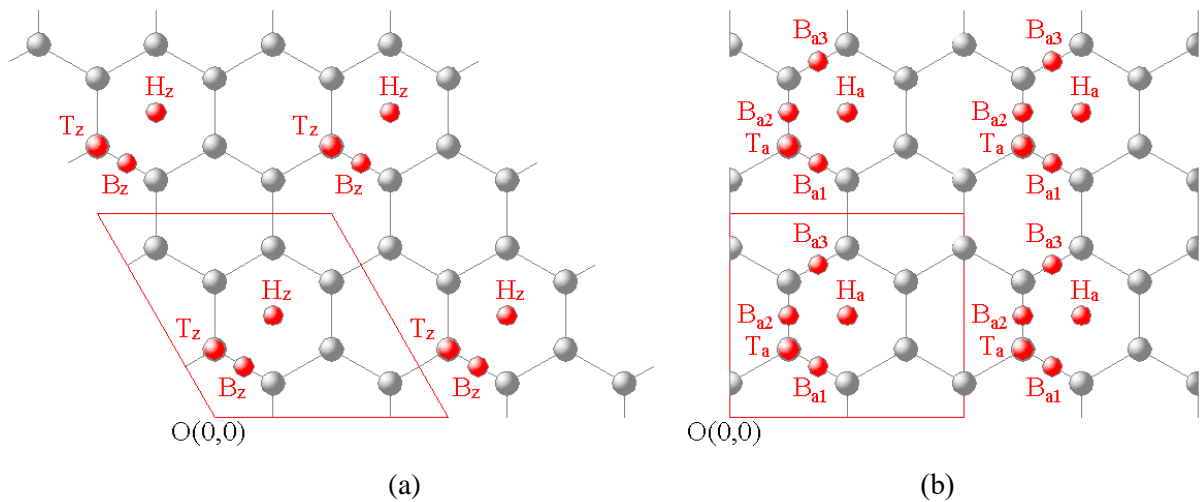


Figure 4.5 Schematic diagrams of adsorption on the graphene supercells for 1:8 atomic ratio, (a) zigzag  $2 \times 2$  and (b) armchair  $2 \times \sqrt{3}$ .  $O(0,0)$  is origin. B, H, T, z, a are bridge, hollow, top, zigzag and armchair.

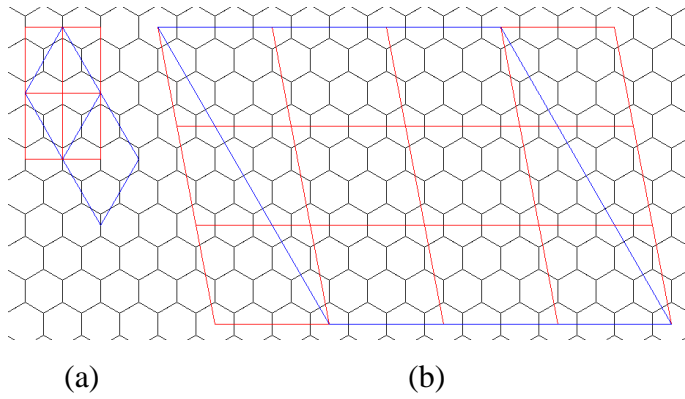


Figure 4.6 Equivalency of graphene supercells, (a) armchair  $1 \times \sqrt{3}$  (red) is equivalent to zigzag  $2 \times 2$  (blue), (b) slant  $3 \times \sqrt{7}$  (red) is equivalent to zigzag  $9 \times 9$  (blue).

### 4.3.1 Bridge Cases

In accordance with this orientation aspect, on the purely geometrical analysis, bridge cases in graphene adsorption are interesting. Changing the orientation from zigzag  $2 \times 2$  to armchair  $2 \times \sqrt{3}$ , breaks the one bridge case ( $B_z$ ) into three bridge cases ( $B_{a1}$ ,  $B_{a2}$  and  $B_{a3}$ ) (see figure 4.5). However, positions  $B_{a1}$  and  $B_{a3}$  are mirror images of each other (see figure 4.7), so the calculation results for positions  $B_{a1}$  and  $B_{a3}$  are expected to be identical.

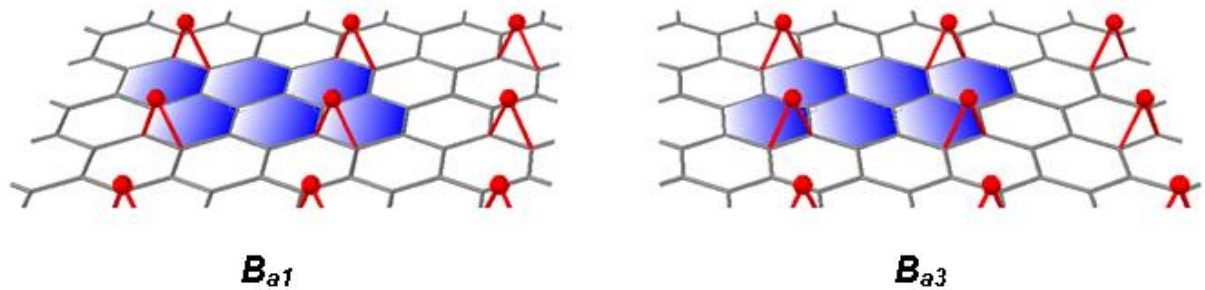


Figure 4.7  $B_{a1}$  and  $B_{a3}$  adsorption position on graphene are mirror images of each other. Shading is to guide the eyes.

Further examination on larger supercells, changing orientation from zigzag  $3 \times 3$  to slant  $3 \times \sqrt{7}$ , breaks the one bridge case ( $B_z$ ) into three bridge cases ( $B_{s1}$ ,  $B_{s2}$  and  $B_{s3}$ ) (see figure 4.8). Changing the orientation from zigzag  $4 \times 4$  to slant  $4 \times \sqrt{13}$ , also breaks the one bridge case ( $B_z$ ) into three bridge cases ( $B_{s1}$ ,  $B_{s2}$  and  $B_{s3}$ ) (see figure 4.9). In general, changing from zigzag to armchair orientation, breaks one bridge case ( $B_z$ ) into two bridge cases ( $B_{a1}$  and  $B_{a2}$ ), and changing from zigzag to slant orientation, breaks one bridge case ( $B_z$ ) into three bridge

cases ( $B_{s1}$ ,  $B_{s2}$  and  $B_{s3}$ ). So the number of adsorption cases on bridge site depends on the adatom orientation, and this does not happen in top or hollow cases.

Although it's expected that the orientation effects for elements are very minimal for graphene supercells larger than zigzag  $3 \times 3$ , but for completeness, the supercell angles and the angle differences between supercells are displayed in figures 4.8 to 4.11. These larger supercells are expected to have effects on molecules or compounds.

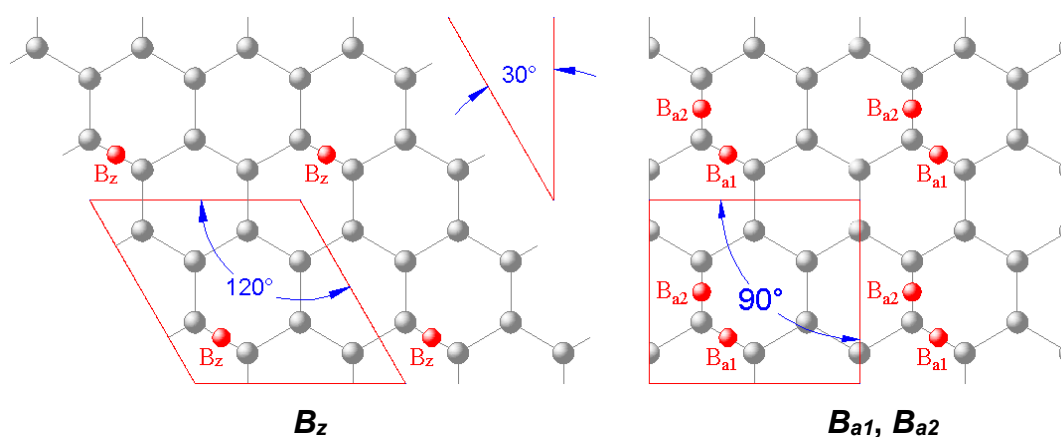


Figure 4.8 Bridge cases on zigzag  $2 \times 2$  ( $B_z$ ) and armchair  $2 \times \sqrt{3}$  ( $B_{a1}$ ,  $B_{a2}$ ) (3 unique positions).

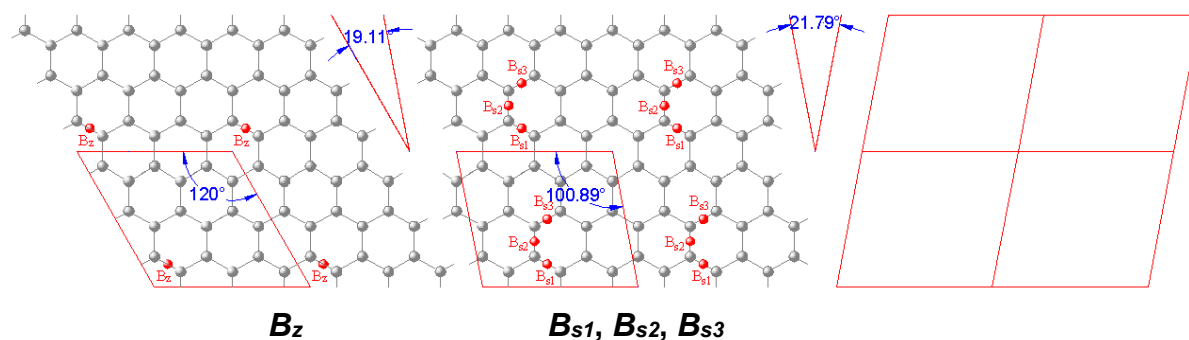


Figure 4.9 Bridge cases on zigzag  $3 \times 3$  ( $B_z$ ), slant  $3 \times \sqrt{7}$  ( $B_{s1}$ ,  $B_{s2}$ ,  $B_{s3}$ ) and mirror of slant  $3 \times \sqrt{7}$  (4 unique positions).

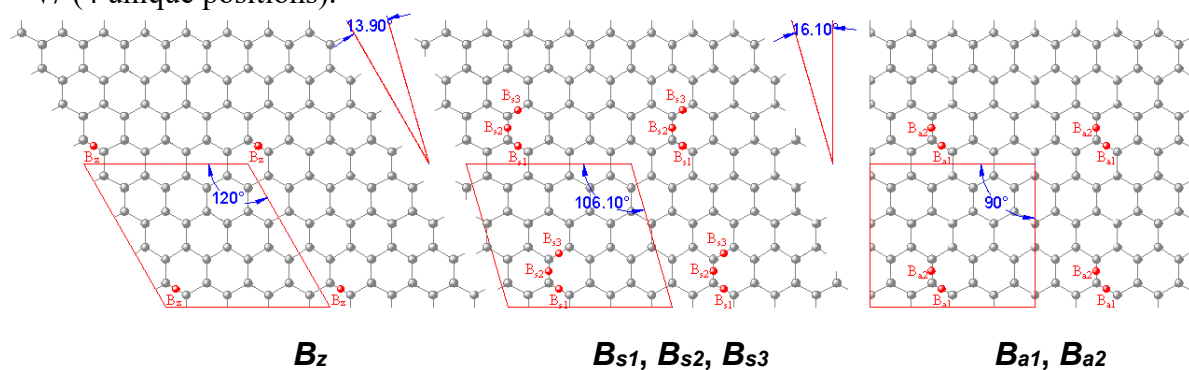


Figure 4.10 Bridge cases on zigzag  $4 \times 4$  ( $B_z$ ), slant  $4 \times \sqrt{13}$  ( $B_{s1}$ ,  $B_{s2}$ ,  $B_{s3}$ ) and armchair  $4 \times 2\sqrt{3}$  ( $B_{a1}$ ,  $B_{a2}$ ) (6 unique positions).

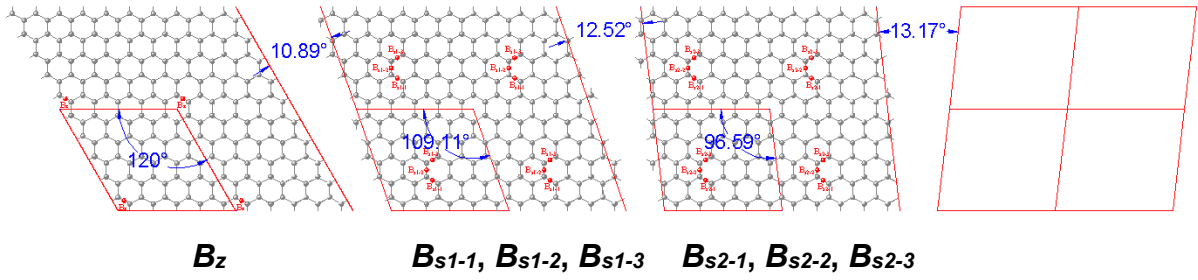


Figure 4.11 Bridge cases on zigzag  $5 \times 5$  ( $B_z$ ), slant<sub>1</sub>  $5 \times \sqrt{21}$  ( $B_{s1-1}$ ,  $B_{s1-2}$ ,  $B_{s1-3}$ ), slant<sub>2</sub>  $5 \times \sqrt{19}$  ( $B_{s2-1}$ ,  $B_{s2-2}$ ,  $B_{s2-3}$ ) and mirror of slant<sub>2</sub> (7 unique positions).

### 4.3.2 Adatom-adatom Interaction

Orientation aspect becomes important if the adatom-adatom interaction is not small. This interaction is represented by its binding energy, as if the graphene were removed from the adatom-adsorbed graphene system. It is expected that the interaction is quite strong at small supercells, but diminishes at larger supercells. At larger supercells, the adatom is unaware of the presence of other adatoms.

As an example, there is interaction difference between zigzag  $2 \times 2$  and armchair  $2 \times \sqrt{3}$ , due to the different adatom's nearest neighbours (see figure 4.12). On zigzag  $2 \times 2$ , there are 6 nearest neighbours of  $r$  in distance; while on armchair  $2 \times \sqrt{3}$ , there are 2 nearest neighbours of  $r$  in distance, 2 of  $\sqrt{3}r/2$  and 4 of  $\sqrt{7}r/2$ .

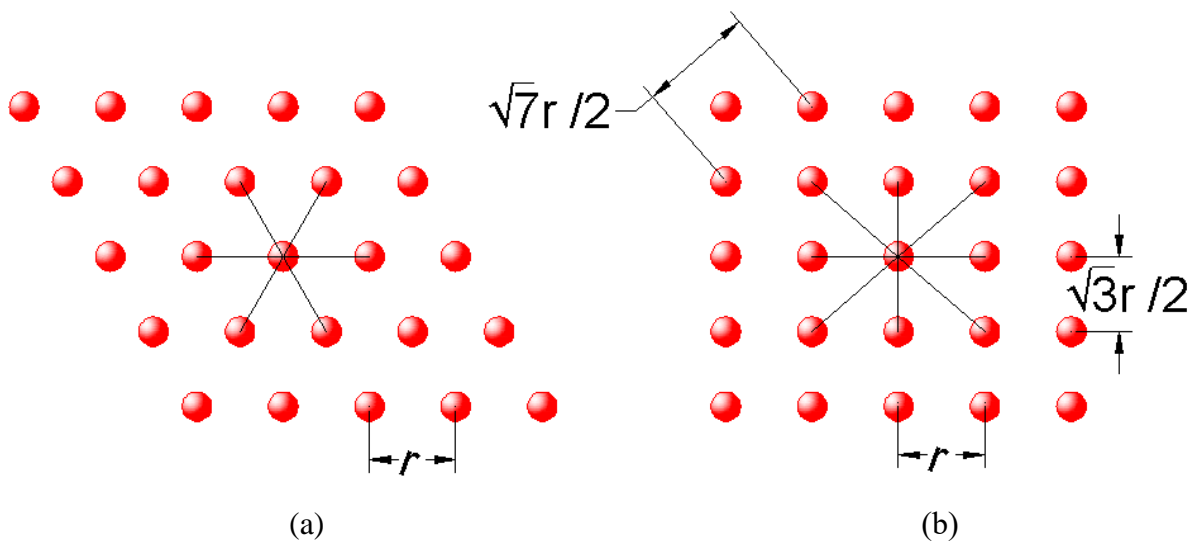


Figure 4.12. Adatom's nearest neighbours, (a) zigzag  $2 \times 2$  and (b) armchair  $2 \times \sqrt{3}$ ,  $r = 4.936 \text{ \AA}$ .

In conclusion, the effects of adsorption site and orientation begin at small graphene cell/supercells and end when the adatom-adatom interaction is very small. Secondly, the number of adsorption cases on bridge site depends on the adatom orientation.

Armed with the trends of elemental adsorption on graphene (see figure 3.10 in Chapter 3), we studied the effects of the orientation as presented in subsequent chapters. Figure 4.13 shows the scope of work for this thesis. The general trends of the elemental adsorption on graphene have been recalculated, and are shown in section 4.4 (supplementary data). In particular, we would like to see the orientation effects in three dimensions across the periodic table of elements : (1) one period (period 3 elements which are Na, Mg, Al, Si, P, S, Cl), (2) one group (halogens which are F, Cl, Br, I), and (3) low to high at.% (F, Cl).

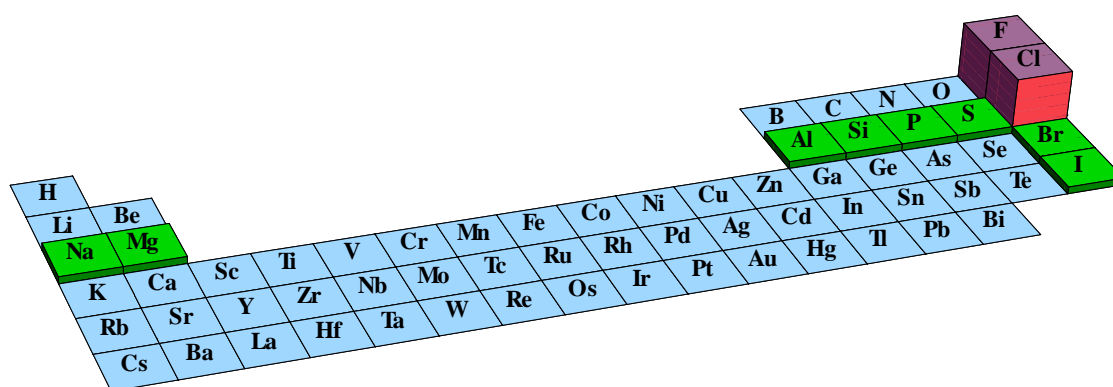


Figure 4.13 Elements-adsorbed graphene inspected in this thesis. Light blue is at 5.6 at.% (single-sided adsorption, no orientation), green is between 5.6 and 16.7 at.% (single-sided adsorption, with orientation), and pink is between 11.1 and 100 at.% (double-sided adsorption, with orientation).

#### 4.4 Supplementary Data

Calculations were performed using the plane-wave DFT code of VASP (Vienna Ab initio Simulation Package)[47]. Calculation methodology consists of spin-polarized PAW-GGA functional [89], van der Waals correction by Grimme (D2) [88] method (for elements H to I), dipole corrections, and a Gaussian smearing. To ensure convergence results, we set the plane wave cut off energy of 500 eV, a tolerance of 0.1 meV for energy and less than 0.05 eV/

Å for forces on each atoms. Zigzag  $3 \times 3$  graphene supercell was selected because of this supercell is relatively small, however it still accommodates the largest element in our calculations, *i.e.* Cs atom.

The binding energy, adatom height, band gap, Fermi energy, charge transfer, magnetization and density of states (DOS) were calculated for all the cases. Binding energy  $E$  is calculated using equation:

$$E = E_{\text{graphene}} + E_{\text{adatoms}} - E_{\text{adatoms-graphene system}} \quad (4.S1)$$

where  $E_{\text{graphene}}$  denotes the energy of the pristine graphene,  $E_{\text{adatoms}}$  signifies the energy of the adatoms and  $E_{\text{adatoms-graphene system}}$  is the total energy of the adatoms and graphene after the adatom is attached to the graphene. For each element, three binding energies based on the adsorption site were computed, *i.e.*  $E_{\text{bridge}}$ ,  $E_{\text{hollow}}$  and  $E_{\text{top}}$ . These three energies were sorted in descending order into  $E_{\text{high}}$ ,  $E_{\text{middle}}$  and  $E_{\text{low}}$ . Migration energy is the difference between the highest ( $E_{\text{high}}$ ) and the second highest ( $E_{\text{middle}}$ ) binding energy. In this analysis, the band gap is determined from the DOS [90, p. 214] analysis, *i.e.* zero DOS at Fermi energy. Zero DOS at Fermi energy signifies that the material is a semiconductor or insulator. Adatom height (Å) is the difference between adatom's  $z$ -coordinate and the average of  $z$ -coordinates of C atoms. The graphene distortion is an indicator of the adatom's presence, which is the total displacement (in Å) of the C atoms in the graphene supercells.

While total charge is the sum of total spin-up and spin-down, magnetization (in Bohr magneton or  $\mu_B$ ) is defined as the difference between total spin up and total spin down of the DOS at the Fermi energy level. Charge transfer is expressed as the scalar quantity charge transferred from adatom to graphene. Positive charge transfer indicates that charge is transferred from adatom to graphene and *vice versa*. Charge transfer has been estimated via the Bader methodology [91]. Calculation results are shown in Figs. 4.S1 – 4.S8. Furthermore, the thresholds in all figures (*e.g.* 2.00 Å in figure 4.S2, 0.10 and 0.50 eV in figure 4.S3, 0.00 and



0.50 electron in figure 4.S4) were set arbitrarily to enhance the visualisation. There is no band gap opening for all recalculation results as indicated by DOS. Figure 4.S8 shows DOS for some elements.

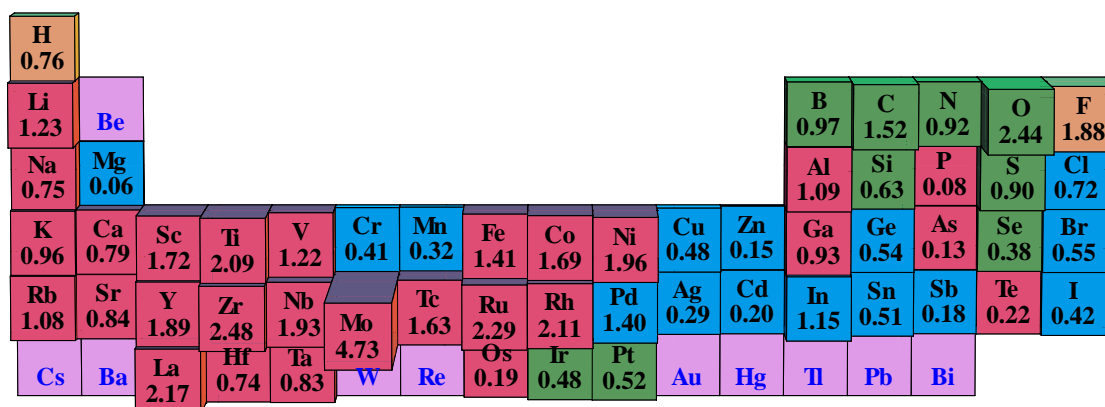


Figure 4.S1 Binding energies (eV) of element-adsorbed on zigzag  $3 \times 3$  graphene supercell. Colours indicate the most stable site, with green, red, yellow are bridge, hollow, top sites. Cyan is site-independent adsorption. Blue elements are unstable adsorption.

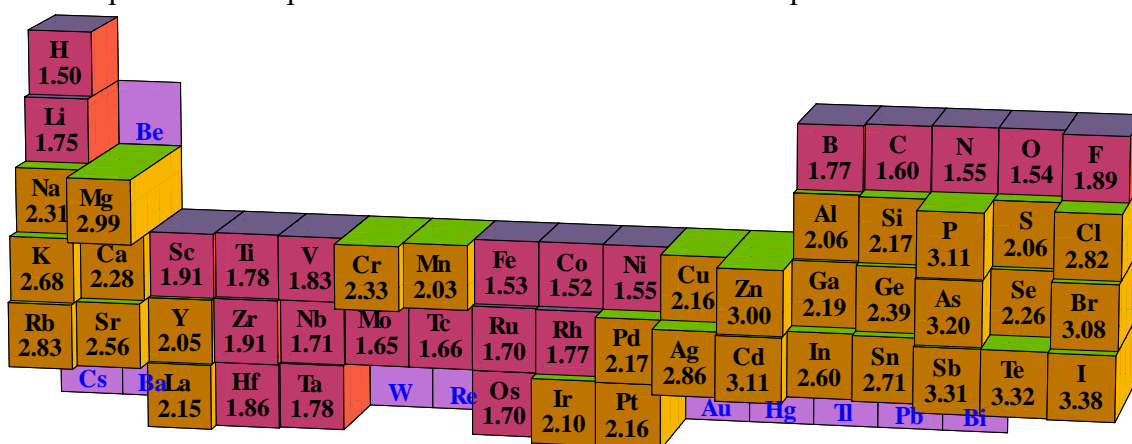


Figure 4.S2 Adatom heights (Å) of element-adsorbed on zigzag  $3 \times 3$  graphene supercell. Red is less than 2.00 Å and yellow is more than 2.00 Å. Blue elements are unstable adsorption.







*Des.*, vol. 89, pp. 27–35, 2016. (*This is publication [1] in the List of Publications*)

For section 4.4 :

H. Widjaja, Z.-T. Jiang, and M. Altarawneh, “Trends on elemental adsorption on graphene,” *Can. J. Phys.*, vol. 94, no. 5, pp. 437-447, 2016. (*This is publication [4] in the List of Publications*)

---

## CHAPTER FIVE

### ALUMINIUM AND SILICON ADSORPTION ON GRAPHENE

---

#### 5.1 Introduction

The calculation procedure developed in chapters 1 to 4 was firstly applied to two elements, *i.e.* aluminium and silicon at 1:8 atomic ratio, as a case of metal (Al) and metalloid (Si).

There are many studies conducted on elemental adsorption on graphene, such as H[43], [92]; Be[93]; O[49], [63], [94]–[96]; F[92], [97]; Si[65]–[67]; Na[98]; Mg[99], [100]; Cl[54], [92]; noble gases[101]; Ca[72]; Ni[102]; Ge[76]; and other metallic elements [20], [103]–[105]. Nakada and Ishii calculated adsorption energy, migration (barrier) energy and most stable site of the adsorbed atom on graphene nonmagnetically, for elements ranging from hydrogen (H) to bismuth (Bi), except the noble gases and lanthanides[45], [46]. Before calculating the electronic properties of graphene with adsorbed elements, it is essential to determine the most stable adatom position correctly. Adatoms are assumed to be adsorbed on one side of the graphene and uniformly distributed throughout the graphene. Many studies predominately examine three sites, *i.e.*, bridge, hollow and top. This is only correct for adatom/graphene atomic ratio of 50% or more. For lower atomic ratio, the orientation (*i.e.* zigzag or armchair) of the adsorbed element needs to be considered as well, as the combination of sites and orientations gives distinct structural information. We define orientation as the position of adatom relative to one another and also relative to graphene. This aspect is surprisingly overlooked (or very marginally discussed) by many previous studies and, as such, it is vital that this facet should be explored to cover the remaining knowledge gaps pertaining to metal-adsorbed graphene systems.

To enhance our understanding of the effects of the orientation of elements adsorbed on graphene, a calculation procedure was developed in the present study to investigate the binding energy, Fermi energy, band gap, magnetization, density of states (DOS) and charge transfer in terms of site and orientation. Two elements, Al and Si, were selected for this study due to their contrasting properties. Firstly, Al is a metallic element with an odd number of electrons, while Si is a metalloid element and has an even number of electrons. Secondly, referring to Nakada and Ishii's work[45], Al and Si, with atomic ratio  $< 50\%$  adsorption, are stable at different sites and are adsorbed relatively weakly (physisorbed) on graphene, thus they do not disrupt the graphene structure significantly. Furthermore, the study of Al adsorbed on graphene can serve as a case for graphene-metal contact which is essential for applying graphene in electronic/mechanical devices [106]–[108]. Whilst the study of Si adsorbed on graphene can loosely be related to the study of graphene growth on SiC[29]. Graphene grown on SiC shows promise for wafer-scale production commercially[30], large-scale patterning[31] and integration with current silicon technology in electronics industry[32]. These aspects make adsorbed Al or Si on graphene an ideal system to study by first-principles electronic structure calculation using density functional theory (DFT) simulation.

This study shows that low atomic adsorption of adatom (Al/Si:C = 1:8) on graphene at specified site and orientation does affect the binding energy, DOS and magnetization properties of the doped graphene. High density micro-scale circuits/devices based on doped graphene sheets may have their overall electronic properties altered even for low adsorbed adatom atomic ratio.

## 5.2 Methods

The calculations were performed using the DFT framework[2], plane-wave method with spin polarization, Perdew-Burke-Wang generalized gradient approximation (GGA)

exchange-correlation functional [89] and projector augmented wave (PAW) pseudopotential[87]. Version 5.3.3 of the *VASP* set of programs was used for the DFT calculations[109]. The effects of adsorption site and orientation begin when atomic ratios are below 50 % and end when the adatom-adatom interaction is very small. In this study, only  $2 \times 2$  and  $2 \times \sqrt{3}$  graphene supercells (figures 5.1e and 5.1f) were used to observe the effect of orientation. In fact, there are three graphene supercells that create atomic ratio of one adatom for every eight carbon atoms (12.5%), *i.e.*  $2 \times 2$ ,  $2 \times \sqrt{3}$  and  $4 \times 1$  (figures 5.1e, 5.1f and 5.1g). However, the  $4 \times 1$  graphene supercell is too narrow in size thus creating very strong adatom-adatom interaction.

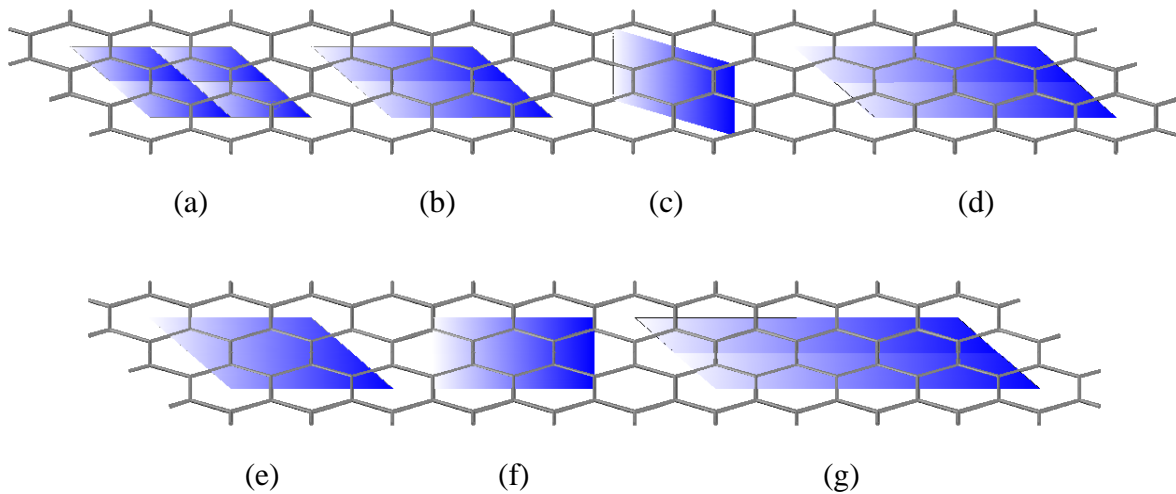


Figure 5.1 Graphene cell/supercells (adsorption atomic ratio, maximum adatom radius):  
 (a) zigzag  $1 \times 1$  (50%,  $\approx 1.23 \text{ \AA}$ ), (b) zigzag  $2 \times 1$  (25%,  $\approx 1.23 \text{ \AA}$ ),  
 (c) zigzag  $\sqrt{3} \times \sqrt{3}$  (16.7%,  $\approx 2.13 \text{ \AA}$ ), (d) zigzag  $3 \times 1$  (16.7%,  $\approx 1.23 \text{ \AA}$ ),  
 (e) zigzag  $2 \times 2$  (12.5%,  $\approx 2.46 \text{ \AA}$ ), (f) armchair  $2 \times \sqrt{3}$  (12.5%,  $\approx 2.13 \text{ \AA}$ ),  
 (g) zigzag  $4 \times 1$  (12.5%,  $\approx 1.23 \text{ \AA}$ ).

One adatom (Al or Si) was placed on these supercells. The calculations include (i) 3 adatom sites: bridge (*B*), hollow (*H*) and top (*T*); and (ii) 2 orientation directions: zigzag (*z*) and armchair (*a*), with an initial adatom height of  $2 \text{ \AA}$ . These sites and orientations are summarized in table 5.1. All the *H* and *T* cases can be represented by one position for zigzag



orientation ( $H_z$  and  $T_z$ ) and one position for armchair orientation ( $H_a$  and  $T_a$ ), while all the  $B$  cases can be represented by one position for zigzag orientation ( $B_z$ ) and three positions for armchair orientation ( $B_{a1}$ ,  $B_{a2}$ ,  $B_{a3}$ ). The lattice parameters were fixed at  $4.936 \text{ \AA} \times 4.936 \text{ \AA}$  for the zigzag  $2 \times 2$  graphene supercell and  $4.936 \text{ \AA} \times 4.275 \text{ \AA}$  for the armchair  $2 \times \sqrt{3}$  graphene supercell, as shown in figure 5.2. At this low adsorption atomic ratio, graphene lattice parameters do not change significantly. The distance between two graphene sheets was also fixed to  $15 \text{ \AA}$ .

Table 5.1 Sites and orientations for elemental adsorbed graphene for  $2 \times 2$  and  $2 \times \sqrt{3}$  supercells.

Site	$B$	$B$	$B$	$B$	$H$	$H$	$T$	$T$
Orientation	$z$	$a1$	$a2$	$a3$	$z$	$a$	$z$	$a$
Site/orientation (position)	$B_z$	$B_{a1}$	$B_{a2}$	$B_{a3}$	$H_z$	$H_a$	$T_z$	$T_a$
Graphene supercell	zigzag $2 \times 2$	armchair $2 \times \sqrt{3}$	armchair $2 \times \sqrt{3}$	armchair $2 \times \sqrt{3}$	zigzag $2 \times 2$	armchair $2 \times \sqrt{3}$	zigzag $2 \times 2$	armchair $2 \times \sqrt{3}$

Huang *et al.* [49] found nonlinearity of the band gap with O-adsorbed on graphene at atomic ratio of O of less than 30%. This nonlinearity appears to be due to the positions of the adatoms relative to one another. For this O case (1:8 ratio) the most stable position is  $B_{a2}$ . Symmetry suggests that there are 8 distinct adsorption positions ( $B_z$ ,  $B_{a1}$ ,  $B_{a2}$ ,  $B_{a3}$ ,  $H_z$ ,  $H_a$ ,  $T_z$ ,  $T_a$ ) for the  $2 \times 2$  and  $2 \times \sqrt{3}$  graphene supercells. The 8 distinct adsorption positions are summarized in the schematic diagrams of figure 5.3. The origin in the real space is set at the bottom left corner of each supercell, marked with O (0, 0). These schematic diagrams and the origin in real space are not unique, but chosen for the simulation. The initial atomic positions are translated from figure 5.3 into table 5.S1 in the supplementary data. However, positions  $B_{a1}$  and  $B_{a3}$  are mirror images of each other and are shown in figure 4.7. The calculation results for

these positions are expected to be identical, so only 7 unique adatom positions were considered in this study ( $B_z$ ,  $B_{a1}$ ,  $B_{a2}$ ,  $H_z$ ,  $H_a$ ,  $T_z$ ,  $T_a$ ).

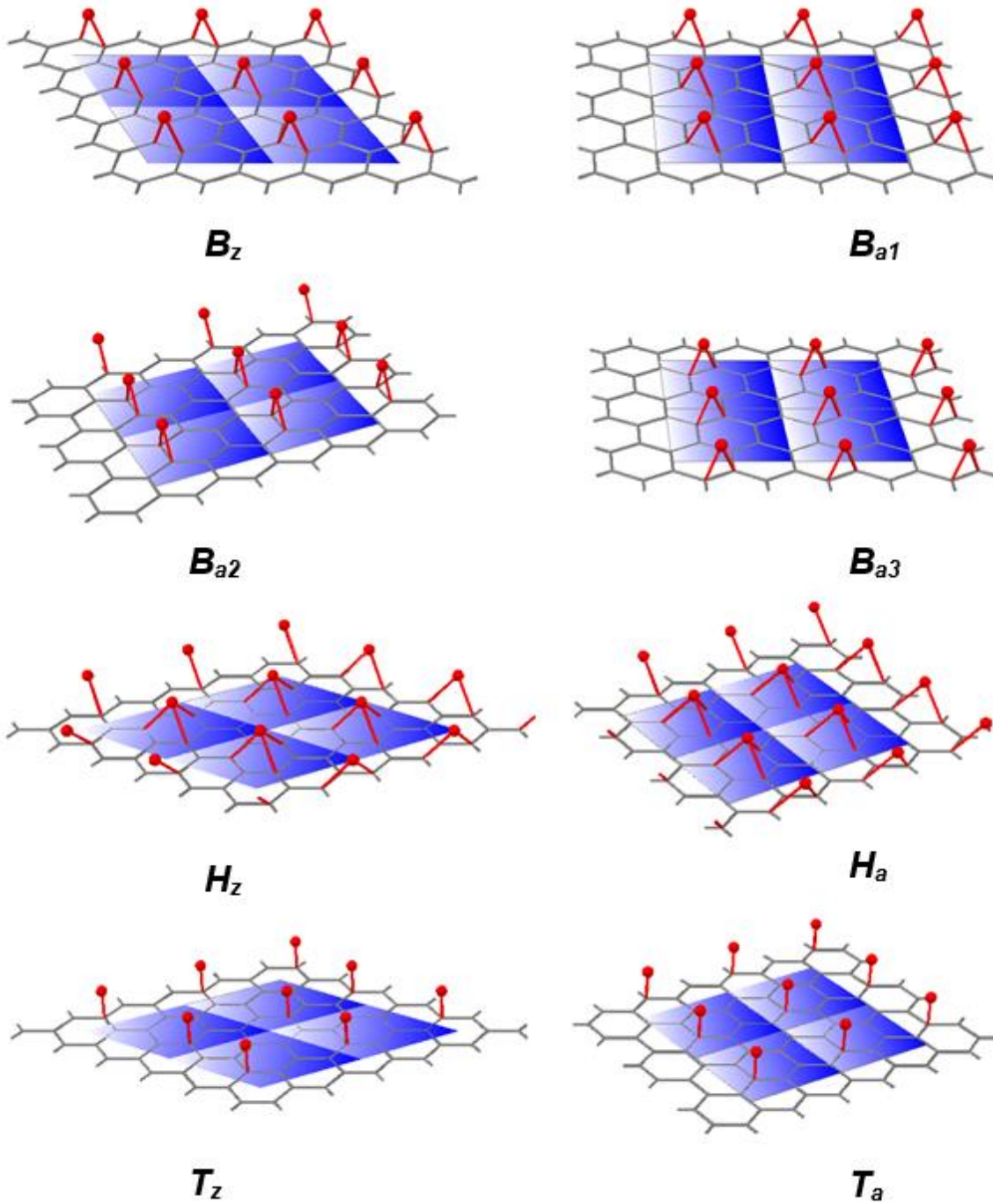


Figure 5.2 The  $2 \times 2$  and  $2 \times \sqrt{3}$  graphene supercells, with 3 sites (8 adatom positions, see table 5.1): bridge ( $B_z$ ,  $B_{a1}$ ,  $B_{a2}$ ,  $B_{a3}$ ), hollow ( $H_z$ ,  $H_a$ ) and top ( $T_z$ ,  $T_a$ ).

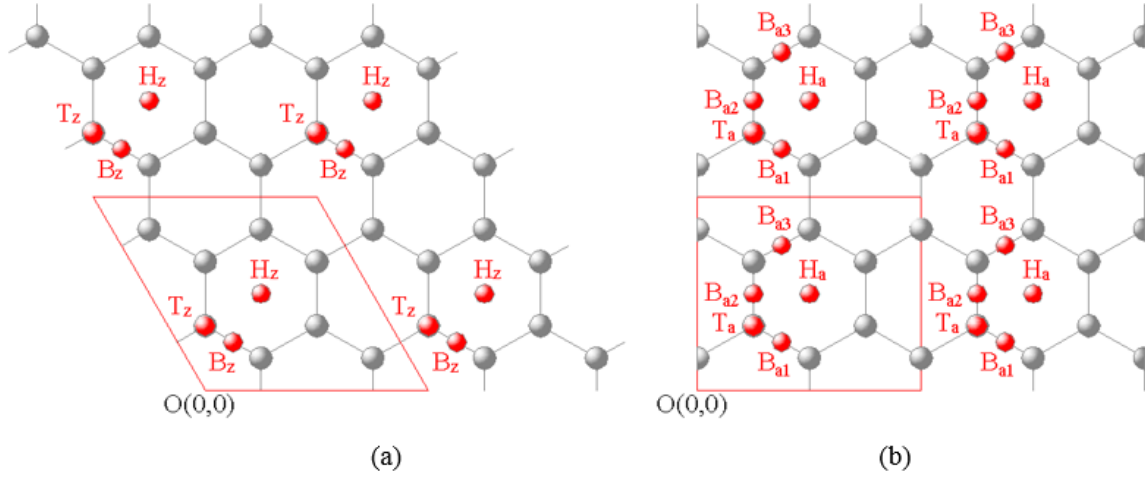


Figure 5.3 Schematic diagrams of adsorption on the graphene supercells for 1:8 atomic ratio, (a) zigzag  $2 \times 2$  and (b) armchair  $2 \times \sqrt{3}$ . O(0,0) is origin.  $4 \times 1$  graphene supercell is excluded.

As the supercells in this study are relatively small, adatom-adatom interaction is present. The calculations were carried out in four stages: (1) adatom and pristine graphene energy, (2) adatom-adatom interaction, (3) graphene-adatom internal structure optimisation, and (4) adatom-graphene density of states (DOS). Adatom-adatom interaction calculations were done for several supercells to compare the interaction strength against the supercell size. To ensure convergence results, all stages used plane wave cut off energy of 600 eV. Completion of iterations entailed tolerances of less than 1  $\mu\text{eV}$  for energy and less than 10  $\text{meV}/\text{\AA}$  for atomic forces. Calculation details ( $k$ -points and supercell sizes) at each stage are shown in table 5.S2 in the supplementary data.

Two types of binding energy,  $E_{binding1}$  and  $E_{binding2}$ , are explored in the present study and they can be determined by using the following equations:

$$E_{binding1} = E_{graphene} + E_{adatom} - E_{adatom-graphene\ system} \quad (5.1)$$

and

$$E_{binding2} = E_{graphene} + E_{adatom-adatom} - E_{adatom-graphene\ system} \quad (5.2)$$

where  $E_{graphene}$  is the energy of the pristine graphene,  $E_{adatom}$  is the energy of the adatom,  $E_{adatom-adatom}$  is the energy of adatom-adatom interaction and  $E_{adatom-graphene\ system}$  is the total energy of

the adatom and graphene after the adatom is attached to the graphene. Adatom-adatom interaction was calculated on the initial condition of adatom-adsorbed graphene as if the graphene sheet were removed from the system. Positive or negative binding energy indicates stability or instability, respectively.

The band gap, adatom height, graphene distortion, DOS, Fermi energy, magnetization and charge transfer for all 7 different adatom positions were calculated. The band gap is the difference between the lowest unoccupied molecular orbital (LUMO) and the highest occupied molecular orbital (HOMO), or Fermi energy. In this analysis, the band gap is determined from the DOS [90, p. 214]. Adatom height ( $\text{\AA}$ ) is the difference between adatom's  $z$ -coordinate and the average of  $z$ -coordinates of C atoms. The graphene distortion is an indicator of the adatom's presence, which is the total displacement (in  $\text{\AA}$ ) of the 8 C atoms in the graphene supercells. Magnetization (in Bohr magneton or  $\mu_B$ ) is defined as the difference between total spin up and total spin down of the DOS at Fermi energy. Charge transfer is defined as how much charge is transferred from adatom to graphene. Positive charge transfer indicates that charge is transferred from adatom to graphene while negative charge transfer indicates charge is transferred from graphene to adatom. Bader analysis was used for the charge transfer calculations [91]. The charge density difference was calculated for the most stable position of the Al and Si case. Charge density difference is defined as:

$$\Delta \rho = \rho_{\text{adatom-graphene system}} - (\rho_{\text{adatom}} + \rho_{\text{graphene}}) \quad (5.3)$$

where  $\rho_{\text{adatom-graphene system}}$  is the charge density of adatom-graphene system,  $\rho_{\text{adatom}}$  is the charge density of adatom as if the graphene sheet is removed from the system, and  $\rho_{\text{graphene}}$  is the charge density of graphene as if the adatom is removed from the system. Charge density difference shows the interactions between adatom and graphene in terms of changes in the spatial distribution of charge density. Version 3.2.1 of Vesta software was used to draw these charge density differences [110].

In our procedure, the adatoms are placed on one side of the graphene with only one adatom added per graphene supercell and all adatoms are uniformly distributed throughout the graphene. Lattice vibrations (in infrared region) were not considered and GW approximation was not applied. In general it is expected that the calculated band gaps are lower than the experimental values. However, these calculations provide indication of band gap presence in elemental adsorption on graphene.

### 5.3 Results and Discussion

The discussion highlights three things, *i.e.* adatom-adatom interaction, Al- / Si-adsorbed graphene, and electronic analysis. Results, using  $2 \times 2$  and  $2 \times \sqrt{3}$  supercells, indicate that the graphene with adsorbed Al or Si does not open band gap as is the case for pristine graphene. However, the Fermi energy of Al- or Si-adsorbed graphene increases from that of pristine graphene. Our result indicates that pristine graphene has a binding energy of  $\approx 7.97$  eV/atom, which is in the deep UV region, and is similar to 7.91 eV/atom calculated by Bhattacharya *et al.* [111].

#### 5.3.1 Adatom-adatom Interaction

Orientation effect becomes important if the adatom-adatom interaction is not small. This interaction is represented by its binding energy, which is  $E_{\text{adatom}} - E_{\text{adatom-adatom}}$  (see figure 5.4). As expected, the interaction is quite strong at small supercells, but diminishes at larger supercells. The binding energy of Si drops more quickly than Al, and the interactions are negligible at zigzag  $3 \times 3$  or larger supercells. At these larger supercells, adatom is unaware of the presence of other adatoms. However, there is interaction difference between zigzag  $2 \times 2$  and armchair  $2 \times \sqrt{3}$ , due to the different adatom's nearest neighbours (see figure 4.12). On zigzag  $2 \times 2$ , there are 6 nearest neighbours at a distance  $r$ . On armchair  $2 \times \sqrt{3}$ , there are 2

nearest neighbours at a distance  $r$ , 2 at  $\sqrt{3}r/2$ , and 4 at  $\sqrt{7}r/2$ . For supercells greater than  $1 \times 1$ , Al-Al interaction is about twice the Si-Si counterpart.

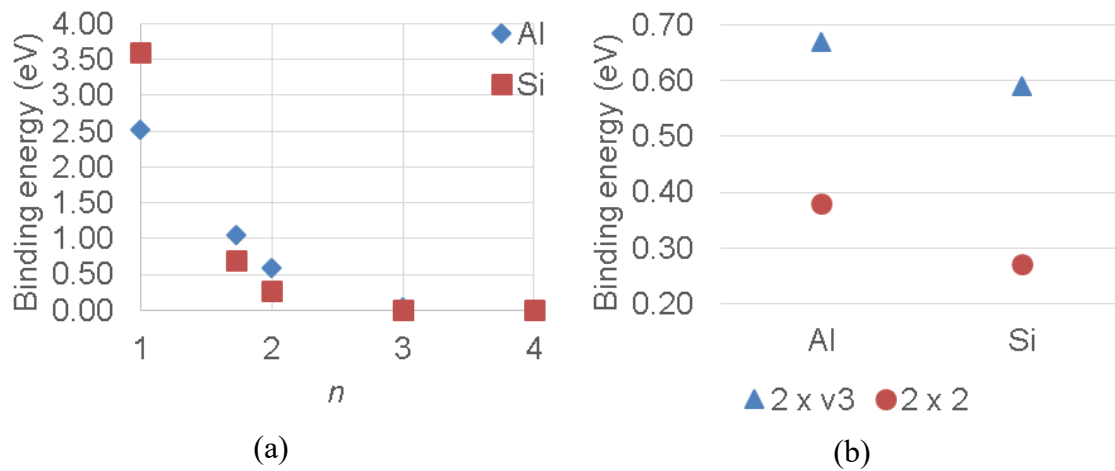


Figure 5.4 Adatom-adatom binding energies for : (a)  $n \times n$  zigzag supercells, (b)  $2 \times \sqrt{3}$  armchair and  $2 \times 2$  zigzag supercells.

### 5.3.2 Al- and Si-adsorbed Graphene

Tables 5.2 and 5.3 are the results for all distinct positions of Al- and Si-adsorbed on graphene. In the following discussion, the  $T_a$  positions for both Al and Si cases were ignored because the adatoms move away from the “top” position after iteration. The most stable position for Al is  $H_z$  and for Si is  $B_{a2}$ . Binding energy 1 is the binding energy of adatom-graphene system relative to free adatom. Binding energy 2 is the binding energy of adatom-graphene system relative to adatom-adatom system. For our Al and Si cases, binding energy 1 is greater than binding energy 2, because the adatom-adatom interaction is not small. Results in tables 5.2 and 5.3, indicate that Si distorts the graphene sheet more than Al.

Binding energy 1 and 2 indicate that  $H_z$  is the most stable position for Al while  $B_{a2}$  is the most stable position for Si. Al-Al interaction is greater than Al-graphene interaction, while Si-Si interaction is comparable to Si-graphene interaction. Comparing binding energy 2 at its most stable position, Si (0.42 eV) binds more strongly than Al (0.33 eV).

Table 5.2 Calculation results for Al-adsorbed graphene (Al:C = 1:8). Spin up and spin down are degenerate. Literature results (at zigzag orientation) are included for  $4 \times 4$  graphene supercell[20] and  $3 \times 3$  graphene supercell[45].

	$B_z$	$B_{a1}$	$B_{a2}$	$B_{a3}$	$H_z^a$	$H_a$	$T_z$	$T_a^b$
Binding energy 1 (eV)	0.83	0.89	0.92	0.89	0.93	0.92	0.80	-
Binding energy 2 (eV)	0.24	0.22	0.25	0.22	0.33	0.25	0.21	-
Binding energy (eV)	0.927[20]	-	-	-	1.042[20] 1.62[45]	-	0.911[20]	-
Adatom height (Å)	2.18 2.22[20]	2.28	2.25	2.28	2.11 2.13[20] 2.04[45]	2.10	2.19 2.22[20]	-
Fermi energy shift (eV) <sup>c</sup>	1.70	1.68	1.61	1.68	1.70	1.73	1.70	-
Graphene distortion (Å)	0.07	0.13	0.11	0.13	0.06	0.10	0.12	-
Magnetization ( $\mu_B$ )	-	-	-	-	-	-	-	-
Migration energy (eV)					0.115[20] 0.05[45]			
Charge transfer (electrons) <sup>d</sup>	1.08	0.97	1.01	0.97	1.24	1.24	1.05	-
Charge transfer (%) <sup>e</sup>	36.0	32.2	33.8	32.2	41.3	41.2	34.9	-

<sup>a</sup> most stable position

<sup>b</sup> adatom moves towards  $B_{a2}$  and the calculation results are close to  $B_{a2}$

<sup>c</sup> Fermi energy shift from pristine graphene

<sup>d</sup> Charge transfer from Al to graphene, initial Al charge is 3

<sup>e</sup> Charge transfer from Al to graphene (% of initial valence electron)

Migration energy or barrier energy is the energy needed for the adatom to move on the graphene surface. To carry out this calculation, the  $B$ ,  $H$ ,  $T$  sites are assumed to be near the true saddle points. For Al adsorption, it is assumed that adatoms move from one  $H$  site to another  $H$  site via a  $B$  site. While for Si, it is assumed that adatoms move from one  $B$  site to another  $B$  site via either an  $H$  or  $T$  site. As an example, for Al migration energy of  $H_z \rightarrow B_z \rightarrow H_z$  is  $0.33 - 0.24 \text{ eV} = 0.09 \text{ eV}$ . While for Si case, migration energy of  $B_z \rightarrow H_z \rightarrow B_z$  or  $B_z \rightarrow T_z \rightarrow B_z$  is  $0.39 - 0.26 \text{ eV} = 0.13 \text{ eV}$ . The example calculations, using binding energy 2, show that the migration energy of Si is greater than Al. Having stronger binding energy and greater migration energy, the Si-graphene system is more stable than the Al-graphene system.

Table 5.3 Calculation results for Si-adsorbed on graphene (Si:C = 1:8). Spin up and spin down are not degenerate. Literature results (at bridge site) are included: armchair orientation on  $4 \times 4$  graphene supercell[67] and zigzag orientation on  $3 \times 3$  graphene supercell[45].

	$B_z$	$B_{a1}$	$B_{a2}^a$	$B_{a3}$	$H_z$	$H_a$	$T_z$	$T_a^b$	Literature
Binding energy 1 (eV)	0.67	0.60	0.81	0.60	0.53	0.24	0.53	-	1.86[45] 0.84[67]
Binding energy 2 (eV)	0.40	0.21	0.42	0.21	0.26	-0.14	0.26	-	-
Adatom height (Å)	2.06	2.06	2.09	2.06	2.00	2.11	1.86	-	2.03[45] 2.05[67]
Fermi energy shift (eV) <sup>c</sup>	1.07	1.18	0.98	1.18	1.33	1.31	1.23	-	-
Graphene distortion (Å)	0.34	0.52	0.48	0.52	0.19	0.12	0.31	-	-
Magnetization ( $\mu_B$ )	0.62	0.38	0.56	0.38	0.00	0.00	0.00	-	0.27[65]
Migration energy (eV)	-	-	-	-	-	-	-	-	0.05[45]
Charge transfer (electrons) <sup>d</sup>	1.38	1.36	1.48	1.36	0.49	0.42	1.49	-	-
Charge transfer (%) <sup>e</sup>	34.5	34.0	36.9	34.0	12.3	10.4	37.1	-	-

<sup>a</sup> most stable position

<sup>b</sup> adatom moves towards  $B_{a2}$  and the calculation results are close to  $B_{a2}$

<sup>c</sup> Fermi energy shift from pristine graphene

<sup>d</sup> Charge transfer from Si to graphene, initial Si charge is 4

<sup>e</sup> Charge transfer from Si to graphene (% of initial valence electron)

The calculated adatom heights, shown in tables 5.2 and 5.3, are in agreement with results of previous studies[20], [45], [67]. The calculated binding energies are also in agreement with findings of previous investigations[20], [67]. However, the calculated binding energies and migration energies are not in agreement with the results of Nakada *et al.* [45], as these authors did not consider spin polarization. Calculation with spin polarization is essential to obtain true ground state energy and reveal magnetic properties of the materials. Tables 5.2 and 5.3 also show that changes of Fermi energy depend on the site and orientation.

Comparison of columns  $B_z$  with  $B_a$  and  $H_z$  with  $H_a$  in tables 5.2 and 5.3, for Al-adsorbed graphene, indicates that different orientation marginally affects the electronic structure. Similar comparison for Si-adsorbed graphene indicates greater effects on the electronic structure due to different orientations. To the best of our knowledge, there is no direct experimental data to



support these results. However, Tao *et al.* [112] demonstrated distinct electronic properties arising from zigzag and armchair graphene nanoribbons. Full experimental verification may be done in the future by utilizing advanced techniques such as scanning tunnelling microscopy (STM).

### 5.3.3 Electronic Analysis

Figure 5.5 are plots of DOS at the most stable positions of  $H_z$  for Al-adsorbed and  $B_{a2}$  for Si-adsorbed graphene. The calculated results agree with results by Chan *et al.* [20] and Sison *et al.* [67]. However, Chan *et al.* DOS values are greater, than those of figure 5.5, as they used larger graphene supercells for their simulations. The Fermi energy of pristine graphene is increased by Al and Si adsorption by 1.70 eV and 0.98 eV respectively. For all Al and Si cases, at the 1:8 (12.5%) adsorption atomic ratio, there is no band gap created at Fermi energy.

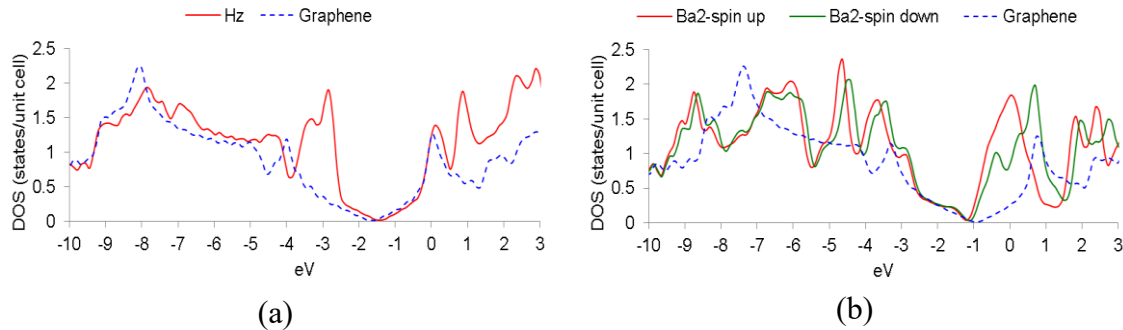


Figure 5.5 DOS and Fermi energy (0 eV) of (a) Al-adsorbed graphene at its most stable position ( $H_z$ ), spin up and spin down are degenerate, (b) Si-adsorbed graphene at its most stable position ( $B_{a2}$ ).

For each adatom position, in general, Al-adsorbed graphene creates identical DOS for both spin up and spin down cases (degenerate and zero magnetization), and in agreement with Liu *et al.*'s calculations [55]. Whilst for Si-adsorbed graphene the DOS are different for spin up and spin down cases with creation of magnetization. This is in qualitative agreement with calculations by Aktürk *et al.* [65], Hu *et al.* [66] and Sison *et al.* [67]. However, Aktürk *et al.*

[65] reported low magnetization of  $0.27 \mu_B$  at 12.5% atomic ratio and high magnetization of  $1.02 \mu_B$  at 1:32 ( $\approx 3.1\%$ ) atomic ratio. Hu *et al.* [66] reported high magnetization of  $1.74 \mu_B$  at 1:72 ( $\approx 1.4\%$ ) atomic ratio. The calculated magnetization at the  $B_z$  position of Si-adsorbed graphene from this study is equal to  $0.62 \mu_B$  ( $B_z$  case) which is more than twice that reported by Aktürk *et al.*

In figure 5.5(a) the DOS near the Dirac point ( $\approx -1.2$  eV) has the same profile and similar values as that of pristine graphene. In figure 5.5(b) the DOS below the Dirac point ( $\approx -2.5$  to  $-1.2$  eV) has the same profile as that of pristine graphene, but is significantly altered above the Dirac point.

Pauling's electronegativity scale was used as the first attempt to see the charge transfer between Al, Si and graphene[21, p. 299]. The electronegativity values used for Al, Si and C are 1.5, 1.8 and 2.5 respectively. It is expected that Al will donate more electrons to the graphene sheet than the Si case. Al donates more electrons to graphene than Si. There is no charge transfer among carbon atoms in graphene.

Bader analysis was used for charge transfer calculations with initial valence electrons of 3 and 4 for Al and Si respectively. After adsorbed to graphene, Al ( $H_z$  case) gives almost half of its valence electrons (41.3% or 1.24 electrons) to graphene, while Si ( $B_{a2}$  case) gives more than a third of its valence electrons (36.9% or 1.48 electrons) to graphene. The largest charge transfers for Al cases are Al- $H_z$  and Al- $H_a$ , with Al- $H_z$  being the most stable configuration. The largest charge transfers for Si cases are Si- $B_{a2}$  and Si- $T_z$ , with Si- $B_{a2}$  being the most stable configuration. This indicates that the most stable configuration is related to the largest charge transfer. Figures 5.6 and 5.7 provide isosurface plots of charge density difference for the most stable positions. The plots show that spatial charge distribution correlates with the symmetry of the adsorption site (where adsorption orientation is implied) regardless of the number of valence electrons. Carbon atoms with the same C-atom distance have identical spatial charge

distribution oriented to the adatom. Finally, orientation effect, noticeable at atomic ratio below 50%, is expected to disappear when the adatom-adatom distance increases resulting in negligible interaction.

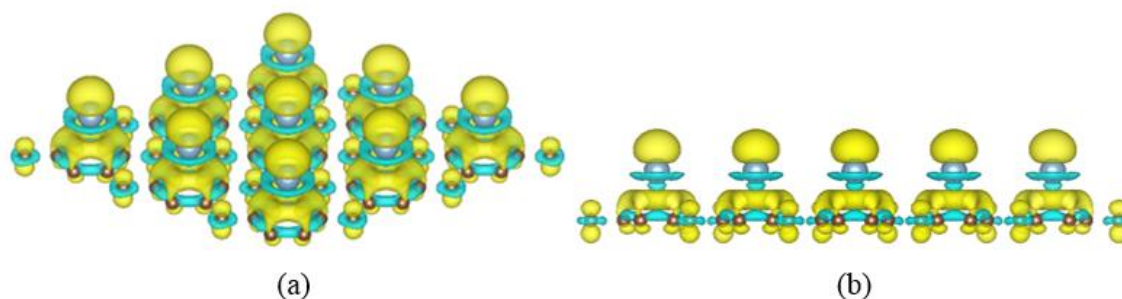


Figure 5.6 Charge density difference of Al-adsorbed graphene,  $H_z$  case, (a) is isometric view, (b) is front view. Brown spheres are C, grey spheres are Al. Yellow surfaces enclose the charge density greater than  $0.015 \text{ electron}/\text{\AA}^3$  (electron surplus), while cyan surfaces enclose the charge density less than  $-0.015 \text{ electron}/\text{\AA}^3$  (electron deficit).

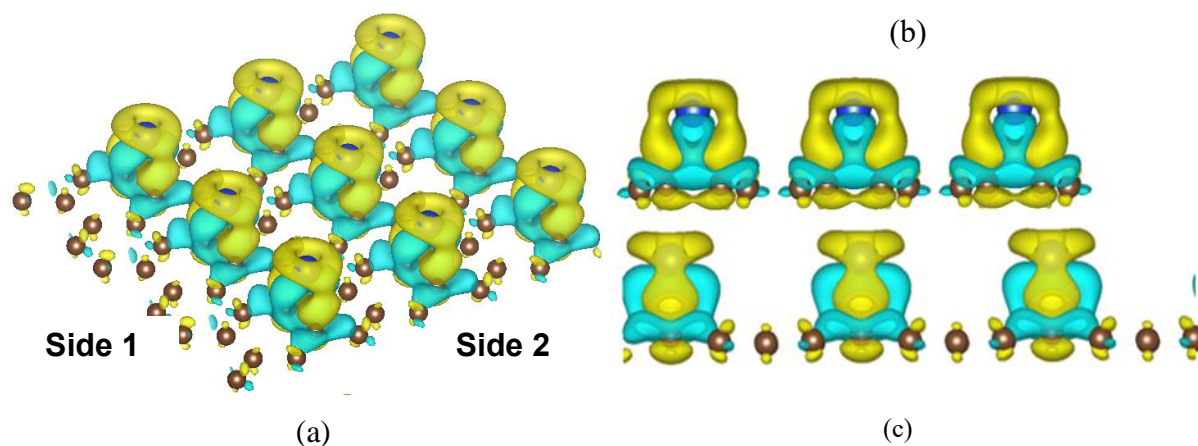


Figure 5.7 Charge density difference of Si-adsorbed graphene,  $B_{a2}$  case, (a) is isometric view, (b) is side 1 view, (c) is side 2 view. Brown spheres are C, blue spheres are Si. Yellow surfaces enclose the charge density greater than  $0.015 \text{ electron}/\text{\AA}^3$  (electron surplus), while cyan surfaces enclose the charge density less than  $-0.015 \text{ electron}/\text{\AA}^3$  (electron deficit).

## 5.4 Conclusions

This contribution deployed the density functional theory (DFT) to investigate the electronic structures and physical properties of a graphene sheet with adsorbed elemental Al and Si. The results indicate that, for adatom/graphene atomic ratio (Al/Si:C = 1:8), the changes in the electronic structure are due to the adsorption site (*i.e.* bridge, hollow or top) and also to

the relative orientation of the adsorbed sites (*i.e.* zigzag or armchair). Furthermore, the number of distinct adsorption positions on bridge site relies on the adatom orientation. The orientation effects of Si-adsorbed graphene were found to be greater than the Al counterpart. Al is most stable at the  $H_z$  and Si is at  $B_{a2}$  positions. Neither Al nor Si create a band gap at the Fermi energy level. However, the Fermi energy of Al- or Si-adsorbed graphene increased from that of pristine graphene. Magnetization of pristine graphene is altered by Si, but not by Al adsorption. The degree of charge transfer is related to the most stable configuration of the adatom on graphene. The spatial charge distribution correlates with the symmetry of the adsorption site regardless of the number of valence electrons. The Si-graphene system incurs more stability when compared with its Al-counterpart.

## 5.5 Supplementary Data

Table 5.S1 Initial atomic positions for each case in figure 5.3 (in fractional coordinate).

Atom	Zigzag	Armchair
C	(1/6, 1/3, 0)	(0, 1/6, 0)
C	(1/3, 1/6, 0)	(1/4, 1/3, 0)
C	(2/3, 1/3, 0)	(1/2, 1/6, 0)
C	(5/6, 1/6, 0)	(3/4, 1/3, 0)
C	(1/6, 5/6, 0)	(0, 5/6, 0)
C	(1/3, 2/3, 0)	(1/4, 2/3, 0)
C	(2/3, 5/6, 0)	(1/2, 5/6, 0)
C	(5/6, 2/3, 0)	(3/4, 2/3, 0)
adatom ( $B_z$ )	(1/4, 1/4, 2/15)	-
adatom ( $B_{a1}$ )	-	(3/8, 1/4, 2/15)
adatom ( $B_{a2}$ )	-	(1/4, 1/2, 2/15)
adatom ( $B_{a3}$ ) <sup>a</sup>	-	(3/8, 3/4, 2/15)
adatom ( $H_z$ )	(1/2, 1/2, 2/15)	-
adatom ( $H_a$ )	-	(1/2, 1/2, 2/15)
adatom ( $T_z$ )	(1/6, 1/3, 2/15)	-
adatom ( $T_a$ )	-	(1/4, 1/3, 2/15)

<sup>a</sup>  $B_{a3}$  is mirror image of  $B_{a1}$

Table 5.S2 Converged  $k$ -points and supercell sizes used in each stage.

Stage	Description of calculation	$k$ -points	Cell/Supercell	Supercell size (Å)
1	Adatom energy	$1 \times 1 \times 1$	cubic	$15 \times 15 \times 15$
	Pristine graphene energy	$24 \times 24 \times 1$	zigzag $2 \times 2$	$4.936 \times 4.936 \times 15$
2	Adatom-adatom interaction	$48 \times 48 \times 1$	zigzag $1 \times 1$	$2.468 \times 2.468 \times 15$
		$28 \times 28 \times 1$	zigzag $\sqrt{3} \times \sqrt{3}$	$4.275 \times 4.275 \times 15$
		$24 \times 28 \times 1$	armchair $2 \times \sqrt{3}$	$4.936 \times 4.275 \times 15$
		$24 \times 24 \times 1$	zigzag $2 \times 2$	$4.936 \times 4.936 \times 15$
		$16 \times 16 \times 1$	zigzag $3 \times 3$	$7.404 \times 7.404 \times 15$
		$12 \times 12 \times 1$	zigzag $4 \times 4$	$9.872 \times 9.872 \times 15$
3	Graphene-adatom internal structure optimisation	$6 \times 6 \times 1$	zigzag $2 \times 2$	$4.936 \times 4.936 \times 15$
		$6 \times 7 \times 1$	armchair $2 \times \sqrt{3}$	$4.936 \times 4.275 \times 15$
4	Graphene-adatom DOS	$24 \times 24 \times 1$	zigzag $2 \times 2$	$4.936 \times 4.936 \times 15$
		$24 \times 28 \times 1$	armchair $2 \times \sqrt{3}$	$4.936 \times 4.275 \times 15$

A manuscript based on the major research outcomes of this chapter was published in :

H. Widjaja, M. Altarawneh, Z.-T. Jiang, C.-Y. Yin, B.-M. M. Goh, N. Mondinos, and B. Z. Dlugogorski, “Geometrical and orientational investigations on the electronic structure of graphene with adsorbed aluminium or silicon,” *Mater. Des.*, vol. 89, pp. 27–35, 2016. (*This is publication [1] in the List of Publications*)

## CHAPTER SIX

### HALOGENS (F-I) ADSORPTION ON GRAPHENE

---

#### 6.1 Introduction

The calculation procedure developed in chapters 1 to 4 was secondly applied to halogens (F, Cl, Br, I) at lower concentration spanning 1:6, 1:8 and 1:18 atomic ratios, in order to elucidate effects of adsorption trends in a group in periodic table of elements. The electronic structure of elemental adsorption on graphene is affected by side of adsorption (single- or double-sided), site of adsorption (*i.e.* bridge, hollow or top), and the relative orientation of the adsorbed sites (*i.e.* zigzag or armchair).

Numerous experimental and theoretical studies have addressed adsorption of halogen on graphene. Karlicky *et al.*[113] reported in their review that fully and partially fluorinated graphene have been synthesized, but only partial coverage for Cl, Br and I have been produced so far. Band gap of fully fluorinated graphene (fluorographene) has been measured to be around 3.0 eV. This makes fluorographene to be one of the thinnest wide-band-gap-semiconductors/insulators, beside graphane (fully hydrogenated graphene) and graphene oxide.

In this regard, two factors appear to play an important role, namely, atomic percent (at.%) and atomic ratio, *e.g.* a 50 at.% has multiple atomic ratios (1:2, 2:4, 3:6, 4:8, ...). Robinson *et al.*[48] synthesized and simulated single-sided fluorinated graphene of 25 at.%. This 25 at.% constitutes the most stable configuration for single-sided case after fluorographene. This configuration cannot be explained using the simplest atomic ratio (1:4), but rather 2:8 (see figure 6.1). The “flower”-like pattern appears out of this configuration. This system opens a band gap of 2.93 eV.

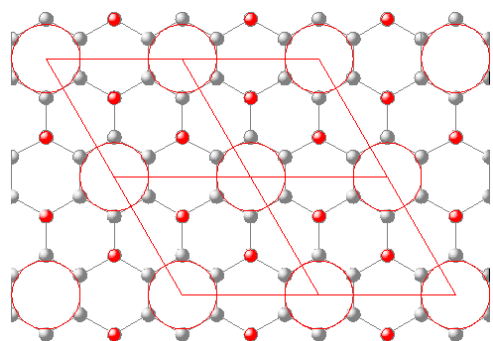


Figure 6.1 Most stable configuration of single-sided fluorinated graphene of 25 at.%, red spheres are F atoms, grey spheres are C atoms, and big red circles are added to guide the eyes[48]. This figure was adopted from figure 4.4.

Wu *et al.* [92] investigated the Cl plasma reaction with graphene and graphene nanoribbon, and contrasted it with the H and F plasma reactions. H and F plasma destroy the network of graphene faster than the Cl plasma. *Ab initio* calculations have indicated that the binding energy of Cl is lower than F and H. It follows that Cl atoms are less reactive toward graphene if compared with F and H. Br has been successfully used as an assisting agent to glue graphene nanoribbons with different widths, due to its weak bond with C[114]. Br atoms are deployed during the gluing process, and then removed from the end products.

On the simulation side, Nakada and Ishii[45], [46] reported in their non-magnetic *ab initio* calculations at 1:18 atomic ratio, that binding energies decreases, adatom heights increases, migration energies decreases, charge transfers (from graphene to adatom) decreases from F to I. However only F shows stability at top site. Although applying non-magnetic calculations appear to be a shortcoming of Nakada and Ishii[45], [46] calculation formalism, their work provide valuable information with regard to the landscape of elemental adsorption on graphene. Analogously, Karki and Adhikari[115] reported in their *ab initio* calculations for halogens adsorbed on  $C_{96}H_{26}$  (1:96 atomic ratio), that binding energies decreases, adatom heights increases, from F to Br. However, charge transfers and band gaps do not follow any trend. Medeiros *et al.*[71] found that fluorographene creates direct band gap of 3.16 eV, while fully chlorinated graphene (chlorographene) opens a direct band gap of 1.53 eV. Br and I do

not open the band gap. Fully halogen-adsorbed graphene systems expand the graphene lattice constant significantly and also crumple the graphene sheet. Binding energies decrease and graphene lattice constants increase from F to I.

Besides site of adsorption (bridge, hollow, top), orientational effects in molecules adsorbed on graphene is obvious (*e.g.* parallel or perpendicular to graphene [116], [117]), however to see orientational effects in single atom adsorbed on graphene requires careful examinations. To this end, the current study deploys density functional theory (DFT) calculations to assess the influence of the orientational effect when the interaction between the adatoms is relatively significant. In estimation of atomic sizes and adatom-adatom interactions, we consider atomic ratio of adatom:C at 1:8. We elucidate the effects of different concentrations using atomic ratios of 1:6 and 1:18. We carry out a thorough geometrical investigation on the orientational effect encountered during the adsorption of the four halogens on graphene. Overall, we highlight some prominent effects of the orientational (*i.e.* zigzag or armchair) and site (*i.e.* bridge, hollow or top) aspects on various properties such as binding energy, Fermi energy, band gap, magnetization, density of states (DOS) and charge transfer.

## 6.2 Methods

We perform all structural optimisations and energy calculations using the plane-wave DFT code of VASP. Calculation methodology comprises spin-polarized PAW-GGA functional [89], van der Waals correction by Grimme (D2) [88] method, dipole corrections along the Z-direction, and a Gaussian smearing.

To investigate the most stable configuration, it is necessary to examine all possible positions. But unfortunately, this is not practical to do, as the number of cases will be unlimited. As such, this study is limited to one adatom per graphene supercells. The adatoms are uniformly distributed throughout the graphene. Only  $2 \times 2$  and  $2 \times \sqrt{3}$  graphene supercells (figures 6.2a



and 6.2b) were used to observe the effect of orientation. We have not utilized a  $4 \times 1$  graphene supercell (figure 6.2c) due to its too narrow size which may induce artificial very strong adatom-adatom interaction, and may not be capable of holding neighbouring Br atoms at their optimum adsorption positions.

It is understood that any non-zigzag graphene supercells (armchairs/slants) can be represented by larger zigzag graphene supercells with the origin  $O(0,0)$  translated/rotated (see figure 6.S1 in the supplementary data) and vice versa. However, in this study, we use armchair graphene supercell, as it is the simplest case to track the effects of the orientation. Finally, the effects of orientation end when the adatom-adatom interaction is very small.

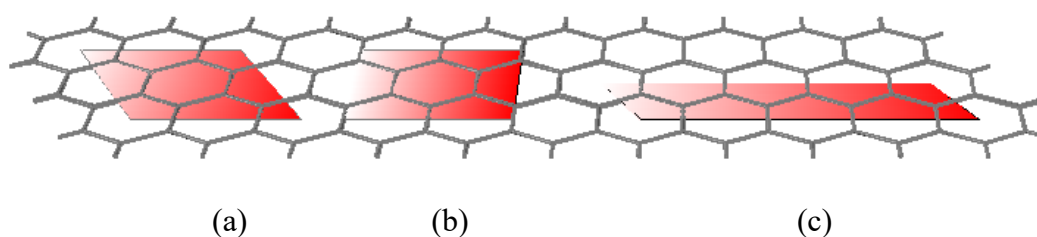


Figure 6.2 Graphene supercells, (a) zigzag  $2 \times 2$ , (b) armchair  $2 \times \sqrt{3}$ , (c) zigzag  $4 \times 1$ .

For 1:8 atomic ratio, the calculations include (i) 3 adatom sites: bridge ( $B$ ), hollow ( $H$ ) and top ( $T$ ); and (ii) 2 orientation directions: zigzag ( $z$ ) and armchair ( $a$ ), with initial adatom height of  $1.5 \text{ \AA}$ . Figures 6.3b and 6.3c summarize these sites and orientations. All the  $H$  and  $T$  cases can be represented by one position for zigzag orientation ( $H_z$  and  $T_z$ ) and one position for armchair orientation ( $H_a$  and  $T_a$ ), while all the  $B$  cases can be represented by one position for zigzag orientation ( $B_z$ ) and two positions for armchair orientation ( $B_{a1}$ ,  $B_{a2}$ ). Thus we only consider 7 unique adatom positions in this study ( $B_z$ ,  $B_{a1}$ ,  $B_{a2}$ ,  $H_z$ ,  $H_a$ ,  $T_z$ ,  $T_a$ ). We fix the lattice parameters at  $4.936 \text{ \AA} \times 4.936 \text{ \AA}$  for the zigzag  $2 \times 2$  graphene supercell and  $4.936 \text{ \AA} \times 4.275 \text{ \AA}$  for the armchair  $2 \times \sqrt{3}$  graphene supercell. At this low adsorption atomic ratio, graphene lattice parameters do not change significantly. We also fix the distance between the two

graphene sheets to 15 Å. We carry out additional calculations for 1:6 and 1:18 atomic ratios and these calculations consider only adsorption sites ( $B$ ,  $H$ ,  $T$ ), as shown in figures 6.3a and 6.3d.

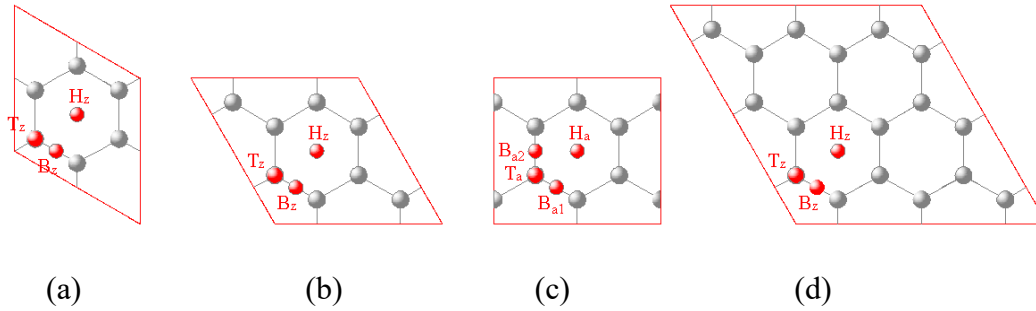


Figure 6.3 Schematic diagrams of adsorption on the graphene supercells for (a) 1:6, (b) 1:8 zigzag  $2 \times 2$ , (c) 1:8 armchair  $2 \times \sqrt{3}$  and (d) 1:18 atomic ratios.

We conduct the calculations in four stages: (1) adatom and pristine graphene energy, (2) adatom-adatom interaction, (3) graphene-adatom internal structure optimisation, and (4) adatom-graphene density of states (DOS) calculation. We do two sets of calculations, with and without van der Waals and dipole corrections, to see the effects of these corrections. We calculate the adatom-adatom interaction for several supercells to compare the interaction strength against the supercell size. To ensure convergence results, all stages used plane wave cut off energy of 600 eV. Completion of iterations entailed tolerances of less than 1  $\mu$ eV for energy and less than 0.02 eV/Å for atomic forces. Table 6.S1 in the supplementary data shows the calculation details ( $k$ -points and supercell sizes) at each stage.

We explore two types of binding energy,  $E_1$  and  $E_2$ , in the present study as expressed in the following two equations:

$$E_1 = E_{\text{graphene}} + E_{\text{adatom}} - E_{\text{adatom-graphene system}} \quad (6.1)$$

and

$$E_2 = E_{\text{graphene}} + E_{\text{adatom-adatom}} - E_{\text{adatom-graphene system}} \quad (6.2)$$

where  $E_{graphene}$  denotes the energy of the pristine graphene,  $E_{adatom}$  signifies the energy of the adatom,  $E_{adatom-adatom}$  stands for the energy of adatom-adatom interaction and  $E_{adatom-graphene\ system}$  is the total energy of the adatom and graphene after the adatom is attached to the graphene. We calculate adatom-adatom interaction on the initial condition of adatom-adsorbed graphene as if the graphene sheet were removed from the system. Positive or negative binding energy indicates stability or instability, respectively.

The band gap, adatom height, graphene distortion, DOS, Fermi energy, magnetization, charge transfer are calculated for all cases. In this analysis, the band gap is determined from the DOS[90, p. 214] analysis, i.e. zero DOS at Fermi energy. Zero DOS at Fermi energy signifies that the material is a semiconductor or insulator. Adatom height ( $\text{\AA}$ ) is the difference between adatom's  $z$ -coordinate and the average of  $z$ -coordinates of C atoms. The graphene distortion is an indicator of the adatom's presence, which is the total displacement (in  $\text{\AA}$ ) of the C atoms in the graphene supercells.

While total charge is the sum of total spin up and spin down, magnetization (in Bohr magneton or  $\mu_B$ ) is defined as the difference between total spin up and total spin down of the DOS at the Fermi energy level. Charge transfer is expressed as the scalar quantity charge transferred from graphene to adatom. Positive charge transfer indicates that charge is transferred from graphene to adatom and negative charge transfer is vice versa. We estimate charge transfer via the Bader methodology[91]. We also calculate charge density difference to show the interactions between adatom and graphene in terms of its spatial distribution. Charge density difference is computed as:

$$\Delta\rho = \rho_{adatom-graphene\ system} - (\rho_{adatom} + \rho_{graphene}) \quad (6.3)$$

where  $\rho_{adatom-graphene\ system}$  is the charge density of adatom-graphene system,  $\rho_{adatom}$  is the charge density of adatom as if the graphene sheet is removed from the system, and  $\rho_{graphene}$  is

the charge density of graphene as if the adatom is removed from the system. The version 3.2.1 of Vesta software facilitates the calculations of charge densities[110].

### 6.3 Results and Discussion

The discussion will focus on adatom-adatom interaction, adatom-adsorbed graphene and electronic analysis. The basic information of graphene and the atoms are shown in table 6.S2 and 6.S3 and figure 6.S2 in the supplementary data. Table 6.S2 shows the atomic/ionic radius and its Pauling's electronegativity[21, pp. 255–257]. Table 6.S3 shows the calculated magnetization and Fermi energy of graphene and the elements. While figure 6.S2 displays the DOS of graphene and the elements.

In general, determining the most stable configuration in elemental adsorption on graphene at arbitrary atomic ratio is very challenging, as the plausible numbers of combination are unlimited. A well-known example is F-adsorbed graphene at 25 at.%, that creates “flower”-like pattern (see again figure 6.1). To verify this problem, advanced techniques to manipulate atoms at precise locations must be used (*e.g.* scanning tunnelling microscopy (STM)). This probably would not be an effective and efficient approach.

Our last verification is that this calculation method has been verified for fluorographene case with excellent agreement with previous studies in terms of DOS and band gap[48], [118] (figure 6.S3 in supplementary data). Subsequently, we apply this method to address the lower atomic ratios. A well-known example of orientation effect is graphene nanoribbon, where zigzag or armchair termination of graphene nanoribbon determines its band gap[25, p. 5]. Zigzag orientation creates metallic materials, while armchair orientation (depending on its width) creates metallic/semiconductor materials. This highlights the importance of a geometric aspect, *i.e.* orientation, on the properties of materials. Xu and Xue[119] carried out a simulation study and reported that oxidation can introduce line defects in graphene, thus unzipping the

pattern of graphene. In relation with this, a potential application for our study is to assist this process, and ultimately to create richer and more controllable patterns, *e.g.* zigzag and armchair graphene nanoribbons.

### 6.3.1 Adatom-adatom Interaction

Elemental adsorption on graphene can be seen as a competition between two parallel surface networks, with the network of C atoms as adsorbent and the network of adatoms as adsorbate. Adatom-adatom interaction in the network of adatoms is represented by its binding energy. As expected, the interaction is quite strong at small supercells, but diminishes at larger supercells. Larger Br and I atoms do not fit when considering a zigzag  $1 \times 1$  graphene cell. Also, the trend of the interaction strengths follows the atomic radius for a zigzag  $\sqrt{3} \times \sqrt{3}$  or larger graphene supercells. This indicates that the larger atomic radius, the stronger adatom-adatom interaction, for the same graphene supercell. In general, armchair  $2 \times \sqrt{3}$  gives greater adatom-adatom interaction than zigzag  $2 \times 2$  (see figure 6.4b).

But this trend does not hold true for  $1 \times 1$  graphene cell for adsorption of F and Cl atoms. This is due to the adatom-adatom repulsion at shorter distance for Cl. The optimised lattice parameter for F-F and Cl-Cl interactions amounts to 2.21 Å and 3.11 Å, respectively. Thus for our  $1 \times 1$  graphene cell (2.468 Å), F interacts strongly with neighbouring F atoms whilst neighbouring Cl atoms experience repulsion from each other.

For all adatoms, the adatom-adatom interactions are small for  $3 \times 3$  or larger graphene supercells. So it is expected that orientation effects of these adatoms on the adatom-adsorbed graphene systems are rather minimal for  $3 \times 3$  or larger graphene supercells. However, there will be no orientation effect for F adsorbate configurations.

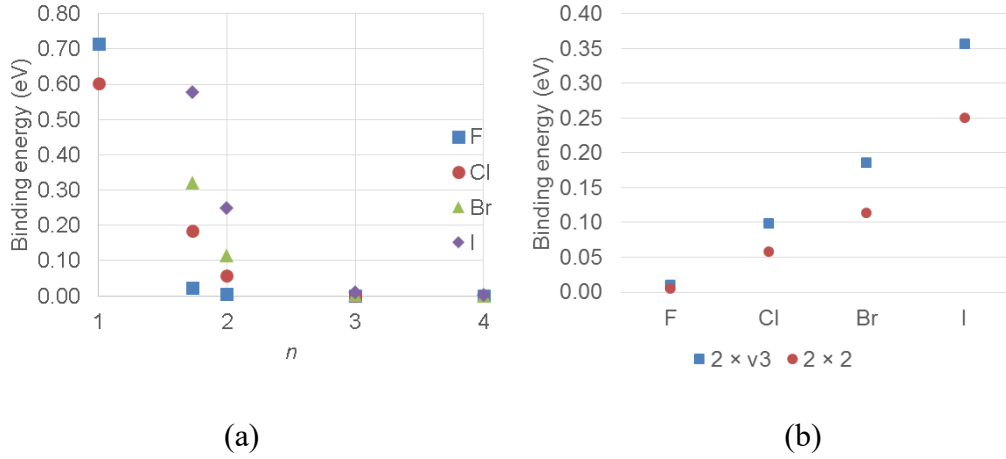


Figure 6.4 Adatom-adatom binding energies for (a) various zigzag  $n \times n$  supercells, (b)  $2 \times \sqrt{3}$  and  $2 \times 2$  supercells.

### 6.3.2 Adatom-adsorbed Graphene

For F cases at all atomic ratios, calculation results on all aspects ( $E_1$ ,  $E_2$ , adatom height, Fermi energy shift, graphene distortion, magnetization and charge transfer) suggest that  $B_z = B_a$ ,  $H_z = H_a$  and  $T_z = T_a$ . For the Cl/Br/I counterparts, calculation results suggest that  $B_z = H_z = T_z$  and  $B_a = H_a = T_a$ . So we group the calculation results of F cases into  $B$ ,  $H$  and  $T$ , while Cl/Br/I cases into  $Z$  and  $A$  (see table 6.1). For these low atomic ratios, calculation with fixed lattice parameter is adequate. For all calculations results at position  $T_a$ , the adatom shifts slightly from its optimum top adsorption site, as indicated by the change of space group between initial and optimised geometries.

Table 6.1 enlists main finding for all systems of adatom-adsorbed graphene. Clearly seen in table 6.1, F is site-dependent, but not orientation-dependent; while Cl, Br and I are orientation-dependent, but not site-dependent. The most stable adsorption site for F atoms is the *top* site. For F cases, the results from zigzag and armchair orientation are the same, as the F-F interaction is very small. The site-independence for Cl, Br and I is in agreement with previous calculations[120]. However, the orientation-dependence for Cl/Br/I is minimal, as the maximum difference of  $E_1$  is  $0.66 - 0.56 = 0.10$  eV (I case at 1:8 atomic ratio). Thus, Cl/Br/I can be placed anywhere on the graphene sheet without considering sites as high symmetry

adsorption points. This implies that Cl/Br/I can occupy multiple sites simultaneously. The value which most likely resides within the accuracy limit of the calculations.

$E_1$  values for Cl/Br/I cases at 1:6 and 1:8 atomic ratio (see table 6.1) do not reflect the highest values, because of the domination of adatom-adatom interactions. To obtain the highest  $E_1$ , further adatom-adatom interaction optimisation with constant cell surface area must be performed. The adatom cell surface area must match to the graphene cell/supercell surface area to maintain the adsorption concentration (at.%). To calculate the adsorption of these adatom cell and graphene cell/supercell, a larger adatom-graphene supercell is required. This in turn creates A : C atomic ratio where  $A > 1$ .

We conclude the general trends from table 6.1 from F to I for each atomic ratio: (1)  $E_2$  decrease; (2) adatom heights increase; (3) charge transfers decrease. The adatom height increase is expected as the atomic/ionic radii increases. Due to stronger interaction, adsorption of F atoms distort the graphene sheet more significantly when compared to adsorptions of the other three halogen atoms. The binding energies of F configurations are around three times stronger compared to Cl/Br/I structures. The trend of charge transfer is in agreement with the Pauling's electronegativity, with F, Cl, Br, I absorb charge from graphene. F has the highest Pauling's electronegativity among all elements. Cl has less binding energies than F, *i.e.* is in agreement with the experimental measurements and theoretical predictions by Wu *et al.* [92]

Table 6.1 Halogen-adsorbed graphene. All cases were calculated using van der Waals and dipole corrections. Bold numbers are the values at the most stable position for F cases. Value in brackets are calculation results from previous studies, with its reference number in the square bracket. *B, H, T, Z, A* are bridge, hollow, top, zigzag and armchair. All cases do not open the band gap at Fermi energy.

	F			Cl		Br		I	
	<i>B</i>	<i>H</i>	<i>T</i>	<i>Z</i>	<i>A</i>	<i>Z</i>	<i>A</i>	<i>Z</i>	<i>A</i>
<i>1:6 atomic ratio</i>									
$E_1$ (eV) ~	1.41	1.02	<b>1.78</b>	0.58 <sup>^</sup>	-	0.64 <sup>^</sup>	-	0.84 <sup>^</sup>	-
$E_2$ (eV) ~~	1.38	1.00	<b>1.76</b>	0.40	-	0.32	-	0.26	-
Adatom height (Å)	1.92	2.28	<b>1.81</b>	3.10	-	3.32	-	3.53	-
Fermi energy shift (eV) #	-1.98	-2.66	<b>-1.43</b>	-1.52	-	-1.14	-	-0.15	-
Graphene distortion (Å)	0.19	0.01	<b>0.57</b>	0.00	-	0.00	-	0.01	-
Magnetization ( $\mu_B$ )	0.00	0.68	<b>0.00</b>	0.79	-	0.83	-	0.56	-
Charge transfer ( <i>e</i> )	0.45	0.37	<b>0.55</b>	0.20	-	0.15	-	0.10	-
<i>1:8 atomic ratio</i>									
$E_1$ (eV) ~	1.50	1.16	<b>1.86</b> (2.00[48])	0.57 <sup>^</sup>	0.59 <sup>^</sup>	0.51 <sup>^</sup>	0.57 <sup>^</sup>	0.56 <sup>^</sup>	0.66 <sup>^</sup>
$E_2$ (eV) ~~	1.49	1.15	<b>1.86</b>	0.51	0.49	0.40	0.39	0.31	0.31
Adatom height (Å)	1.97	2.28	<b>1.82</b>	2.97	3.00	3.24	3.26	3.50	3.48
Fermi energy shift (eV) #	-1.88	-2.44	<b>-1.23</b>	-1.60	-1.61	-1.30	-1.30	-0.50	-0.51
Graphene distortion (Å)	0.21	0.02	<b>0.58</b>	0.02	0.04	0.01	0.03	0.01	0.04
Magnetization ( $\mu_B$ )	0.15	0.61	<b>0.12</b>	0.75	0.74	0.80	0.79	0.84	0.61
Charge transfer ( <i>e</i> )	0.48	0.42	<b>0.55</b>	0.25	0.25	0.19	0.19	0.13	0.13
<i>1:18 atomic ratio</i>									
$E_1$ (eV) ~	1.66	1.45	<b>1.97</b> (2.90[45])	0.77 (1.27[45])	-	0.60 (0.98[45])	-	0.47 (0.75[45])	-
$E_2$ (eV) ~~	1.66	1.45	<b>1.96</b>	0.77	-	0.60	-	0.47	-
Adatom height (Å)	2.13	2.41	<b>1.90</b> (1.87[45])	2.98 (2.56[45])	-	3.19 (2.78[45])	-	3.42 (3.26[45])	-
Fermi energy shift (eV) #	-1.51	-1.78	<b>-0.93</b>	-1.50	-	-1.34	-	-0.92	-
Graphene distortion (Å)	0.19	0.05	<b>0.91</b>	0.06	-	0.06	-	0.07	-
Magnetization ( $\mu_B$ )	0.43	0.49	<b>0.00</b>	0.59	-	0.65	-	0.72	-
Charge transfer ( <i>e</i> )	0.54	0.51	<b>0.57</b> (0.59[46])	0.39 (0.41[46])	-	0.32 (0.34[46])	-	0.24 (0.28[46])	-

~ Binding energy with respect to adatom.

~~ Binding energy with respect to adatom-adatom interaction.

# Fermi energy shift from pristine graphene.

<sup>^</sup> This value is our calculation result only and does not reflect the highest value.



The trend from Cl to I sees the decrease in Fermi energy shifts. Thus for Cl to I, the stronger interaction with graphene, the wider the shift in Fermi energy shift. But the site dependence of F cases derive nonlinearity in Fermi energy shifts trends. However, magnetizations do not exhibit any trends. Via examining the group 14 in the periodic table of elements, Akturk *et al.* [65] found that: (1) binding energy of Si-adsorbed graphene is higher than Ge counterpart; (2) adatom height of Si-adsorbed is shorter than Ge counterpart. These two trends are similar to the trends of our results on Cl- and Br-adsorbed graphene. The main difference for Cl, Br and I cases is the  $E_1$ , which is solely caused by the adatom-adatom interaction. This finding highlights the importance of orientation. However, there is a noticeable difference in magnetization for zigzag ( $0.84\mu_B$ ) and armchair ( $0.61\mu_B$ ) orientation for I case at 1:8 atomic ratio.

Following the trends of atomic ratios, as the atomic ratios decrease: (1) the  $E_2$  increase; (2) F adatom heights slightly increase; (3) Cl/Br/I adatom heights slightly decrease; (4) Cl/Br/I charge transfers increase. The increase in binding energies and charge transfers are due to more C atoms pull the adatoms. The trends of adatom heights are not so obvious, as their maximum difference is less than  $0.13 \text{ \AA}$ . The site-independence of Cl, Br, I is probably due to the adatoms' size or mass compared to carbon's atomic size or mass. F has comparable atomic radius to C, but Cl, Br and I are 29%, 48% and 73% larger than C in radius. F is slightly heavier than C, but Cl, Br and I are 3, 7 and 11 times heavier than C.

In table 6.2, we show the difference between the results with and without van der Waals and dipole corrections. These two corrections have relatively small impacts for F cases, but have significant impacts for Cl/Br/I cases. The corrections alter  $E_2$  for F cases for  $\approx 4.6\%$ , but from 6.9% to 52.0% for Cl/Br/I cases. This signifies the importance of these corrections. Based on  $E_2$  in table 6.2, we can derive an additional trend that van der Waals and dipole corrections are increasing (1) from F to I at each atomic ratio and (2) from low to high atomic ratio.

Based on the analysis above, we can summarize the trends accompanying halogen adsorption on graphene in figure 6.5. These trends may provide guidelines for future experimental studies.

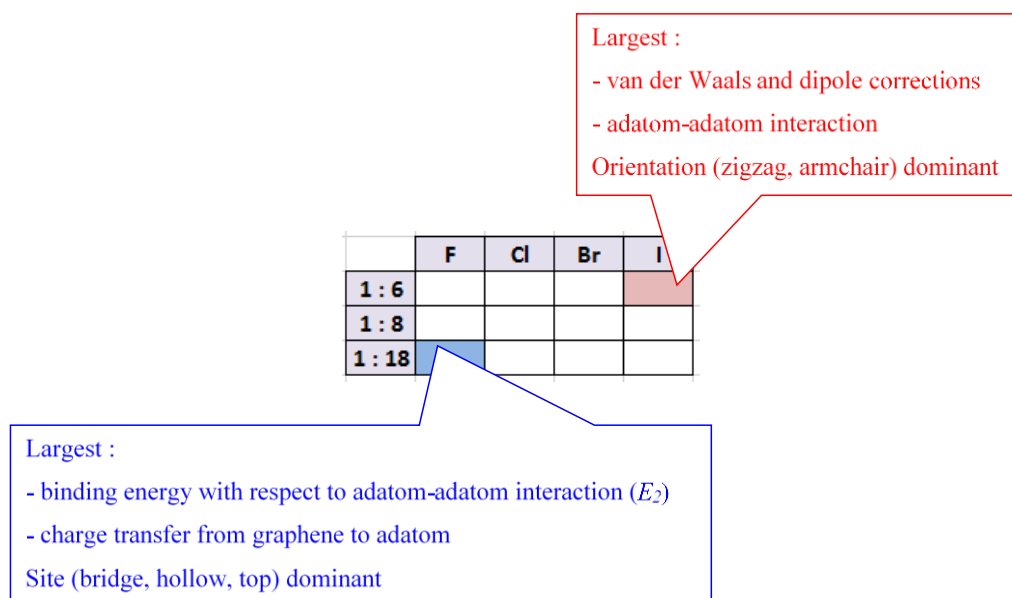


Figure 6.5 Some trends for halogen adsorption on graphene at 1:6, 1:8 and 1:18 atomic ratios.

Table 6.2 Difference between calculations with and without van der Waals and dipole corrections in halogen-adsorbed graphene. All values are in %. *B, H, T, Z, A* are bridge, hollow, top, zigzag and armchair.

<i>Atomic ratio</i>	F			Cl		Br		I		
	<i>B</i>	<i>H</i>	<i>T</i>	<i>Z</i>	<i>A</i>	<i>Z</i>	<i>A</i>	<i>Z</i>	<i>A</i>	
<i>1:6</i>	$E_1 \sim$	3.4	0.3	4.8	13.1	-	22.6	-	30.6	-
	$E_2 \sim\sim$	3.2	0.6	4.7	14.0	-	29.5	-	52.0	-
	Adatom height	0.1	2.0	0.2	7.0	-	10.9	-	14.3	-
	Fermi energy shift #	0.2	1.1	0.6	1.1	-	0.2	-	3.7	-
	Graphene distortion	0.5	4.3	0.1	28.4	-	67.1	-	69.4	-
	Magnetization	-	1.3	-	1.9	-	2.7	-	5.3	-
	Charge transfer	0.0	2.3	0.5	6.7	-	7.6	-	4.3	-
<i>1:8</i>	$E_1 \sim$	3.0	0.5	4.6	13.8	11.9	24.7	21.6	35.0	30.2
	$E_2 \sim\sim$	3.0	0.6	4.5	13.7	12.4	26.4	25.3	45.6	44.7
	Adatom height	0.1	2.3	0.2	6.5	5.7	8.9	9.1	10.3	11.8
	Fermi energy shift #	0.2	1.4	0.8	2.5	2.0	1.5	1.2	2.4	2.3
	Graphene distortion	0.4	24.8	0.5	45.8	9.0	47.9	16.8	62.1	14.5
	Magnetization	0.5	2.3	5.4	1.2	1.7	1.4	2.3	1.0	1.4
	Charge transfer	0.1	2.7	0.6	6.1	5.3	5.6	5.6	3.6	3.4
<i>1:18</i>	$E_1 \sim$	2.8	1.3	4.5	6.9	-	16.2	-	32.5	-
	$E_2 \sim\sim$	2.8	1.3	4.5	6.9	-	16.3	-	33.1	-
	Adatom height	0.6	0.1	0.4	5.3	-	7.9	-	8.1	-
	Fermi energy shift #	0.8	0.1	1.0	2.0	-	1.8	-	1.8	-
	Graphene distortion	4.7	40.9	2.8	42.2	-	50.8	-	42.7	-
	Magnetization	1.2	0.1	-	2.2	-	2.6	-	1.6	-
	Charge transfer	1.3	0.0	0.3	3.5	-	3.4	-	2.4	-

~ Binding energy with respect to adatom.

~~ Binding energy with respect to adatom-adatom interaction.

# Fermi energy shift from pristine graphene.

### 6.3.3 Electronic analysis

Figure 6.6 displays plotted DOS curves for all considered cases. The most striking feature in this figure is that all cases do not open the band gap at Fermi energy, thus all cases exhibit metallic character. It is seen that F cases are different from Cl/Br/I cases. Graphene DOS is altered significantly by F atoms. This indicates that there is strong bond between F and graphene. On the contrary, Cl/Br/I-graphene DOS are nearly algebraic addition of graphene

DOS and the element's DOS (see figures 6.S2 in the supplementary data). This indicates that the bonds between Cl/Br/I and graphene are relatively weak (physisorption). For Cl, Br, I cases, the peaks near Fermi energy belong to  $2p^5$ ,  $3p^5$  and  $4p^5$  electronic occupation with 3 spin up and 2 spin down.

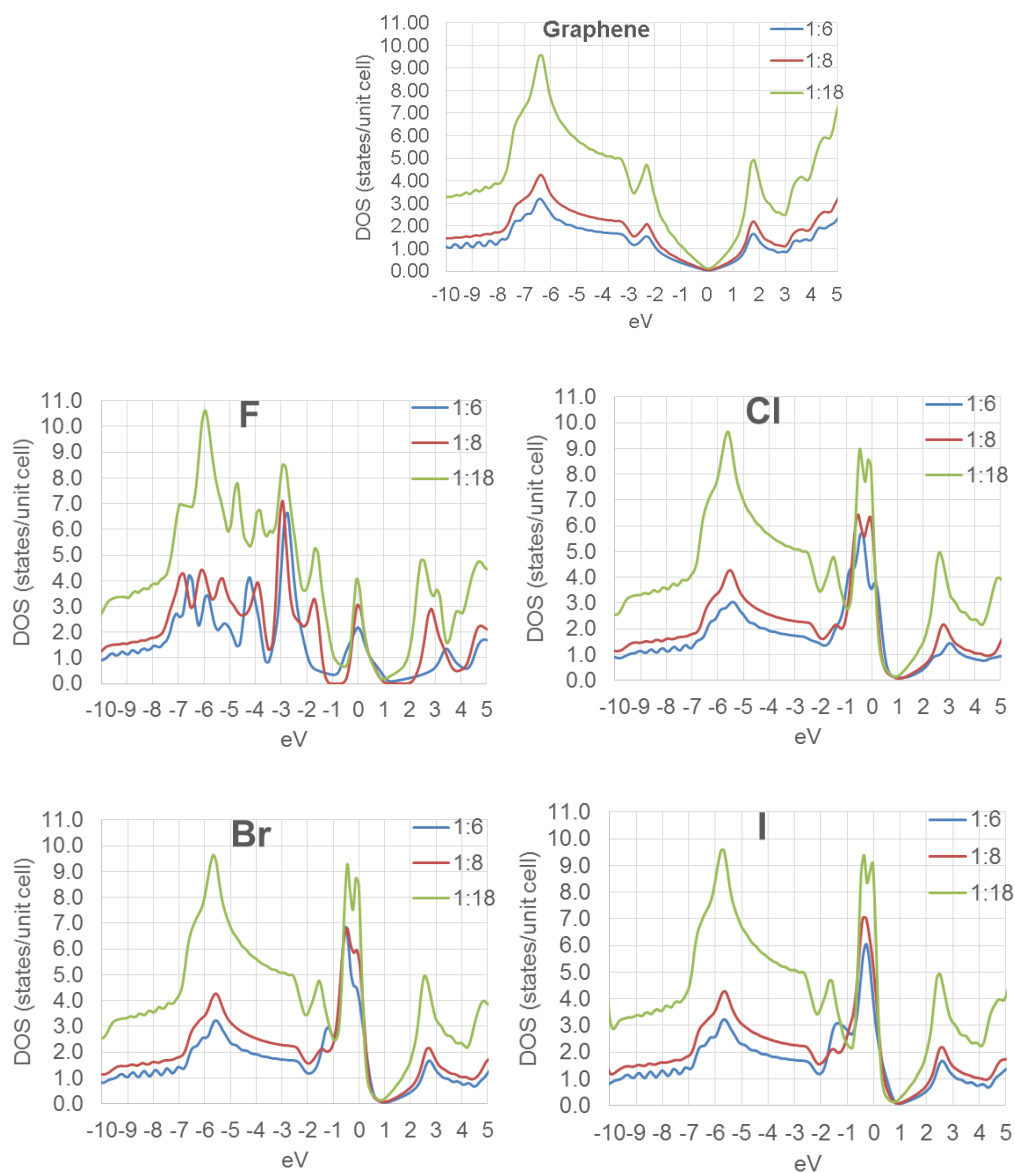


Figure 6.6 DOS (total spin) and Fermi energy (0 eV) of halogen-adsorbed graphene at 3 different atomic ratios (1:6, 1:8 and 1:18). F is top ( $T$ ) cases, Cl/Br/I are the average values of zigzag ( $Z$ ) and armchair ( $A$ ) cases.

To illustrate how the charges are distributed in the system, charge density differences were calculated for two typical cases, F and Br at 1:8 atomic ratio,  $T_z$  case (see figures 6.7 and

6.8). All other F cases are expected to exhibit very similar charge distribution to the one shown in figure 6.7. Similarly, other Cl/Br/I are anticipated to be similar to charge distribution in figure 6.8. These two figures clearly show: (1) that electron charges are transferred from graphene to the adatoms, and (2) interaction of F-graphene is stronger than Cl/Br/I-graphene.

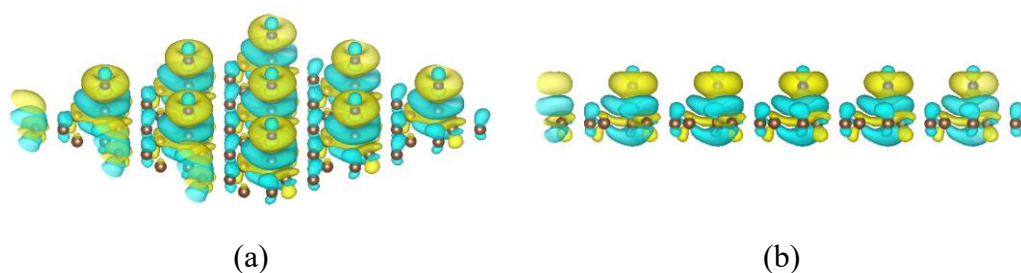


Figure 6.7 Charge density difference of F-adsorbed graphene at 1:8 atomic ratio,  $T_z$  case, (a) is isometric view, (b) is side view. Brown spheres are C, grey spheres are F. Yellow surfaces enclose the charge density greater than  $0.01 \text{ electron}/\text{\AA}^3$  (electron surplus), while cyan surfaces enclose the charge density less than  $-0.01 \text{ electron}/\text{\AA}^3$  (electron deficit).

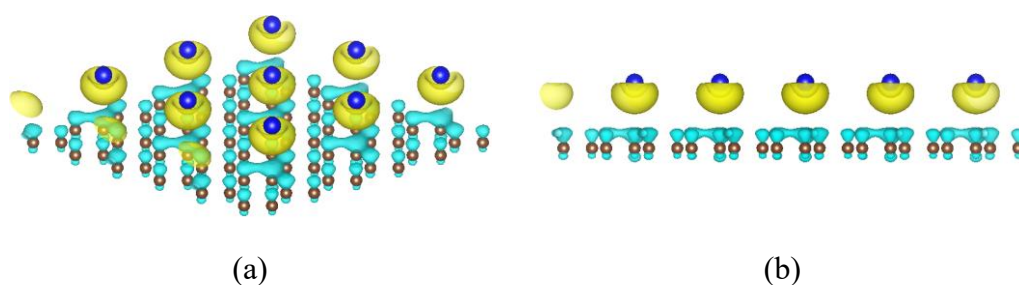


Figure 6.8 Charge density difference of Br-adsorbed graphene at 1:8 atomic ratio,  $T_z$  case, (a) is isometric view, (b) is side view. Brown spheres are C, blue spheres are Br. Yellow surfaces enclose the charge density greater than  $0.01 \text{ electron}/\text{\AA}^3$  (electron surplus), while cyan surfaces enclose the charge density less than  $-0.01 \text{ electron}/\text{\AA}^3$  (electron deficit).

## 6.4 Conclusions

The electronic structure of elemental adsorption on graphene is affected by both site of adsorption (*i.e.* bridge, hollow or top), and also the relative orientation of the adsorbed sites (*i.e.* zigzag or armchair). Overall, we have shown that geometry and orientation are important in elemental adsorption on graphene. It is found that adsorption of F is merely site-dependent (top), but adsorption of Cl, Br and I has merely small orientation-dependent. F is adsorbed to graphene at about three times stronger than Cl/Br/I. Cl/Br/I-adsorbed graphene carries similar

properties, as confirmed by the density of states (DOS) and charge density distribution. General trends from F at low concentration to I at high concentration are binding energies with respect to adatom-adatom interaction, charge transfers from graphene to adatom, site domination decrease; while van der Waals and dipole corrections, adatom-adatom interactions, orientation domination increase. All cases do not open the band gap at Fermi energy.

## 6.5 Supplementary Data

Table 6.S1 Converged  $k$ -points and supercell sizes used in each stage.

Stage	Description of calculation	$k$ -points	Atomic ratio	Cell/Supercell	Supercell size (Å)
1	Adatom energy	$1 \times 1 \times 1$	-	cubic	$15 \times 15 \times 15$
	Pristine graphene energy	$24 \times 24 \times 1$	-	zigzag $2 \times 2$	$4.936 \times 4.936 \times 15$
2	Adatom-adatom interaction	$48 \times 48 \times 1$	-	zigzag $1 \times 1$	$2.468 \times 2.468 \times 15$
		$28 \times 28 \times 1$	-	zigzag $\sqrt{3} \times \sqrt{3}$	$4.275 \times 4.275 \times 15$
		$24 \times 28 \times 1$	-	armchair $2 \times \sqrt{3}$	$4.936 \times 4.275 \times 15$
		$24 \times 24 \times 1$	-	zigzag $2 \times 2$	$4.936 \times 4.936 \times 15$
		$16 \times 16 \times 1$	-	zigzag $3 \times 3$	$7.404 \times 7.404 \times 15$
		$12 \times 12 \times 1$	-	zigzag $4 \times 4$	$9.872 \times 9.872 \times 15$
3	Graphene-adatom internal structure optimisation	$7 \times 7 \times 1$	1:6	zigzag $\sqrt{3} \times \sqrt{3}$	$4.275 \times 4.275 \times 15$
		$6 \times 6 \times 1$	1:8	zigzag $2 \times 2$	$4.936 \times 4.936 \times 15$
		$6 \times 7 \times 1$	1:8	armchair $2 \times \sqrt{3}$	$4.936 \times 4.275 \times 15$
		$4 \times 4 \times 1$	1:18	zigzag $3 \times 3$	$7.404 \times 7.404 \times 15$
4	Graphene-adatom DOS	$28 \times 28 \times 1$	1:6	zigzag $\sqrt{3} \times \sqrt{3}$	$4.275 \times 4.275 \times 15$
		$24 \times 24 \times 1$	1:8	zigzag $2 \times 2$	$4.936 \times 4.936 \times 15$
		$24 \times 28 \times 1$	1:8	armchair $2 \times \sqrt{3}$	$4.936 \times 4.275 \times 15$
		$16 \times 16 \times 1$	1:18	zigzag $3 \times 3$	$7.404 \times 7.404 \times 15$

Table 6.S2 Atomic/ionic radius and Pauling's electronegativity[21, pp. 255–257].

Atom	Radius (Å)	Pauling's electronegativity	Ion	Radius (Å)
C	0.77	2.5	-	-
F	0.71	4.0	F <sup>-</sup>	1.19
Cl	0.99	3.0	Cl <sup>-</sup>	1.67
Br <sup>#</sup>	1.14	2.8	Br <sup>-</sup>	1.82
I <sup>#</sup>	1.33	2.5	I <sup>-</sup>	2.06

# Relatively big atom

Table 6.S3 Calculation results of graphene and the elements.

	No. of valence electrons	Magnetization ( $\mu_B$ )	Fermi energy (eV)
Graphene	24, 32, 72 <sup>^</sup>	0	-2.29
C	4	2	-6.03
F	7	1	-10.26
Cl	7	1	-8.08
Br	7	1	-7.41
I	7	1	-6.67

<sup>^</sup> for 1:6, 1:8, 1:18 atomic ratios

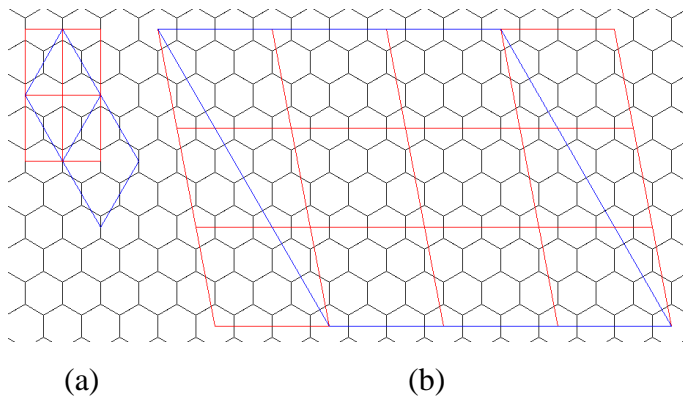


Figure 6.S1 Equivalency of graphene supercells, (a) armchair  $1 \times \sqrt{3}$  (red) is equivalent to zigzag  $2 \times 2$  (blue), (b) slant  $3 \times \sqrt{7}$  (red) is equivalent to zigzag  $9 \times 9$  (blue). This figure was adopted from figure 4.6.

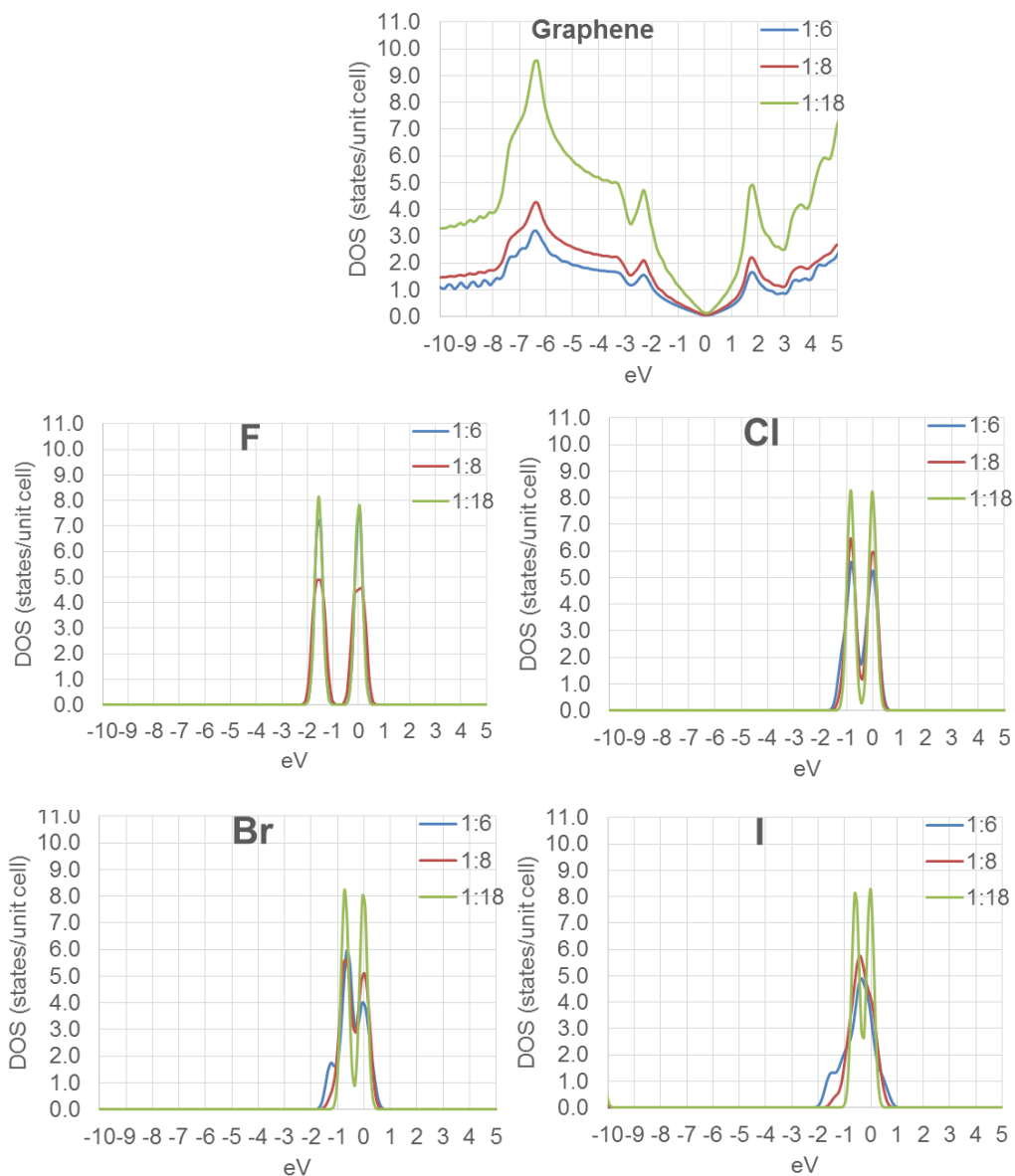


Figure 6.S2 DOS (total spin) and Fermi energy (0 eV) of graphene and the elements at 3 atomic ratios. Average values of zigzag (*Z*) and armchair (*A*) cases are used.

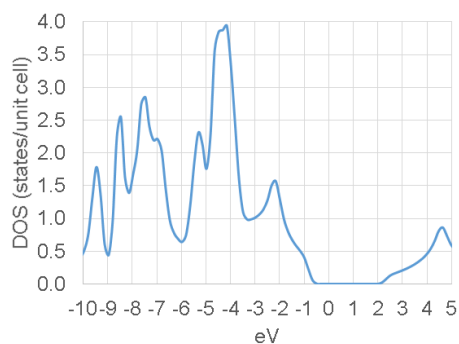


Figure 6.S3 DOS (total spin) and Fermi energy (0 eV) of fluorographene, band gap  $\approx 2.99$  eV.



---

A manuscript based on the major research outcomes of this chapter was published in :

H. Widjaja, Z.-T. Jiang, M. Altarawneh, C.-Y. Yin, B.-M. Goh, N. Mondinos, and B. Z. Dlugogorski, “Towards a better understanding of the geometrical and orientational aspects of the electronic structure of halogens (F–I) adsorption on graphene,” *Appl. Surf. Sci.*, vol. 356, pp. 370–377, 2015. (*This is publication [2] in the List of Publications*)

---

# CHAPTER SEVEN

## DOUBLE-SIDED FLUORINE AND CHLORINE ADSORPTION ON GRAPHENE

---

### 7.1 Introduction

The calculation procedure developed in chapters 1 to 4 was thirdly applied to F and Cl at various atomic ratios, spanning from very low atomic ratio (C: F/Cl = 18:2) to full adsorption (C:F/Cl = 2:2), in order to elucidate effects of adsorption trends in a wide range of atomic ratios. Properties of elemental adsorption on graphene have been calculated in terms of site (bridge, hollow, top), *e.g.* metal adatoms [20], H – Bi (except noble gases and lanthanides) adatoms [45]. However, graphene with adsorbed O at atomic ratio of O/C of less than 30% was found to have a nonlinear band gap [49]. This nonlinearity appears to be due to the positions of the adatoms relative to one another. This suggests that the electronic structure of elemental adsorption on graphene is affected not only by side of adsorption (single- or double-sided) and site of adsorption (bridge, hollow or top), but also to the relative orientation of the adsorbed sites (zigzag or armchair) (figure 7.1) [121].

Numerous syntheses, progress reports, simulations, experimental and theoretical studies have addressed adsorption of halogens on graphene[48], [54], [71], [92], [113], [115], [122], [123]. There are two well-known results for fluorinated graphene. Fully fluorinated graphene (fluorographene/CF) is the most stable configuration for double-sided case, while CF<sub>0.250</sub> (figure 7.2) is the counterpart for single-sided case. In regards to figure 7.2, two factors appear to play an important role, namely, atomic percent/concentration (at.%) and atomic ratio, *e.g.* a 25 at.% has multiple C:F atomic ratios (4:1, 8:2, 12:3, 16:4, ...). CF<sub>0.250</sub> cannot be explained using the simplest 4:1 atomic ratio, but rather 8:2 atomic ratio with certain adatom configuration. CF expands the graphene cell lattice constant of  $\approx 0.13 \text{ \AA}$  and opens a band gap

of  $\approx 3.00$  eV, while  $\text{CF}_{0.250}$  opens a band gap of  $\approx 2.93$  eV[48]. Liu *et al.* calculated fluorinated graphene from 3.1 at.% (C:F = 32:1) to 100 at.% (C:F = 2:2) with zigzag graphene cell/supercells [122]. There are some concerns on Liu *et al.*'s work, in relation to drawing trends on  $\text{CF}_a$  ( $a$  = atomic concentration). Firstly, the cases are mixed between single- and double-sided. Secondly, one-side-atom-addition/removal might be less stable than two-side-atom-addition/removal.

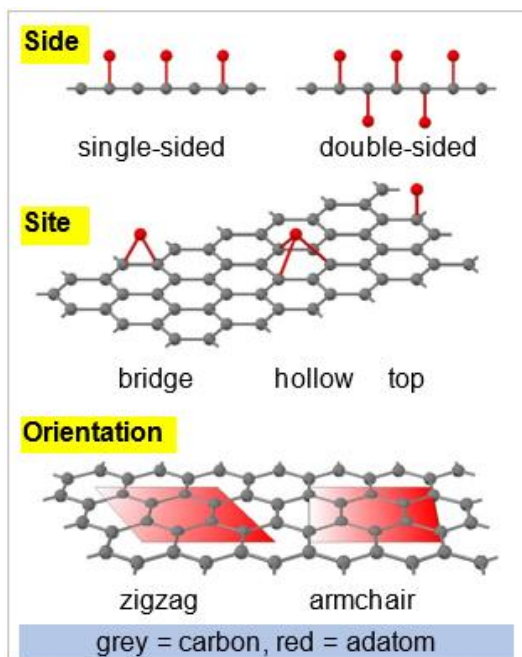


Figure 7.1 Side, site and orientation in elemental adsorption on graphene.

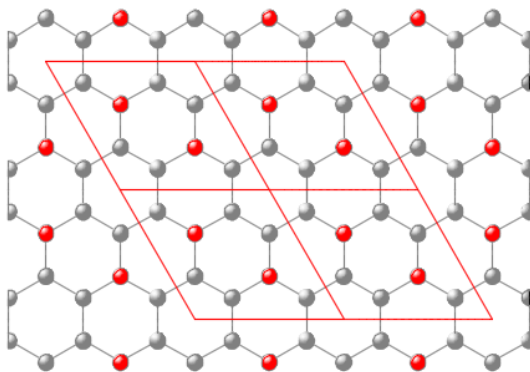


Figure 7.2 Most stable configuration of single-sided fluorinated graphene of 25 at.%, red spheres are F atoms, grey spheres are C atoms [48]. This figure was adopted from figure 6.1.

In this contribution, density functional theory (DFT) calculations were applied to perform investigation on the electronic structures of F and Cl adsorption on graphene in terms of adsorption orientation, at various atomic ratios, spanning from very low atomic ratio (C:F/Cl = 18:2) to full adsorption (C:F/Cl = 2:2). The side is fixed to double-sided, to give consistent trends on the results and can account for high atomic concentrations. The site is fixed to top, as it is adequate for the calculations. The most stable site for F is top, while Cl is site-independent, so any site for Cl can be picked. Overall, it is highlighted some prominent effects of orientation aspects on various properties such as binding energy, graphene cell lattice constant expansion, adatom height, band gap, Fermi energy, charge transfer, magnetization and density of states (DOS).

## 7.2 Methods

To investigate the most stable configuration, it is necessary to examine all possible positions. Unfortunately, this is not practical, as the number of cases will be infinite. As such, this study is limited to the cases with same number of adatom addition/removal on both sides of graphene supercells. So the calculations for F/Cl-adsorbed to graphene were set to the following atomic ratios (X=F/Cl) :  $CX_{0.500}$  (8:4), CX (2:2), and pairs {adatom addition and removal} of { $CX_{0.111}$  (18:2) and  $CX_{0.889}$  (18:16)}; { $CX_{0.250}$  (8:2) and  $CX_{0.750}$  (8:6)}; { $CX_{0.333}$  (6:2) and  $CX_{0.667}$  (6:4)}. Five graphene cells/supercells were used (figures 7.3a – 7.3e). However, slant  $3 \times \sqrt{7}$  was not used, because the adatoms (F/Cl) are too far to interact with one another. As such, the results for  $3 \times 3$  are expected to be the same as  $3 \times \sqrt{7}$ .

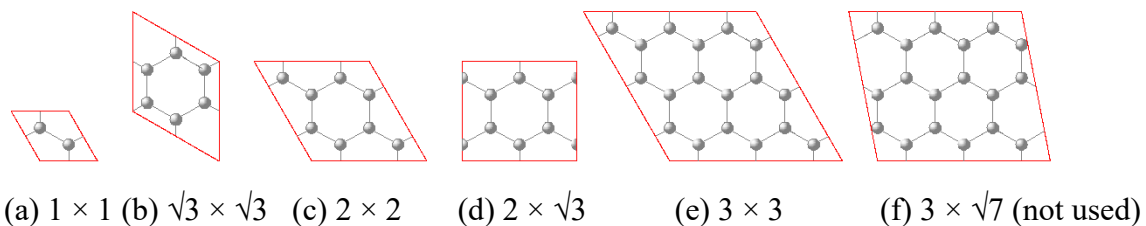


Figure 7.3 Graphene cells/supercells, all are zigzag orientation, except  $2 \times \sqrt{3}$  is armchair and  $3 \times \sqrt{7}$  is slant.

All structural optimisations and energy calculations were performed using the plane-wave DFT code of VASP. Calculation methodology comprises spin-polarized PAW-GGA functional [89], HSE06 functional [19], van der Waals correction by Grimme (D2) [88] method, and a Gaussian smearing. For our cases, dipole correction to  $z$  direction is not needed, as the number of adatom is the same on both sides of the graphene.

The calculations were conducted four stages: (1) adatom and pristine graphene energy, (2) geometrical analysis for positioning the adatoms using GGA, (3) graphene-adatom lattice expansion with internal structure optimisation using GGA, and (4) adatom-graphene density of states (DOS) calculation using both GGA and HSE06. In the third stage, the calculations were performed using symmetrical lattice expansion (lattice parameters  $a$  and  $b$  are at constant proportion,  $c = 15 \text{ \AA}$ ,  $\alpha = \beta = 90^\circ$ ,  $\gamma = 120^\circ$ ). We set the plane wave cut off energy of 500 eV. In all structures, we deployed a tolerance of less than 0.1 meV for energy and less than 0.05 eV/Å for forces on each atoms.

The binding energy, lattice constant expansion, adatom height, band gap, Fermi energy, charge transfer, magnetization and DOS were calculated for all the cases. Binding energy  $E$  is calculated using equation :

$$E = (E_{\text{graphene}} + E_{\text{upper adatoms}} + E_{\text{lower adatoms}} - E_{\text{adatoms-graphene}}) / \text{number of adatoms} \quad (7.1)$$

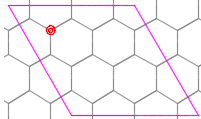
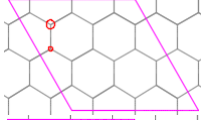
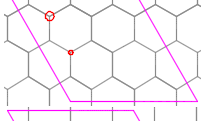

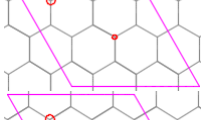
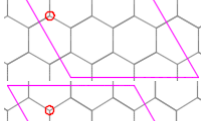
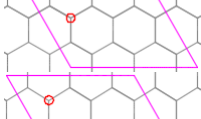
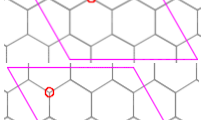
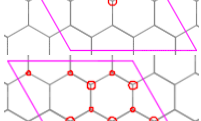
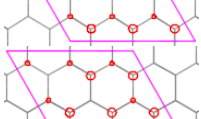
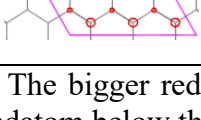
where  $E_{\text{graphene}}$  denotes the energy of the pristine graphene,  $E_{\text{upper adatoms}}$  signifies the energy of the relaxed adatoms above the graphene (without graphene sheet),  $E_{\text{lower adatoms}}$  signifies the energy of the relaxed adatoms below the graphene (without graphene sheet) and  $E_{\text{adatoms-graphene system}}$  is the total energy of the adatoms and graphene after the adatom is attached to the graphene. At a lattice constant of *e.g.*  $a_0$ , all four energy terms were relaxed at  $a_0$ .

Herein, we compute the band gap based on the DOS [90, p. 214] analysis in which a zero DOS value marks the Fermi energy. Adatom height ( $\text{\AA}$ ) signifies the difference in  $z$ -coordinate between adatom's and the average of  $z$ -coordinates of carbon atoms. Total charge is estimated as the sum of total spin-up and spin-down values whereas magnetisation is expressed as the variation between total spin up and total spin down at the Fermi energy level. We calculate charge transfer (as a scalar quantity) based on the Bader's [91] formalism. A positive value of charge transfer indicates that charge is shifted from graphene to adsorbates.

### 7.3 Results and Discussion

At high atomic ratio, it is well known that chair structure of CF and CCl [113] is the most stable configuration. At low atomic ratio, Yuan and co-researchers concluded that F atoms tend to form in pairs during fluorination [124]. Whilst at low atomic ratio for Cl case, Şahin and co-researchers stated that single Cl vacancy on one side of the graphene imposes another single Cl vacancy on the other side of the graphene [54]. Armed with these aforementioned findings, we did extensive tests on many geometrical configurations using GGA functional, and table 7.1 summarizes the most important test results.

Table 7.1 Configurations and binding energies for F- and Cl-adsorbed graphene.

Configuration <sup>a</sup>	F case		Cl case	
	Lattice constant (Å)	Binding energy (eV/adatom)	Lattice constant (Å)	Binding energy (eV/adatom)
	7.40	2.06	7.40	1.01
	7.40	2.55 <sup>b</sup>	7.40	1.08 <sup>b</sup>
	7.40	1.88	7.40	1.00
	7.40	2.31	7.40	0.83
	7.40	1.86	7.40	0.72
	7.40	0.92	7.40	0.10
	7.40	0.53	7.40	0.10
	7.40	1.06	7.40	0.10
	7.40	1.77	7.40	0.61
	7.74	2.18 <sup>c</sup>	7.61 (non-bonding) 8.51 (bonding)	0.12 (non-bonding) 0.31 <sup>c</sup> (bonding)
	7.74	2.02	7.61 (non-bonding) 8.51 (bonding)	0.14 (non-bonding) 0.20 (bonding)

<sup>a</sup> The bigger red circle is the adatom above the graphene while the smaller red circle is the adatom below the graphene.

<sup>b</sup> The most stable configuration (adatom addition).

<sup>c</sup> The most stable configuration (adatom removal).

Based on table 7.1, we can verify that for F/Cl-adsorbed graphene (CX, X=F/Cl) : (1) at the same atomic concentration, double-sided is more stable than single-sided adsorption; (2)  $C_2X_2$  cluster configuration of figure 7.4 gives stability for both addition and removal. This finding facilitates the positioning of adatoms on both side of the graphene in a more manageable manner. For clarity in the subsequent figures, configuration shown in figure 7.4 is represented using a triangle (figure 7.5). Unfortunately for  $CX_{0.500}$ , further simplification for cluster with four adatoms cannot be verified from our cases. As a result, there are more than ten combinations appear for  $CX_{0.500}$ . So all possible initial configurations can now be determined as shown in figure 7.6.

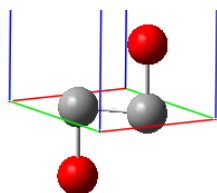


Figure 7.4 Most stable  $C_2X_2$  cluster (X=F/Cl), grey is C, red is F/Cl.

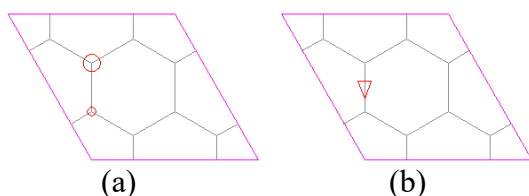


Figure 7.5 Two-adatom adsorbed on graphene, big red circle is adatom at the upper side of graphene, small red circle is adatom at the lower side of graphene (a) is represented using a triangle (b).



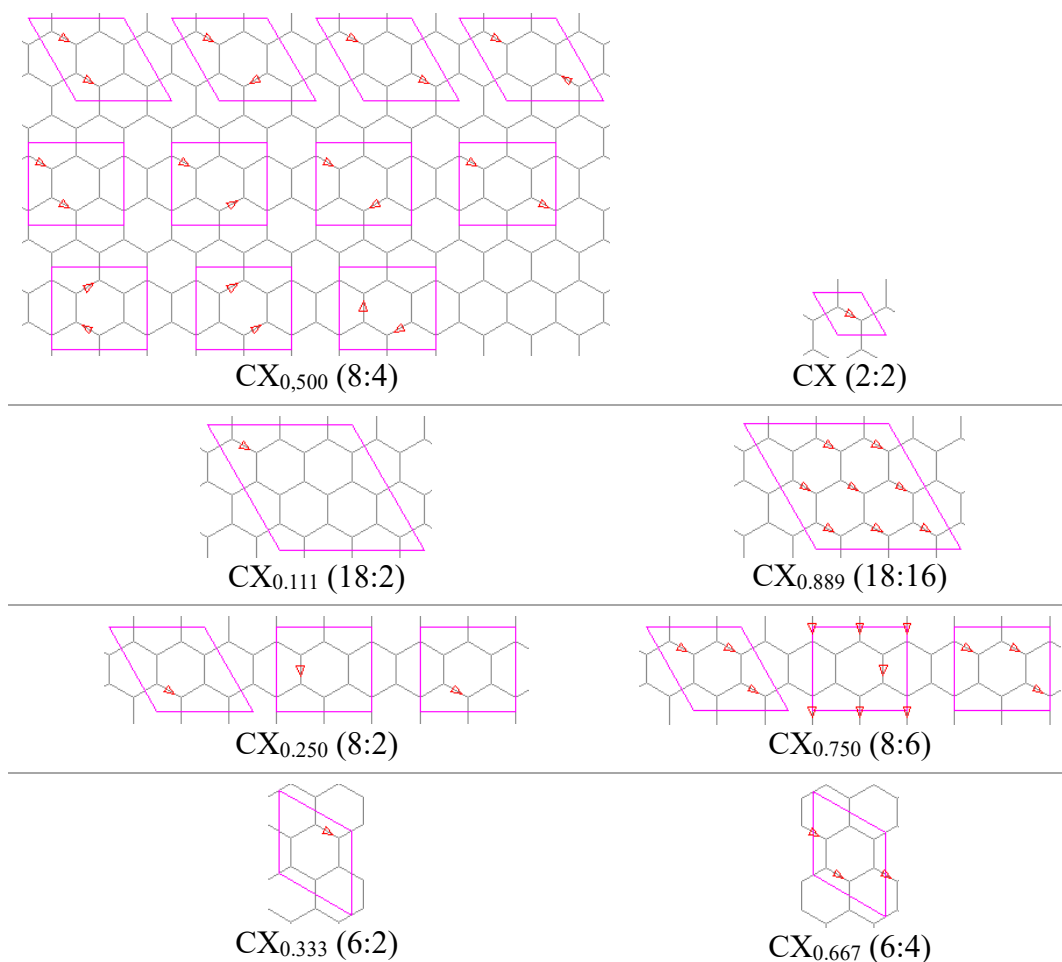


Figure 7.6 All possible initial configurations for F/Cl-adsorbed graphene based on the used atomic ratios, red triangle is a pair of F/Cl adsorbed on the upper and lower side of the graphene ( $X=F/Cl$ ).

Figures 7.7 – 7.9 show the calculation results. The most stable orientation for  $CX_{0.250}$  and  $CX_{0.750}$  is armchair,  $CF_{0.500}$  is zigzag and  $CCl_{0.500}$  is armchair. This shows that orientation does affect the stability of  $CX_a$ . Although F and Cl are in a group (halogens) in periodic table of elements, their adsorption trends on graphene are very dissimilar (figure 7.9). This indicates that having similar electronic configuration ( $s^2p^5$  or one unpaired valence electron) does not give similar trends when adsorbed to graphene. Adatom's size and mass compared to carbon's size and mass seem to have greater influence. F has comparable atomic radius to C, but Cl is 29% larger than C in radius. F is slightly heavier than C, but Cl is three times heavier than C. Van den Broek and co-researchers [125] showed in their calculations, that fully adsorbed F on silicene (SiF) and germanene (GeF) exhibit some similarities to CF, *e.g.* most stable at top site

with CF-like structure. So, our surmise is within the same group in the periodic table of elements, applying smaller/lighter adsorbate atom (or bigger/heavier adsorbent atom) may show similarities. On comparing atomic size and mass, F-adsorbed graphene might be analogous to Cl-adsorbed on silicene, but this needs further examinations in future research.

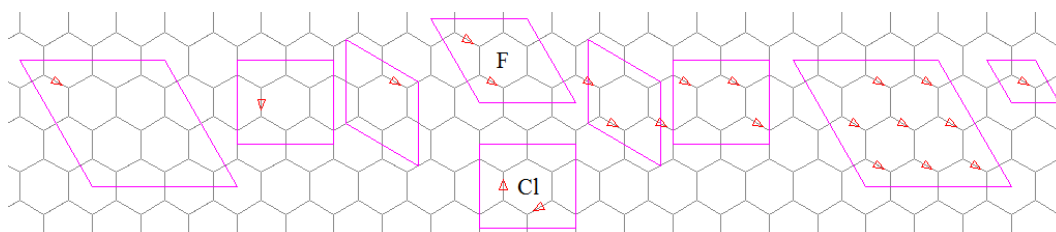
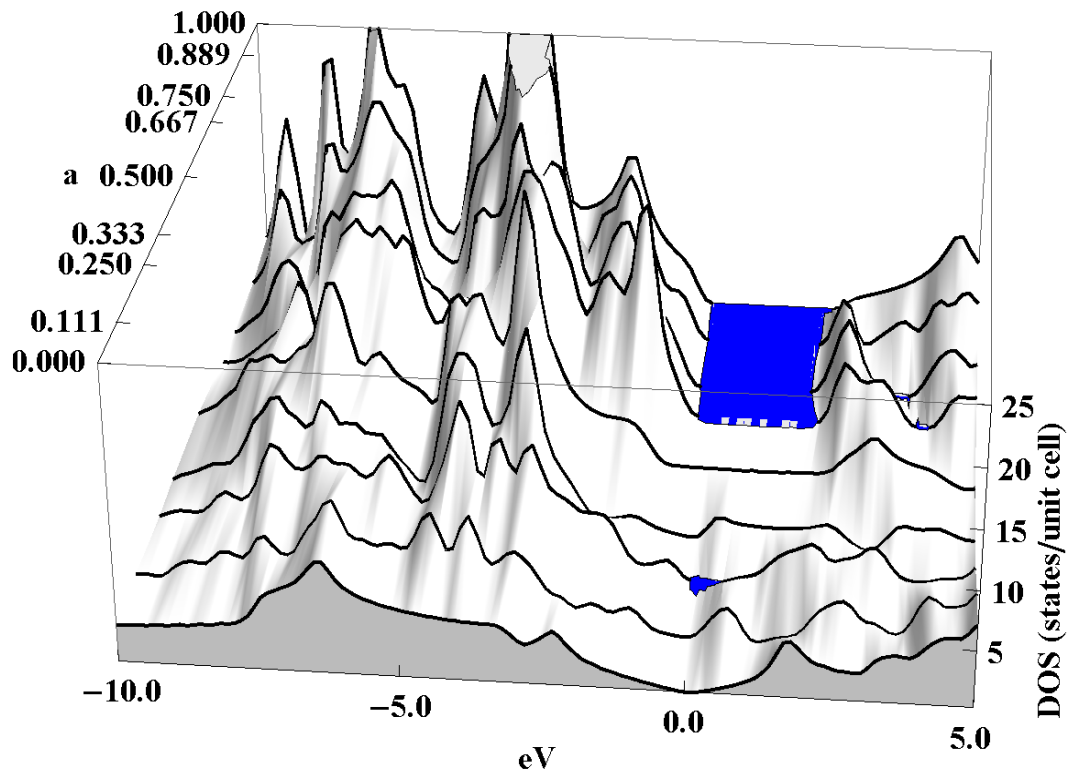
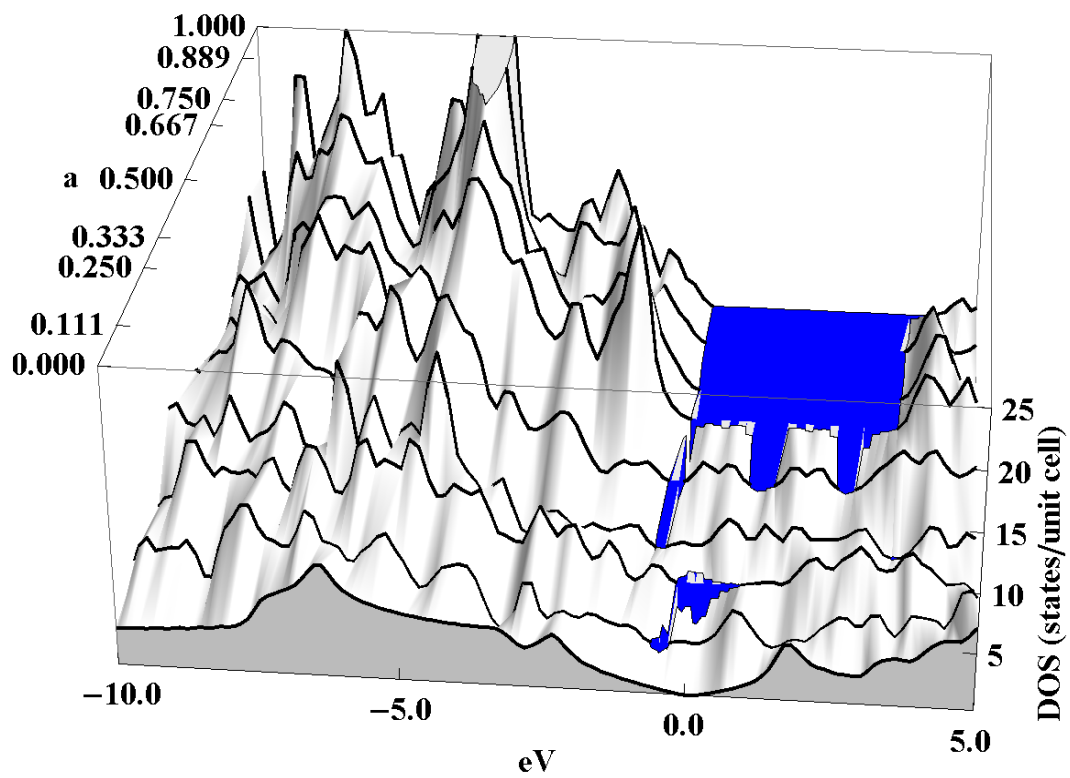


Figure 7.7 Initial configurations that produce the most stable configurations for F/Cl-adsorbed graphene based on the used atomic ratios, red triangle is a pair of identical adatoms adsorbed on upper and lower side of the graphene, from left to right ( $X=F/Cl$ ):  $CX_{0.111}$  (18:2),  $CX_{0.250}$  (8:2),  $CX_{0.333}$  (6:2),  $CX_{0.500}$  (8:4),  $CX_{0.667}$  (6:4),  $CX_{0.750}$  (8:6),  $CX_{0.889}$  (18:16),  $CX$  (2:2).

DOS landscapes (figure 7.8) were created by scaling the original DOS to our largest supercell (zigzag  $3 \times 3$ ) to give consistent picture across the atomic concentrations. Band gaps (blue areas in figure 7.8) were extracted from the scaled DOS. The numerical results on band gaps at Fermi energy are shown in figure 7.9d. With this threshold, our result for CF ( $\approx 2.61$  eV) is somewhat lower than the experiment (3 eV[126], 3.8 eV[127], 5 eV[128]) or calculations by others (3.1 eV (PBE)[129], 8.3 eV (GW)[130], 3.09 eV (PBE) and 4.88 eV (HSE06)[131], 6.3 eV (GW)[124]). The band gap difference between ours ( $\approx 2.61$  eV) and other DFT calculations (*e.g.* 3.1 eV[130]) is mainly because of the DOS threshold selection. Picking up different DOS threshold results different band gap. This lower band gap result is also due to the nature of the pure DFT calculations that underestimate the band gap. To achieve more accurate results, we have performed calculations based on the GGA optimised structures with HSE06 functional (figures 7.8b, 7.8d, 7.9d, 7.9e and 7.9f).



(a)



(b)

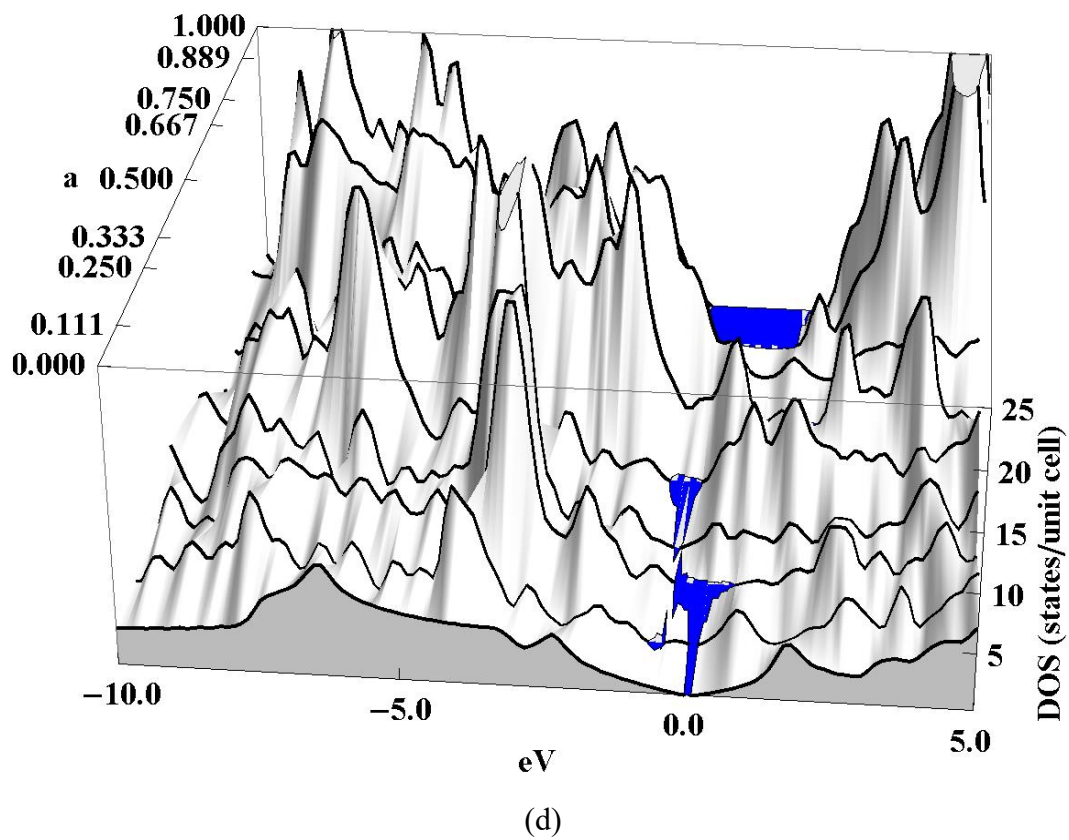
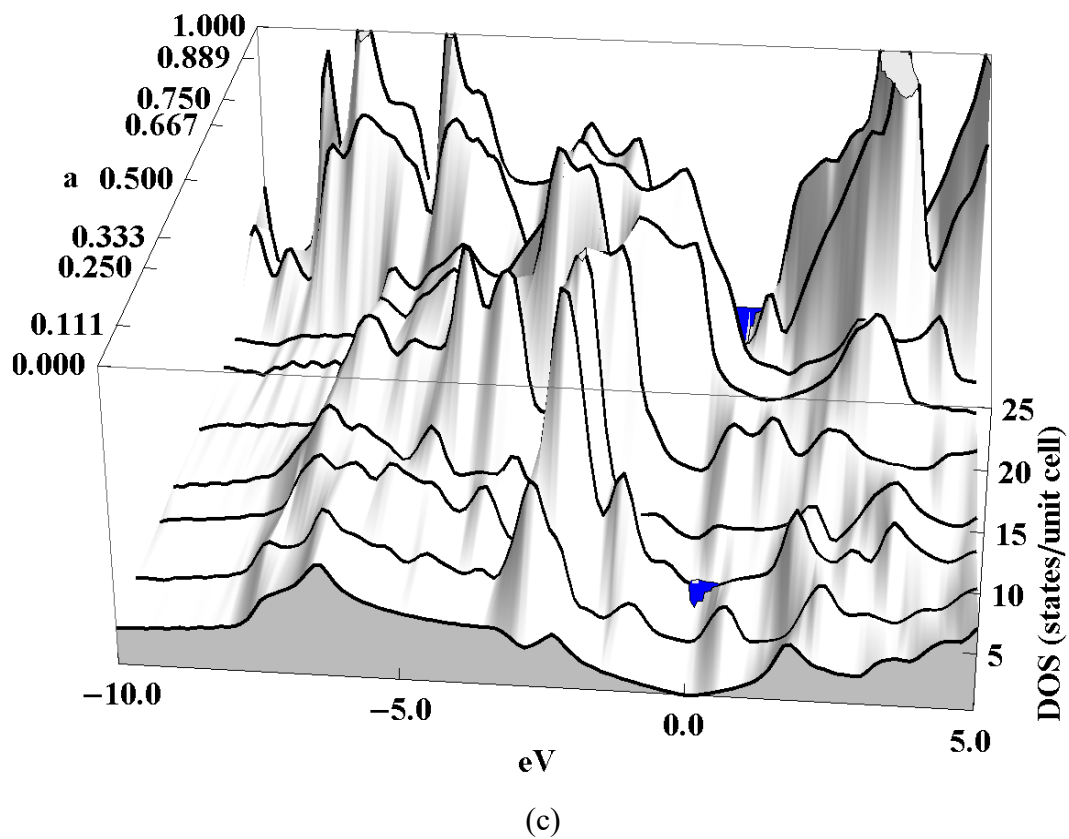


Figure 7.8 DOS (total spin) and Fermi energy (0.0 eV) of (a)  $\text{CF}_a$  - GGA, (b)  $\text{CF}_a$  - HSE06, (c)  $\text{CCl}_a$  - GGA, (d)  $\text{CCl}_a$  - HSE06. The blue areas denote zero DOS.

For F cases, binding energies, graphene cell lattice constants and adatom heights are relatively linear at high atomic concentration. However, band gaps and Fermi energy shifts show nonlinearity. Binding energies are inversely proportional to adatom heights. Graphene cell lattice constants start increasing significantly when the adsorption is more than 50 at.%.

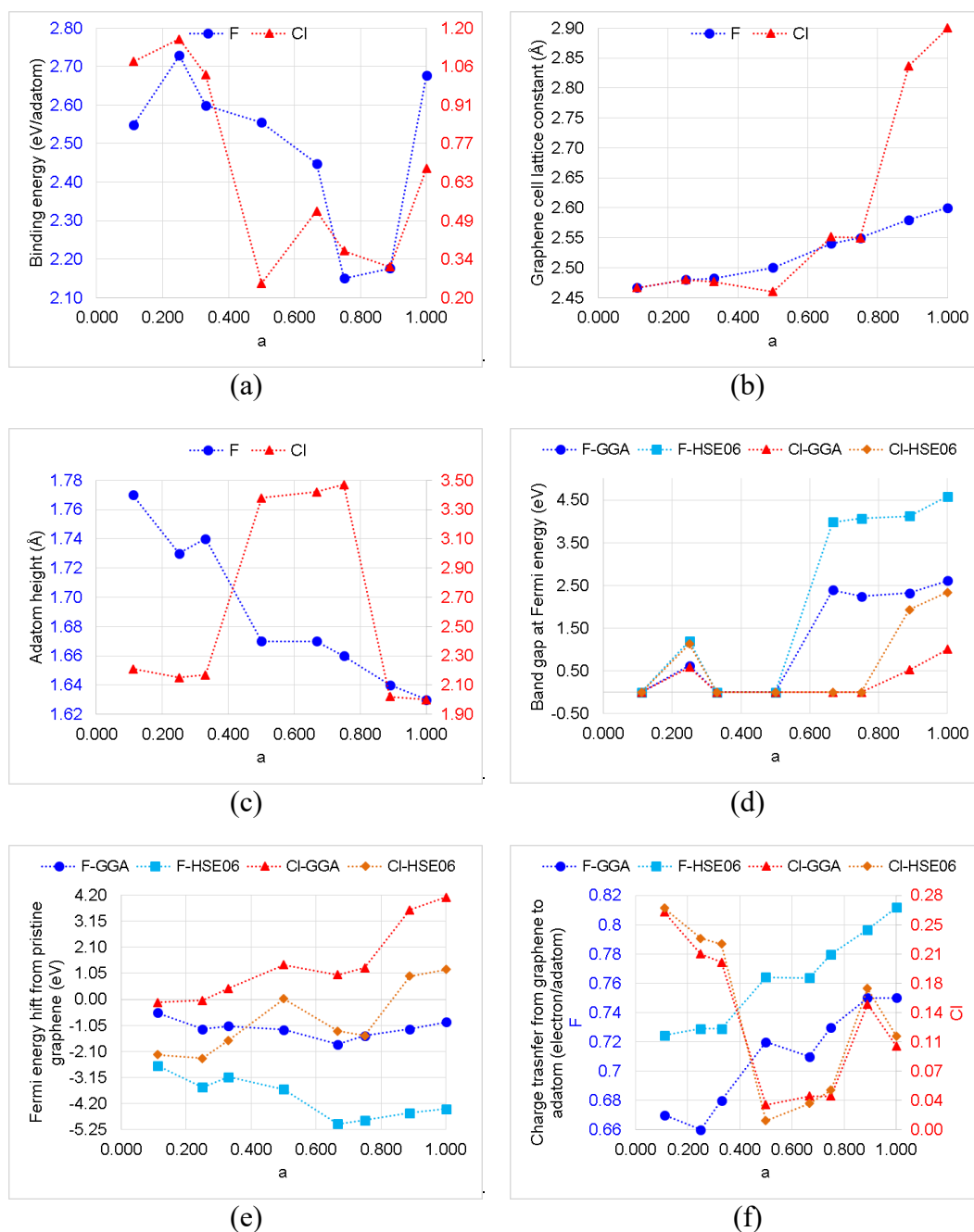


Figure 7.9 Calculated trends for  $CF_a$  and  $CCl_a$ . None creates magnetization. Dotted lines are added as guides and do not imply continuity.

Binding energies (normalized to the CF binding energy) are higher for double-sided addition/removal (our results) than single-sided addition/removal results of Liu *et al.* [122]. This double-sided adsorption results in huge difference on band gaps. This also delays our graphene cell lattice expansion at around 50 at.%. Figures 7.10 are plots of the calculated trends for CF<sub>a</sub> compared with results from Liu *et al.* [122].

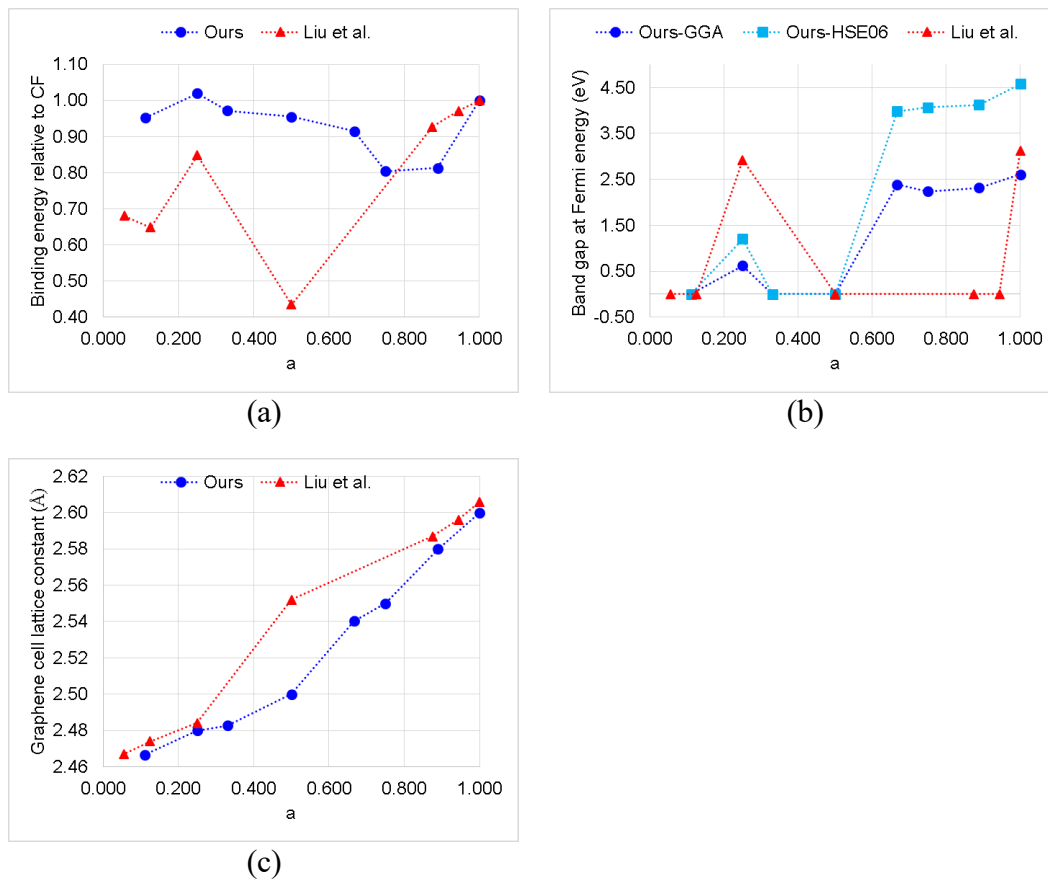


Figure 7.10 Calculated trends for CF<sub>a</sub> compared to Liu *et al.*'s work [122]. Dotted lines are added as guides and do not imply continuity.

Medeiros and co-researchers [71] calculated two different CCl configurations, *i.e.* non-bonding and bonding. Non-bonding configuration has lower total energy. Although having lower total energy, Şahin and co-researchers [54] calculated that non-bonding is dynamically unstable, because Cl atom can roam on the graphene surface without barrier energy. This is supported by Nakada and Ishii's calculation [46], which stated that migration energy for Cl-

adsorbed graphene is minimal (0.02 eV). Our previous study [121] also supports this and we concluded that non-bonding Cl-adsorbed graphene is basically site-independent. Furthermore, Şahin and co-researchers also reported that bonding configuration is dynamically stable at 0 K and possibly at room temperature, but with graphene lattice expansion of more than 15%. Using the binding energy formula (equation 7.1), our results show that there is competition between bonding and non-bonding configuration, which non-bonding wins at 50% to 75% atomic ratios. At these atomic ratios, the adsorption becomes weak (physisorbed), as indicated by the decreasing binding energies, large adatom heights are approximately 3.50 Å, zero band gaps at Fermi energy and miniscule charge transfers (figure 7.9).

F is adsorbed to graphene at least two times stronger than Cl (figure 7.9a). CF<sub>a</sub> is most stable at full and 25% coverage, while CCl<sub>a</sub> is most stable at 25% coverage. Adatom heights for F are inversely proportional to atomic concentrations, but adatom heights exhibit discreteness for Cl (figure 7.9c). For both F and Cl cases, open band gap (at Fermi energy) at certain atomic concentration coverage (figure 7.9d). However, magnetization is not created due to the adatom addition/removal that is done in pairs.

## 7.4 Conclusions

The electronic structures of F and Cl adsorption (double-sided, top site) on graphene were investigated and analysed geometrically in terms of adsorption orientation, at a wide range of atomic ratios. At the same atomic concentration, double-sided adsorption is more stable single-sided. Despite of being in the halogens group, F- and Cl-adsorbed graphene cases show contrasting trends. Their electronic structures are affected by the relative orientation of the adsorbed sites (zigzag or armchair) and possibly the relative size/mass of the adatoms and carbon. This calls for careful consideration of the orientation effect in element-graphene systems. F is adsorbed to graphene more strongly than Cl. F favours full and 25% adsorption

coverage, while Cl favours 25% coverage. Finally, taking adsorption orientation into account, both F and Cl cases open band gap (at Fermi energy) at certain atomic concentration coverage, but none creates magnetization.

---

A manuscript based on the major research outcomes of this chapter was published in :

H. Widjaja, Z.-T. Jiang, M. Altarawneh, C.-Y. Yin, B.-M. Goh, N. Mondinos, A. Amri, and B. Z. Dlugogorski, “Double-sided F and Cl adsorptions on graphene at various atomic ratios: Geometric, orientation and electronic structure aspects,” *Appl. Surf. Sci.*, vol. 373, pp. 65-72, 2016. (*This is publication [3] in the List of Publications*)

---



## CHAPTER EIGHT

### PERIOD 3 ELEMENTS (Na – Cl) ADSORPTION ON GRAPHENE

---

#### 8.1 Introduction

The calculation procedure developed in chapters 1 to 4 was lastly applied to period 3 elements (Na, Mg, Al, Si, P, S, Cl) at lower concentration spanning 1:6, 1:8 and 1:18 atomic ratios, in order to elucidate effects of adsorption trends in a period in periodic table of elements. The electronic structure of elemental adsorption on graphene is affected by side of adsorption (single- or double-sided), site of adsorption (*i.e.* bridge, hollow or top), and the relative orientation of the adsorbed sites (*i.e.* zigzag or armchair).

Numerous experimental and theoretical studies have addressed adsorption/substitution of period 3 elements on graphene, which is shown in table 8.1. Table 8.1 is only an indicator, because of the uniqueness of experimental conditions and assumptions in theoretical methods in each paper. Nakada and Ishii's work provide most of the data in table 8.1, but their calculations were performed nonmagnetically[45], [46]. To see the trends of these properties, unified experiments or simulations across period 3 elements are needed.

To this end, the current study deploys density functional theory (DFT) calculations to assess the influence of the orientational effect when the interaction between the adatoms is relatively significant. Considering the atomic sizes and adatom-adatom interactions, we set the atomic ratio to adatom:C at 1:8. We also included the effects of different concentrations using atomic ratios of 1:6 and 1:18 and conducted a thorough geometrical investigation on the orientational effect encountered during the adsorption of the seven period 3 elements on graphene - aspects which has been overlooked in previous studies. Overall, we highlight some prominent effects of the orientational (zigzag or armchair) and site (bridge, hollow or top)

aspects on various properties such as binding energy, adatom height, Fermi energy shift, graphene distortion, magnetization, charge transfer and band gap.

Table 8.1 Adatom-adsorbed/doped graphene results from previous studies, atomic ratios are printed in parenthesis.

	Na	Mg	Al	Si	P	S	Cl
Most stable site (1:18)[45]	Hollow	Hollow	Hollow	Bridge	Bridge	Bridge	Top
Binding energy (eV)	0.72 <sub>(1:18)</sub> [45] 0.462 <sub>(1:32)</sub> [20]	0.03 <sub>(1:18)</sub> [45]	1.62 <sub>(1:18)</sub> [45]	1.86 <sub>(1:18)</sub> [45]	2.30 <sub>(1:18)</sub> [45]	2.34 <sub>(1:18)</sub> [45]	1.27 <sub>(1:18)</sub> [45]
Adatom height (Å)	2.22 <sub>(1:18)</sub> [45] 2.28 <sub>(1:32)</sub> [20]	3.21 <sub>(1:18)</sub> [45]	2.04 <sub>(1:18)</sub> [45]	2.3 <sub>(1:18)</sub> [45]	2.09 <sub>(1:18)</sub> [45]	2.8 <sub>(1:18)</sub> [45]	2.56 <sub>(1:18)</sub> [45]
Fermi energy shift# (eV)	0.86 <sub>(1:32)</sub> [20]	-	0.94 <sub>(1:32)</sub> [20] 0.49 <sub>(graphene-metal)</sub> [103] 0.57 <sub>(graphene-metal)</sub> [105] 0.8 <sub>(1:31)</sub> [64]	-	-	-	-
Magnetization ( $\mu_B$ )	0.27 <sub>(1:32)</sub> [20] 0.0 <sub>(1:72)</sub> [55]	0.0 <sub>(1:72)</sub> [55]	0.00 <sub>(1:32)</sub> [20] 0.0 <sub>(1:72)</sub> [55]	0.27 <sub>(1:8)</sub> [65] 1.02 <sub>(1:32)</sub> [65] 1.74 <sub>(1:72)</sub> [66] 0 <sub>(1:32)</sub> [67]	1 <sub>(1:31-1:127)</sub> [64] 1 <sub>(1:31-1:241)</sub> [70]	0 <sub>(1:31-1:241)</sub> [70]	-
Charge transfer <sup>^</sup> ( $e$ )	0.62 <sub>(1:18)</sub> [46]	0.10 <sub>(1:18)</sub> [46]	0.81 <sub>(1:18)</sub> [46]	0.72 <sub>(1:18)</sub> [46]	0.38 <sub>(1:18)</sub> [46]	-0.04 <sub>(1:18)</sub> [46]	-0.41 <sub>(1:18)</sub> [46]
Migration energy (eV)	0.13 <sub>(1:18)</sub> [45] 0.069 <sub>(1:32)</sub> [20]	0.02 <sub>(1:18)</sub> [45]	0.05 <sub>(1:18)</sub> [45]	0.05 <sub>(1:18)</sub> [45]	0.45 <sub>(1:18)</sub> [45]	0.46 <sub>(1:18)</sub> [45]	0.02 <sub>(1:18)</sub> [45]
Band gap <sup>~</sup> (eV)	-	-	metallic <sub>(1:31-1:127)</sub> [64]	0.00 <sub>(1:31)</sub> [64] 0.08 <sub>(1:71)</sub> [64] 2.02 <sub>(1:1)</sub> [68] 2.13 <sub>(1:1)</sub> [69]	0.67 <sub>(1:31)</sub> [64] 0.14 <sub>(1:71)</sub> [64] 0.50 <sub>(1:127)</sub> [70]	0.57 <sub>(1:31)</sub> [64] 0.01 <sub>(1:71)</sub> [64] 0.80 <sub>(1:31)</sub> [70]	1.21 <sub>(2:2)</sub> bonding [54] 0.00 <sub>(2:2)</sub> non-bonding [71]

# Charge transfer from adatom to graphene

<sup>^</sup> Fermi energy shift from pristine graphene

<sup>~</sup> Band gap at Fermi energy

## 8.2 Methods

We perform all structural optimisations and energy calculations using the plane-wave DFT code of VASP. Calculation methodology comprises spin-polarized PAW-GGA functional [89], van der Waals correction by Grimme (2) [88] method, dipole corrections along the  $Z$ -direction, and a Gaussian smearing.

For 1:8 atomic ratio, the calculations include (i) 3 adatom sites: bridge ( $B$ ), hollow ( $H$ ) and top ( $T$ ); and (ii) 2 orientation directions: zigzag ( $z$ ) and armchair ( $a$ ), with initial adatom height of 1.5 Å. Figures 8.1b and 8.1c summarize these sites and orientations. All the  $H$  and  $T$  cases can be represented by one position for zigzag orientation ( $H_z$  and  $T_z$ ) and one position for armchair orientation ( $H_a$  and  $T_a$ ), while all the  $B$  cases can be represented by one position for

zigzag orientation ( $B_z$ ) and two positions for armchair orientation ( $B_{a1}$ ,  $B_{a2}$ ). Thus, we only considered 7 unique adatom positions in this study ( $B_z$ ,  $B_{a1}$ ,  $B_{a2}$ ,  $H_z$ ,  $H_a$ ,  $T_z$ ,  $T_a$ ). We fixed the lattice parameters at  $4.936 \text{ \AA} \times 4.936 \text{ \AA}$  for the zigzag  $2 \times 2$  graphene supercell and  $4.936 \text{ \AA} \times 4.275 \text{ \AA}$  for the armchair  $2 \times \sqrt{3}$  graphene supercell. At this low adsorption atomic ratio, graphene lattice parameters do not change significantly. We also fixed the distance between the two graphene sheets to  $15 \text{ \AA}$ . Additional calculations for 1:6 and 1:18 atomic ratios and these calculations consider only adsorption sites ( $B$ ,  $H$ ,  $T$ ) has also been performed, as shown in figures 8.1a and 8.1d. However, we did not use slant  $3 \times \sqrt{7}$ , because the adatoms are too far to interact with one another. As such, the results for  $3 \times 3$  are expected to be the same as  $3 \times \sqrt{7}$ .

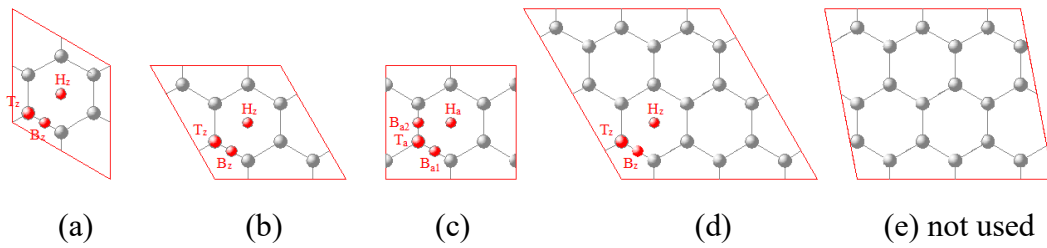


Figure 8.1 Schematic diagrams of adsorption on the graphene supercells for (a) 1:6 zigzag  $\sqrt{3} \times \sqrt{3}$ , (b) 1:8 zigzag  $2 \times 2$ , (c) 1:8 armchair  $2 \times \sqrt{3}$ , (d) 1:18 zigzag  $3 \times 3$ , and (e) 1:18 slant  $3 \times \sqrt{7}$ . (e) is not used.

We conducted the calculations in four stages: (1) adatom and pristine graphene energy, (2) adatom-adatom interaction, (3) graphene-adatom internal structure optimisation, and (4) adatom-graphene density of states (DOS) calculation. We calculated the adatom-adatom interaction for several supercells to compare the interaction strength against the supercell size. To ensure convergence results, all stages used plane wave cut off energy of  $600 \text{ eV}$ . Completion of iterations entailed tolerances of less than  $1 \text{ } \mu\text{eV}$  for energy and less than  $0.02 \text{ eV/\AA}$  for atomic forces.

We explored two types of binding energy,  $E_1$  and  $E_2$ , in the present study as expressed in the following two equations:

$$E_1 = E_{graphene} + E_{adatom} - E_{adatom-graphene\ system} \quad (8.1)$$

and

$$E_2 = E_{graphene} + E_{adatom-adatom} - E_{adatom-graphene\ system} \quad (8.2)$$

where  $E_{graphene}$  denotes the energy of the pristine graphene,  $E_{adatom}$  signifies the energy of the adatom,  $E_{adatom-adatom}$  stands for the energy of adatom-adatom interaction and  $E_{adatom-graphene\ system}$  is the total energy of the adatom and graphene after the adatom is attached to the graphene. We calculated adatom-adatom interaction on the initial condition of adatom-adsorbed graphene as if the graphene sheet were removed from the system. Positive or negative binding energy indicates stability or instability, respectively.

The adatom height, Fermi energy shift, graphene distortion, magnetization, charge transfer, band gap and DOS were calculated for all cases. In this analysis, the band gap is determined from the DOS [90, p. 214] analysis, *i.e.* zero DOS at Fermi energy. Zero DOS at Fermi energy signifies that the material is a semiconductor or insulator. Adatom height (Å) is the difference between adatom's  $z$ -coordinate and the average of  $z$ -coordinates of C atoms. The graphene distortion is an indicator of the adatom's presence, which is the average displacement (in picometer/carbon atom) of the C atoms in the graphene supercells.

While total charge is the sum of total spin-up and spin-down, magnetization (in Bohr magneton or  $\mu_B$ ) is defined as the difference between total spin up and total spin down of the DOS at the Fermi energy level. Charge transfer is expressed as the scalar quantity charge transferred from adatom to graphene (electrons/adatom). Positive charge transfer indicates that charge is transferred from adatom to graphene and *vice versa*. Charge transfer estimation has been calculated via the Bader methodology [91].

## 8.3 Results and Discussion

The discussion focuses on adatom-adatom interaction and adatom-adsorbed graphene. The basic information of graphene and the atoms are shown in Table 8.S1 and 8.S2 in the supplementary data. Table 8.S1 shows the atomic/ionic radius and its Pauling's electronegativity [21, pp. 255–257]. Table 8.S2 shows the calculated magnetization and Fermi energy of graphene and the elements.

### 8.3.1 Adatom-adatom Interaction

Adatom-adatom interaction in the network of adatoms is represented by its binding energy, which is  $E_{\text{adatom}} - E_{\text{adatom-adatom}}$ . As expected, the interaction is quite strong at small supercells, but diminishes at larger supercells. Larger Na and Mg atoms do not fit when considering a zigzag  $1 \times 1$  graphene cell. Also, the trend of the interaction strengths follows the atomic radius for a zigzag  $\sqrt{3} \times \sqrt{3}$  or larger graphene supercells. This indicates that the larger atomic radius, the stronger adatom-adatom interaction, for the same graphene supercell. In general, armchair  $2 \times \sqrt{3}$  gives greater adatom-adatom interaction than zigzag  $2 \times 2$ , except Na and P (figure 8.2b).

However, this trend does not hold true for  $1 \times 1$  graphene cell for adsorption of Al and Si atoms. This is due to the adatom-adatom repulsion at shorter distance for Si. The optimised lattice parameter for Al-Al and Si-Si interactions amounts to 2.79 Å ( $120^\circ$  rhombus lattice) and 2.49 Å (square lattice), respectively. Thus for our  $1 \times 1$  graphene cell (2.468 Å), Si interacts strongly with its neighbouring atoms whilst neighbouring Al atoms experience repulsion from each other. While P has very low P-P interaction starting at  $\sqrt{3} \times \sqrt{3}$  graphene supercells.

For all adatoms, the adatom-adatom interactions are small for  $3 \times 3$  or larger graphene supercells. So it is expected that orientation effects of these adatoms on the adatom-adsorbed graphene systems are rather minimal for  $3 \times 3$  or larger graphene supercells.

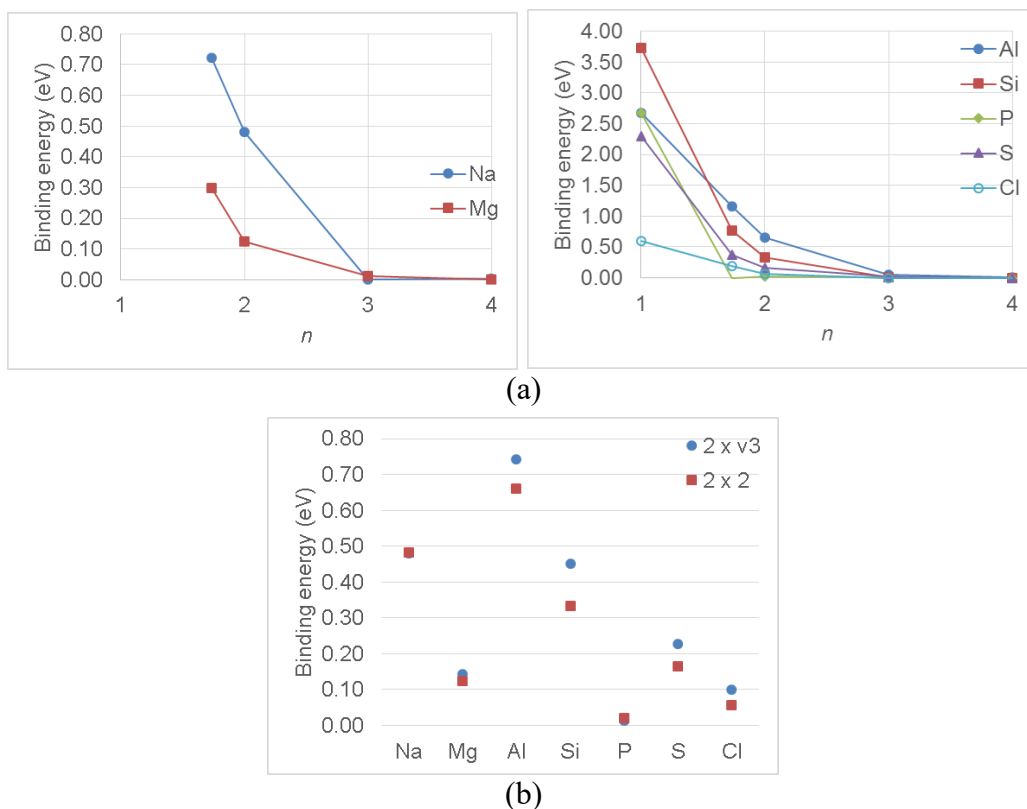


Figure 8.2 Adatom-adatom binding energies for (a) various zigzag  $n \times n$  supercells, (b)  $2 \times \sqrt{3}$  and  $2 \times 2$  supercells. Connecting lines have been added as guidance.

### 8.3.2 Adatom-adsorbed Graphene

Calculation results are summarized in table 8.2 and figures 8.3 and 8.4, with the numerical details are in table 8.S3 in supplementary data. Na, Mg, Al are metals; Si is metalloid; P, S, Cl are nonmetals. At these low atomic concentrations, Na shows site-only dependence ( $H$ ), Mg and Cl show orientation-only dependence, and Al, Si, P, S show site-and-orientation dependence. Orientation was inspected at 1:8 atomic ratio, which gives extra information in addition to the most stable site (Al is zigzag, while Si, P, S are armchair). All adatoms are larger in size than C. Mg and P exhibit weak adsorption to graphene, while Al and S exhibit strong adsorption (figures 8.3a). As expected, binding energies are qualitatively inversely proportional to adatom heights (figures 8.3a and 8.3c). Fermi energy shifts trend (figure 8.3d) is similar to Pauling's electronegativities trend. There is no clear trend for

graphene distortions across the adatoms (figure 8.3e), but in general, the lower adatom concentration, the lower distortion. Mg, Al and S do not create magnetization, while Na, Si, P and Cl do (figure 8.3f). This is in agreement with previous studies shown in table 8.1. The very weak bonding in P 1:18 case causes the magnetization of P atom is preserved ( $3 \mu_B$ ) after adsorbed to graphene. There is also no clear trend for charge transfers across the adatoms (figure 3g), but we can at least predict the direction of the charge transfer based on Pauling's electronegativity (Na – P are positive, while S and Cl are negative). Strong bonding to graphene creates an opportunity to open the band gap, as in S 1:8 case (figure 8.3h). The DOS details for extracting the band gaps are shown in figure 8.S1 in the supplementary data.

Table 8.2 Results for period 3-elements adsorbed graphene at three atomic ratios. *B, H, T, Z, A*, +, – are bridge, hollow, top, zigzag, armchair, positive and negative. Atomic ratios printed in parenthesis override the atomic ratio column.

	atomic ratio(s)	Na	Mg	Al	Si	P	S	Cl
	1:6	<i>H</i>	<i>Z</i>	<i>Z</i>	<i>B</i>	<i>B</i>	<i>B</i>	<i>Z</i>
Most stable position	1:8	<i>H</i>	<i>A</i>	<i>H<sub>z</sub></i>	<i>B<sub>a2</sub></i>	<i>B<sub>a2</sub></i>	<i>B<sub>a2</sub></i>	<i>Z</i>
	1:18	<i>H</i>	<i>Z</i>	<i>H</i>	<i>B</i>	<i>H</i>	<i>B</i>	<i>Z</i>
Magnetization	1:6-1:18	Yes	No	No	Yes	Yes	No	Yes
Fermi energy shift #	1:6-1:18	+	+	+	+	+	+	–
Charge transfer ^	1:6-1:18	+	+	+	+	+	–	–
Band gap ~	1:6-1:18	No	No	No	No	No	Yes <sub>(1:8)</sub>	No

# Fermi energy shift from pristine graphene

^ Charge transfer from adatom to graphene

~ Band gap at Fermi energy

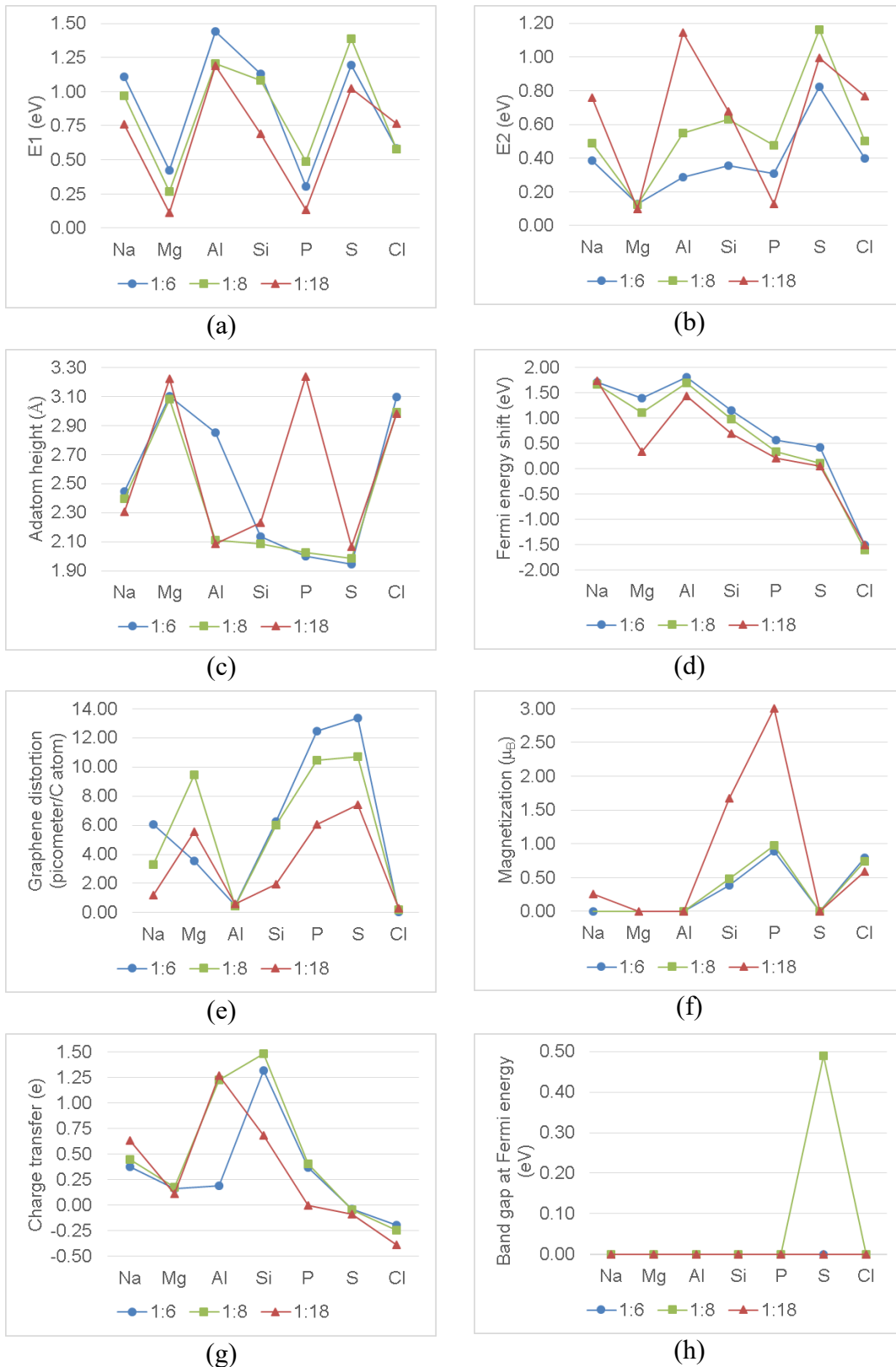


Figure 8.3 Calculation results for period-3 elements adsorbed on graphene, lines are added as a guidance.  $E_1$  is binding energy with respect to adatom,  $E_2$  is binding energy with respect to adatom-adatom interaction.



For all adatoms except P, the difference between  $E_1$  and  $E_2$  decreases as the atomic ratio decreases, and becomes miniscule at 1:18 atomic ratio (figure 8.4).

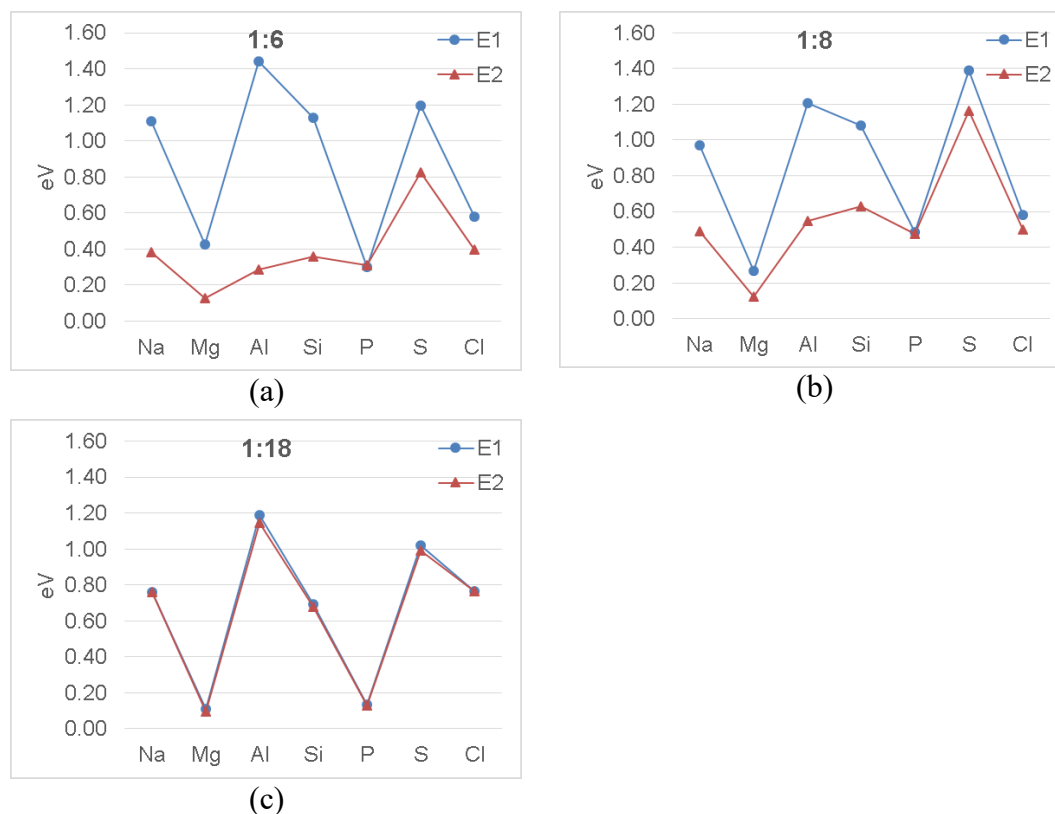


Figure 8.4 Binding energies for period-3 elements adsorbed on graphene, lines are added as a guidance.  $E_1$  is binding energy with respect to adatom,  $E_2$  is binding energy with respect to adatom-adatom interaction.

## 8.4 Conclusions

We have performed geometrical analysis and first principles calculations using DFT to investigate the electronic structures of period 3 elements (Na, Mg, Al, Si, P, S, Cl) adsorbed on graphene at lower concentrations spanning 1:6, 1:8 and 1:18 atomic ratios, in terms of site of adsorption (bridge, hollow or top), and the relative orientation of the adsorbed sites (zigzag or armchair). In these atomic ratios, we found that some elements are site-dependent (Na), orientation-dependent (Mg, Cl), and site-and-orientation-dependent (Al, Si, P, S). None shows both site-and-orientation-independency. Mg and P show weak adsorption, while Al and S show stronger adsorption. Pauling's electronegativity has been useful in predicting the Fermi energy

shifts and charge transfers trends. Mg, Al and S cases do not create magnetization. Only S opens a band gap at 1:8 atomic ratio.

## 8.5 Supplementary Data

Table 8.S1 Atomic/ionic radius and Pauling's electronegativity[21, pp. 255–257].

Atom	Radius (Å)	Pauling's electronegativity	Ion	Radius (Å)
C	0.77	2.5	-	-
Na <sup>#</sup>	1.54	0.9	Na <sup>+</sup>	1.16
Mg <sup>#</sup>	1.30	1.2	Mg <sup>2+</sup>	0.86
Al	1.18	1.5	Al <sup>3+</sup>	0.68
Si	1.11	1.8	-	-
P	1.06	2.1	-	-
S	1.02	2.5	S <sup>2-</sup>	1.70
Cl	0.99	3.0	Cl <sup>-</sup>	1.67

# Relatively big atom

Table 8.S2 Calculation results of graphene and the elements.

	No. of valence electrons	Magnetization ( $\mu_B$ )	Fermi energy (eV)
Graphene	24, 32, 72 <sup>^</sup>	0	-2.29
C	4	2	-6.03
Na	1	1	-2.21
Mg	2	0	-3.76
Al	3	1	-3.01
Si	4	2	-4.50
P	5	3	-5.25
S	6	2	-6.12
Cl	7	1	-8.08

<sup>^</sup> for 1:6, 1:8, 1:18 atomic ratios

Table 8.S3 Period 3-elements adsorbed graphene. Bold numbers are the values at the most stable position. *B, H, T, Z, A* are bridge, hollow, top, zigzag and armchair.

1:6 atomic ratio	Na			Mg	Al	Si			P			S			Cl
	<i>B</i>	<i>H</i>	<i>T</i>	<i>Z</i>	<i>Z</i>	<i>B</i>	<i>H</i>	<i>T</i>	<i>B</i>	<i>H</i>	<i>T</i>	<i>B</i>	<i>H</i>	<i>T</i>	<i>Z</i>
$E_1$ (eV) ~	1.04	<b>1.11</b>	1.04	0.43	1.44	<b>1.13</b>	0.93	1.04	<b>0.30</b>	0.10	0.07	<b>1.19</b>	0.53	0.93	0.58
$E_2$ (eV) ~	0.32	<b>0.38</b>	0.32	0.13	0.29	<b>0.36</b>	0.16	0.27	<b>0.31</b>	0.11	0.08	<b>0.82</b>	0.15	0.56	0.40
Adatom height (Å)	2.63	<b>2.44</b>	2.65	3.10	2.85	<b>2.14</b>	3.08	2.29	<b>2.00</b>	3.31	2.11	<b>1.94</b>	3.18	2.07	3.10
Fermi energy shift (eV) #	1.69	<b>1.70</b>	1.71	1.39	1.80	<b>1.14</b>	1.09	1.14	<b>0.56</b>	0.46	0.60	<b>0.43</b>	-	0.36	1.52
Graphene distortion *	2.89	<b>6.08</b>	2.90	3.57	0.50	<b>6.24</b>	0.01	3.50	<b>12.47</b>	6.29	10.76	<b>13.38</b>	4.39	11.34	0.05
Magnetization ( $\mu_B$ )	0.00	<b>0.00</b>	0.00	0.00	0.00	<b>0.38</b>	0.57	0.00	<b>0.89</b>	2.98	0.94	<b>0.00</b>	1.93	0.00	0.79
Charge transfer ( <i>e</i> )	0.32	<b>0.38</b>	0.32	0.16	0.19	<b>1.32</b>	0.05	0.86	<b>0.37</b>	0.01	0.26	<b>-0.04</b>	0.08	-0.05	0.20
Band gap (eV) ^	0.00	<b>0.00</b>	0.00	0.00	0.00	<b>0.00</b>	0.00	0.00	<b>0.00</b>	0.00	0.00	<b>0.00</b>	0.00	0.07	0.00

1:8 atomic ratio	Na			Mg	
	<i>B</i>	<i>H</i>	<i>T</i>	<i>Z</i>	<i>A</i>
$E_1$ (eV) ~	0.89	<b>0.97</b>	0.89	0.22	<b>0.27</b>
$E_2$ (eV) ~	0.41	<b>0.49</b>	0.41	0.09	<b>0.12</b>
Adatom height (Å)	2.57	<b>2.40</b>	2.58	3.20	<b>3.08</b>
Fermi energy shift (eV) #	1.63	<b>1.66</b>	1.64	0.91	<b>1.11</b>
Graphene distortion *	3.44	<b>3.29</b>	4.50	11.58	<b>9.46</b>
Magnetization ( $\mu_B$ )	0.00	<b>0.00</b>	0.00	0.00	<b>0.00</b>
Charge transfer ( <i>e</i> )	0.39	<b>0.45</b>	0.39	0.13	<b>0.17</b>
Band gap (eV) ^	0.00	<b>0.00</b>	0.00	0.00	<b>0.00</b>

1:8 atomic ratio	Al						Si					
	<i>Bz</i>	<i>Ba1</i>	<i>Ba2</i>	<i>Hz</i>	<i>Ha</i>	<i>Tz</i>	<i>Bz</i>	<i>Ba1</i>	<i>Ba2</i>	<i>Hz</i>	<i>Ha</i>	<i>Tz</i>
$E_1$ (eV) ~	1.14	1.21	1.24	<b>1.21</b>	1.20	1.13	0.95	0.86	<b>1.08</b>	0.81	0.72	0.82
$E_2$ (eV) ~	0.48	0.47	0.50	<b>0.55</b>	0.46	0.47	0.62	0.41	<b>0.63</b>	0.48	0.27	0.48
Adatom height (Å)	2.20	2.32	2.28	<b>2.11</b>	2.09	2.18	2.05	3.06	<b>2.08</b>	1.98	1.91	1.95
Fermi energy shift (eV) #	1.69	1.67	1.60	<b>1.70</b>	1.72	1.68	1.08	1.16	<b>0.98</b>	1.48	1.19	1.19
Graphene distortion *	0.71	1.49	1.46	<b>0.46</b>	0.87	1.38	4.04	0.15	<b>6.02</b>	2.20	15.41	2.93
Magnetization ( $\mu_B$ )	0.00	0.00	0.00	<b>0.00</b>	0.00	0.00	0.59	0.48	<b>0.48</b>	0.00	0.00	0.00
Charge transfer ( <i>e</i> )	1.06	0.92	0.98	<b>1.22</b>	1.24	1.05	1.39	1.34	<b>1.48</b>	0.51	2.07	1.32
Band gap (eV) ^	0.00	0.00	0.00	<b>0.00</b>	0.00	0.00	0.00	0.00	<b>0.00</b>	0.00	0.00	0.00

1:8 atomic ratio	P						S						Cl	
	<i>Bz</i>	<i>Ba1</i>	<i>Ba2</i>	<i>Hz</i>	<i>Ha</i>	<i>Tz</i>	<i>Bz</i>	<i>Ba1</i>	<i>Ba2</i>	<i>Hz</i>	<i>Ha</i>	<i>Tz</i>	<i>Z</i>	<i>A</i>
$E_1$ (eV) ~	0.12	0.10	<b>0.49</b>	0.13	0.12	-0.15	0.96	0.97	<b>1.39</b>	0.36	0.40	0.73	0.57	0.59
$E_2$ (eV) ~	0.10	0.08	<b>0.48</b>	0.11	0.11	-0.17	0.80	0.74	<b>1.16</b>	0.19	0.17	0.57	0.51	0.49
Adatom height (Å)	1.97	1.99	<b>2.02</b>	3.27	3.30	2.10	1.96	1.97	<b>1.98</b>	3.09	3.12	2.10	2.97	3.01
Fermi energy shift (eV) #	0.45	0.50	<b>0.34</b>	0.44	0.38	0.56	0.20	0.14	<b>0.11</b>	-0.54	-0.55	-0.11	-1.60	-1.61
Graphene distortion *	6.60	8.52	<b>10.44</b>	12.90	13.42	3.98	7.84	8.29	<b>10.71</b>	10.85	11.38	5.29	0.20	0.16
Magnetization ( $\mu_B$ )	0.51	0.85	<b>0.98</b>	3.00	2.99	0.99	0.00	0.00	<b>0.00</b>	1.92	1.91	0.00	0.75	0.74
Charge transfer ( <i>e</i> )	0.36	0.37	<b>0.41</b>	0.00	0.00	0.24	-0.07	-0.05	<b>-0.05</b>	-0.10	-0.10	-0.12	-0.25	-0.24
Band gap (eV) ^	0.08	0.00	<b>0.00</b>	0.00	0.00	0.00	0.00	0.00	<b>0.49</b>	0.00	0.00	0.00	0.00	0.00

1:18 atomic ratio	Na			Mg
	<i>B</i>	<i>H</i>	<i>T</i>	<i>Z</i>
$E_1$ (eV) ~	0.63	<b>0.76</b>	0.62	0.11
$E_2$ (eV) ~	0.63	<b>0.76</b>	0.62	0.10
Adatom height (Å)	2.43	<b>2.31</b>	2.42	3.22
Fermi energy shift (eV) #	1.63	<b>1.73</b>	1.63	0.34
Graphene distortion *	1.17	<b>1.19</b>	1.28	5.58
Magnetization ( $\mu_B$ )	0.43	<b>0.26</b>	0.42	0.00
Charge transfer ( <i>e</i> )	0.59	<b>0.64</b>	0.59	0.11
Band gap (eV) ^	0.00	<b>0.00</b>	0.00	0.00

1:18 atomic ratio	Al			Si			P			S			Cl
	<i>B</i>	<i>H</i>	<i>T</i>	<i>B</i>	<i>H</i>	<i>T</i>	<i>B</i>	<i>H</i>	<i>T</i>	<i>B</i>	<i>H</i>	<i>T</i>	<i>Z</i>
$E_1$ (eV) ~	1.08	<b>1.19</b>	1.08	<b>0.72</b>	0.06	<b>0.69</b>	0.05	<b>0.13</b>	-0.41	<b>1.02</b>	0.30	0.62	0.77
$E_2$ (eV) ~	1.04	<b>1.15</b>	1.03	<b>0.71</b>	0.04	<b>0.68</b>	0.04	<b>0.13</b>	-0.41	<b>0.99</b>	0.27	0.60	0.77
Adatom height (Å)	2.22	<b>2.09</b>	2.18	<b>2.19</b>	1.88	<b>2.23</b>	2.09	<b>3.23</b>	2.19	<b>2.07</b>	3.09	2.20	2.98
Fermi energy shift (eV) #	1.38	<b>1.44</b>	1.37	<b>0.69</b>	1.31	<b>0.70</b>	0.07	<b>0.20</b>	0.35	<b>0.05</b>	-0.71	-0.32	-1.50
Graphene distortion *	0.56	<b>0.60</b>	1.03	<b>3.46</b>	1.10	<b>1.97</b>	7.45	<b>6.05</b>	3.44	<b>7.42</b>	5.28	4.71	0.32
Magnetization ( $\mu_B$ )	0.00	<b>0.00</b>	0.00	<b>1.52</b>	0.00	<b>1.67</b>	0.94	<b>3.00</b>	1.10	<b>0.00</b>	1.85	0.00	0.59
Charge transfer ( <i>e</i> )	1.09	<b>1.27</b>	1.09	<b>1.00</b>	0.75	<b>0.68</b>	0.42	<b>0.00</b>	0.13	<b>-0.09</b>	-0.17	-0.27	-0.39
Band gap (eV) ^	0.00	<b>0.00</b>	0.00	<b>0.00</b>	0.00	<b>0.00</b>	0.00	<b>0.00</b>	0.00	<b>0.00</b>	0.00	0.00	0.00

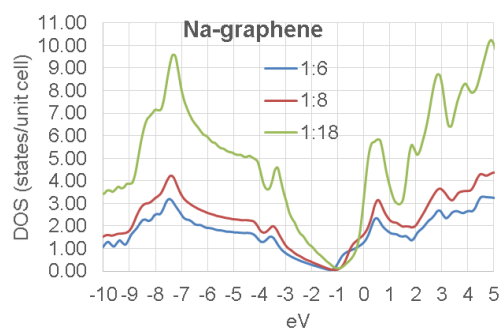
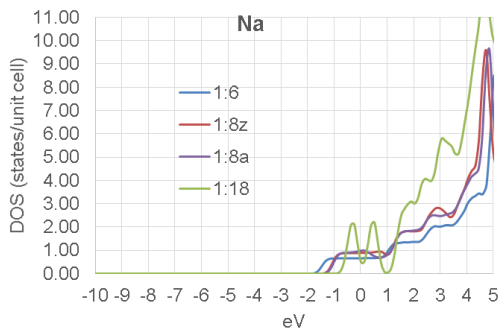
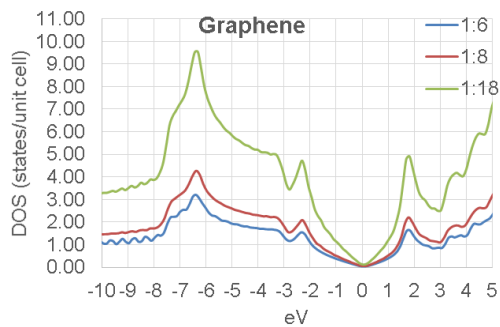
~ Binding energy with respect to adatom.

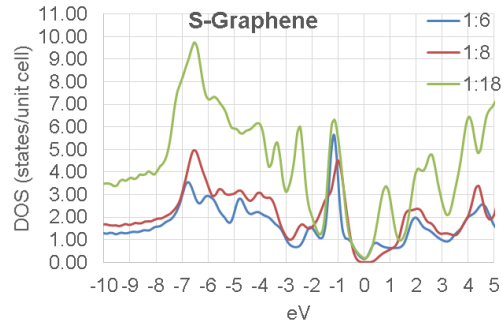
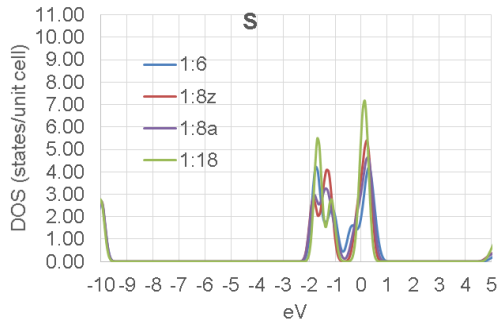
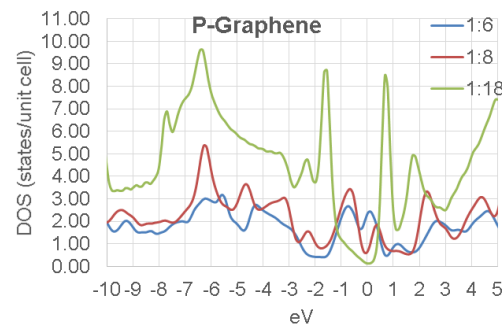
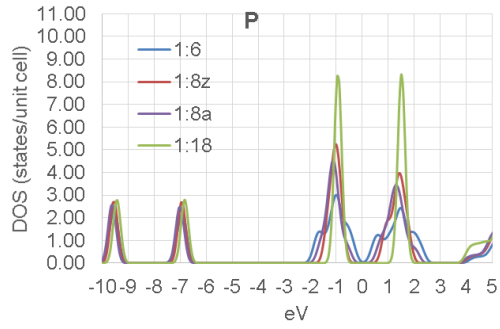
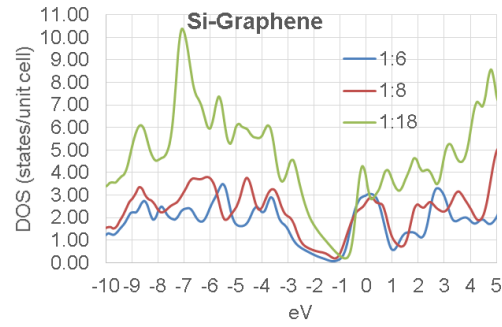
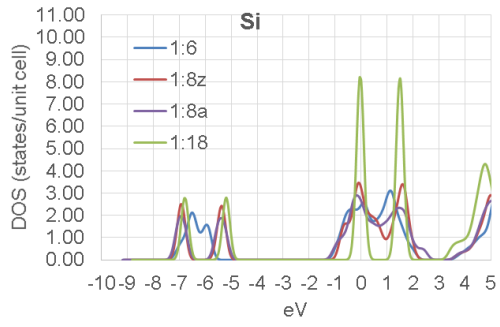
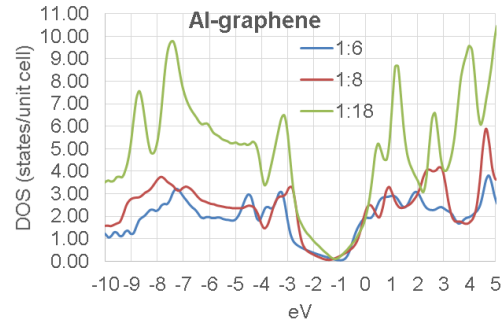
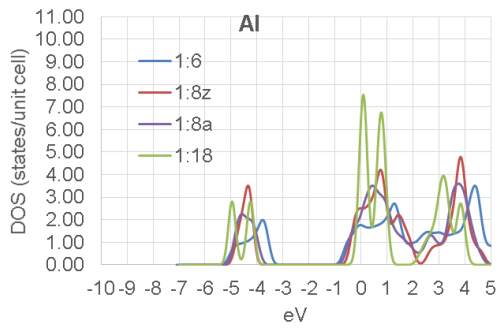
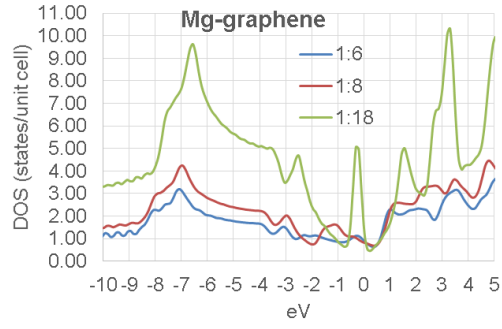
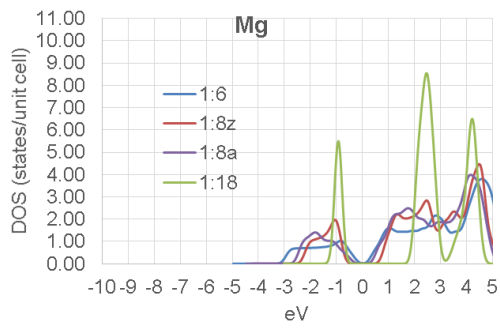
~ Binding energy with respect to adatom-adatom interaction.

# Fermi energy shift from pristine graphene.

\* in picometer/carbon atom.

^ Band gap at Fermi energy.





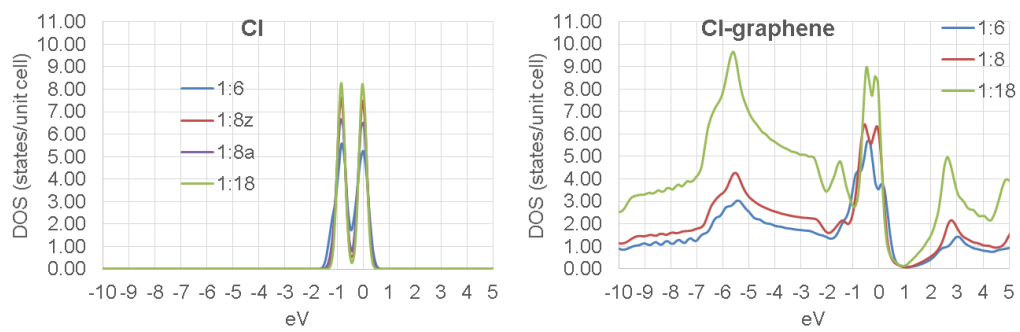


Figure 8.S1 DOS (total spin) and Fermi energy (0 eV) of element-adsorbed graphene at 3 atomic ratios,  $z$  is zigzag,  $a$  is armchair.

# CHAPTER NINE

## CONCLUDING REMARKS

### 9.1 Consolidated Results

This section is intended to consolidate all the results before concluding this study. Based on the scope of this thesis for ten adatoms (figure 4.13), this section shows : (1) the summary the overall trends from previous studies in section 3.3 (see table 9.1) and our results in chapters 5 – 8 (see table 9.2), (2) the comparison of tables 9.1 and 9.2.

Table 9.1 Results from previous studies for period 3-elements and halogens adsorbed/doped graphene. *B, H, T, +, -* are bridge, hollow, top, positive and negative. Grey is cell with no data. Atomic ratios printed in parenthesis override the atomic ratio column.

#### (a) period 3-elements

	atomic ratio(s)	Na	Mg	Al	Si	P	S	Cl
Most stable positions	1:18	<i>H</i>	<i>H*</i>	<i>H</i>	<i>B</i>	<i>B</i>	<i>B</i>	<i>T*</i>
Magnetization	< 50 at.%	Yes	No	No	Yes	Yes	No	
Charge transfer ^	1:18	+	+	+	+	+	-	-
Band gap ~	> 50 at.%			No(<50at%)	Yes	Yes(<50at%)	Yes	Yes

#### (b) halogens

	atomic ratio(s)	F	Cl	Br	I
Most stable positions	1:18	<i>T</i>	<i>T*</i>	<i>T*</i>	<i>T*</i>
Magnetization	< 50 at.%	Yes			
Charge transfer ^	1:18	-	-	-	-
Band gap ~	> 50 at.%	Yes	Yes	No	Yes(<50at%)

^ Charge transfer from adatom to graphene

~ Band gap at Fermi energy

\* with very tiny migration energy

Table 9.2 Results from our calculations for period 3-elements and halogens adsorbed graphene. *B, H, T, Z, A, +, -* are bridge, hollow, top, zigzag, armchair, positive and negative. Atomic ratios printed in parenthesis override the atomic ratio column.

(a) period 3-elements

	atomic ratio(s)	Na	Mg	Al	Si	P	S	Cl
	1:6	<i>H</i>	<i>Z</i>	<i>Z</i>	<i>B</i>	<i>B</i>	<i>B</i>	<i>Z</i>
Most stable position	1:8	<i>H</i>	<i>A</i>	<i>H<sub>z</sub></i>	<i>B<sub>a2</sub></i>	<i>B<sub>a2</sub></i>	<i>B<sub>a2</sub></i>	<i>Z</i>
	1:18	<i>H</i>	<i>Z</i>	<i>H</i>	<i>B</i>	<i>H</i>	<i>B</i>	<i>Z</i>
Magnetization	1:6-1:18	Yes	No	No	Yes	Yes	No	Yes
Fermi energy shift #	1:6-1:18	+	+	+	+	+	+	-
Charge transfer ^	1:6-1:18	+	+	+	+	+	-	-
Band gap ~	1:6-1:18	No	No	No	No	No	Yes <sub>(1:8)</sub>	Yes <sub>(25 and &gt;80 at.%) *</sub>

(b) halogens

	atomic ratio(s)	F	Cl	Br	I
	1:6	<i>T</i>	<i>Z</i>	<i>Z</i>	<i>Z</i>
Most stable position	1:8	<i>T</i>	<i>Z</i>	<i>A</i>	<i>A</i>
	1:18	<i>T</i>	<i>Z</i>	<i>Z</i>	<i>Z</i>
Magnetization	1:6-1:18	No	Yes	Yes	Yes
Fermi energy shift #	1:6-1:18	-	-	-	-
Charge transfer ^	1:6-1:18	-	-	-	-
Band gap ~	1:6-1:18	Yes <sub>(25 and &gt;50at%)*</sub>	Yes <sub>(25 and &gt;80 at.%) *</sub>	No	No

# Fermi energy shift from pristine graphene

^ Charge transfer from adatom to graphene

~ Band gap at Fermi energy

\* Based on double-sided adsorption

Orientation information has been added in this elemental adsorption on graphene study. Adatoms that have tiny migration energy in the previous study (Mg, Cl, Br, I) becomes orientation-only-dependent in this thesis. Magnetizations are in agreement between previous studies and this thesis, except for F. However, the F case from the previous study is a doping case, and not adsorption. In the literature review (figure 3.6), it is surmised that charge transfer and Fermi energy shift trends might at least have the same sign (positive/negative). In our case, it is generally correct, except for S case. This is because S and C have very close Pauling's electronegativity (figure 3.S1). Finally, for band gaps are also in agreement between previous results and this thesis, except for P, I and Cl. However, the P and I cases from the previous study are also doping cases, and not adsorption. For Cl case, the previous studies use bonding



state of CCl, while this thesis uses bonding or non-bonding state, depending on the atomic ratio.

## 9.2 Conclusions

Nano-sized materials are promising to serve human kind now and in the future, as it has richer properties than normal-sized materials. It is natural because quantum physics that governs nano-sized materials is the superset of classical physics that governs normal-sized materials. Many quantum effects do not have classical analog, but not in reverse. To harvest these opportunities, extensive studies must be done experimentally and theoretically.

DFT as a quantum mechanical computational method has been successfully applied to investigate the electronic properties nano-sized materials in this thesis, within reasonable time and cost. Many simulation software (Gaussian 09W, NWChem, Quantum Espresso, Abinit and VASP) have been tried, but finally VASP was picked to execute all the calculations.

In this thesis, it is studied and examined the elemental adsorption on graphene. Extensive trends based on previous studies have been elucidated, in terms of binding energy (stability), the most stable site (bridge, hollow or top), migration (barrier) energy, adatom height, graphene distortion, Fermi energy, magnetization, charge transfer, and band gap at Fermi energy.

For non-magnetic calculations, the trends are visible. Number of adatom unpaired valence electrons are qualitatively proportional to binding energies. Knowing the trend of binding energies, adatom heights and migration energies trends can be loosely predicted, with adatoms heights are inversely proportional, while migration energies are proportional to the binding energies. Pauling's electronegativity gives good indicator for charge transfer and Fermi energy shift. Most metals are stable at hollow site, most metalloids and nonmetals are stable at bridge site, while H and halogens are stable at top site. Some adatoms create magnetization or

open the band gap. While for magnetic calculations, the trends are not simple. This indicates that spin-polarization modifies significantly the calculation results.

Furthermore, it is shown that geometry and orientation are important in elemental adsorption on graphene. To proof this idea, it was created a calculation procedure using DFT to investigate the electronic structures of elemental adsorption on graphene in terms of side (single-, double-sided), site (bridge, hollow, top) and orientation (zigzag, armchair), and applied it to 10 elements : Na, Mg, Al, Si, P, S, F, Cl, Br, and I.

The results are summarized as follows. Geometrically, the number of adsorption cases on bridge site relies on the adatom orientation, one bridge case for zigzag orientation, two bridge cases for armchair orientation, and three bridge cases for slant orientation. At lower atomic ratios (adatom:C), some elements are site-dependent (Na, F); orientation-dependent (Mg, Cl, Br, I); both site-and-orientation-dependent (Al, Si, P, S); but none shows both site-and-orientation-independency.

In one group (halogens), there are two contrast characteristics, F in one side, and Cl/Br/I in the other side. F is adsorbed to graphene at about three times stronger than Cl/Br/I. Cl/Br/I share similar properties in this adsorption. Our calculations on F and Cl adsorbed at a wide range of atomic ratios (11 – 100 at.%) also support these contrast characteristics. F favours full and 25% adsorption coverage, while Cl favours 25% coverage. This suggests that adatoms size/mass compared to carbon atom size/mass has prominent effect, beside its valence electron. F opens band gap at both low and high atomic ratios (25 at.% and greater than 50 at.%), while Cl open small band gap at around 25 at.% and greater than 80 at.%.

In a period (period 3 elements), Mg and P exhibit weak adsorption to graphene, while Al and S exhibit strong adsorption. Some trends are not simple. However, Pauling's electronegativity is still useful in predicting the Fermi energy shifts and charge transfers trends.

Mg, Al and S cases do not create magnetization. Only S opens a band gap at 1:8 atomic ratio. To have better understandings, it is strongly suggested to inspect elements in other periods.

Finally, the trends have been improved with extra information, *i.e.* orientation. This orientation aspect adds one degree of freedom in elemental adsorption on graphene, and thus improves the accuracy and correctness to predict. This demands many of previous studies by others to be re-examined in terms of orientation, and also the inclusion of orientation as a routine procedure in the future studies.

### 9.3 Future Work

The method developed in this thesis could be applied to the other elements, molecules or compounds. It is also applicable to the other emerging 2D materials (*e.g.* silicene, germanene, stanene, phosphorene, boron nitride). These results can be used to assist, accelerate and direct the experiments. Further approximations can be done, *e.g.* utilising time-dependent DFT, taking strongly correlated materials into account, applying GW approximation and considering lattice vibrations. GW approximation is a well-known method to overcome band gap underestimation in DFT.

More features can be calculated, *e.g.* work function, vibration energies, mechanical stress and band structure. Experimenting elemental adsorption on graphene is quite challenging, as manipulation at atomic level is required.

## REFERENCES

- [1] H.-E. Schaefer, *Nanoscience The Science of the Small in Physics, Engineering, Chemistry, Biology and Medicine*. Berlin, Heidelberg: Springer Berlin Heidelberg, 2010.
- [2] W. Kohn, “Nobel Lecture Electronic structure of matter-wave functions and density functionals,” *Rev. Mod. Phys.*, vol. 71, no. 5, pp. 1253–66, 1999.
- [3] K. S. Novoselov, A. K. Geim, S. V Morozov, D. Jiang, Y. Zhang, S. V Dubonos, I. V Grigorieva, and A. A. Firsov, “Electric field in atomically thin carbon films,” *Science (80-. )*, vol. 306, no. 5696, pp. 666–669, 2004.
- [4] P. Jennings, Z.-T. Jiang, N. W. M. W. Wyatt, D. Parlevliet, C. Creagh, C.-Y. Yin, H. Widjaja, and N. Mondinos, “Characterization of silicon nanowires grown on silicon, stainless steel and indium tin oxide substrates,” *Appl. Phys. A*, vol. 113, no. 3, pp. 723–728, 2013.
- [5] A. Amri, Z.-T. Jiang, P. A. Bahri, C.-Y. Yin, X. Zhao, Z. Xie, X. Duan, H. Widjaja, M. M. Rahman, and T. Pryor, “Surface Electronic Structure and Mechanical Characteristics of Copper–Cobalt Oxide Thin Film Coatings: Soft X-ray Synchrotron Radiation Spectroscopic Analyses and Modeling,” *J. Phys. Chem. C*, vol. 117, no. 32, pp. 16457–16467, Aug. 2013.
- [6] M. M. Rahman, Z. Jiang, Z. Xie, X. Duan, Z. Zhou, P. C. Wo, C. Yin, N. Mondinos, Q. Gu, H. Widjaja, K. Jack, A. Yago, and A. Amri, “Understanding Local Bonding Structures of Ni-Doped Chromium Nitride Coatings through Synchrotron Radiation NEXAFS Spectroscopy,” *J. Phys. Chem. C*, vol. 118, pp. 18573–9, 2014.
- [7] D. Griffiths, *Introduction to Elementary Particles*. John Wiley & Sons, 1987.
- [8] D. J. Griffiths, *Introduction to Quantum Mechanics*. New Jersey: Prentice Hall, 1995.
- [9] J. Walker, D. Halliday, and R. Resnick, *Fundamentals of Physics*, 10th ed. John Wiley & Sons, 2014.
- [10] B. Weber Mahapatra, S., Ryu, H., Lee, S., Fuhrer, A. Reusch, T.C.G., Thompson, D.L., Lee, W.C.T., Klimeck, G., Hollenberg, L.C.L. & Simmons, M.Y., “Ohm’s Law Survives to the Atomic Scale,” *Science (80-. )*, vol. 335, pp. 64–67, 2012.
- [11] K. S. Novoselov, V. I. Fal’ko, L. Colombo, P. R. Gellert, M. G. Schwab, and K. Kim, “A roadmap for graphene,” *Nature*, vol. 490, no. 7419, pp. 192–200, Oct. 2012.
- [12] A. Amri, “Structural, Optical and Mechanical Characterizations of Nanostructured Copper Cobalt Oxide Coatings Synthesized via Sol-gel Method for Solar Selective Absorber,” Murdoch University, 2013.
- [13] M. Joshi, A. Bhattacharyya, and S. W. Ali, “Characterization techniques for nanotechnology application in textiles,” *Indian J. Fibre Text. Res.*, vol. 33, no. 3, pp. 304–317, 2008.
- [14] D. A. Skoog, F. J. Holler, and S. R. Crouch, *Principles of Instrumental Analysis*, 6th ed. Belmont California: Thomson Brooks/Cole, 2007.
- [15] S. Kan, T. Mokari, E. Rothenberg, and U. Banin, “Synthesis and size-dependent properties of zinc-blende semiconductor quantum rods,” *Nat Mater*, vol. 2, no. 3, pp. 155–158, 2003.
- [16] W. E. & C. Buhro V.L, “Semiconductor nanocrystals Shape matters,” *Nat. Mater.*, vol. 2, pp. 138–139, 2003.
- [17] V. I. Artyukhov, M. Liu, and B. I. Yakobson, “Mechanically Induced Metal-Insulator Transition in Carbyne,” *Nano Lett.*, Jul. 2014.
- [18] J. B. Foresman and Æ. Frisch, *Exploring Chemistry with Electronic Structure Methods*, 2nd ed. Pittsburgh Pennsylvania: Gaussian, Inc., 1996.
- [19] A. V Krukau, O. A. Vydrov, A. F. Izmaylov, and G. E. Scuseria, “Influence of the exchange screening parameter on the performance of screened hybrid functionals,” *J.*

- Chem. Phys.*, vol. 125, no. 22, 2006.
- [20] K. T. Chan, J. B. Neaton, and M. L. Cohen, “First-principles study of metal adatom adsorption on graphene,” *Phys. Rev. B*, vol. 77, p. 235430, Jun. 2008.
- [21] T. L. Brown, J. H. Eugene LeMay, B. E. Bursten, C. J. Murphy, and P. M. Woodward, *Chemistry The Central Science*, 12th ed. Boston: Prentice Hall, 2012.
- [22] A. Beiser, *Concepts of Modern Physics*, 6th ed. McGraw-Hill, 2003.
- [23] K. S. Novoselov, A. K. Geim, S. V Morozov, D. Jiang, Y. Zhang, S. V Dubonos, I. V Grigorieva, and A. A. Firsov, “Electric field effect in atomically thin carbon films,” *Science*, vol. 306, no. 5696, pp. 666–9, Oct. 2004.
- [24] A. K. Geim and K. S. Novoselov, “The rise of graphene,” *Nat. Mater.*, vol. 6, no. 3, pp. 183–192, 2007.
- [25] W. Choi and J. Lee, Eds., *Graphene Synthesis and Applications*. Boca Raton Florida: CRC Press, 2012.
- [26] M. S. Dresselhaus, “Fifty years in studying carbon-based materials,” *Phys. Scr.*, vol. T146, p. 014002, Jan. 2012.
- [27] A. K. Geim, “Graphene prehistory,” *Phys. Scr.*, vol. T146, p. 014003, Jan. 2012.
- [28] T. Kobayashi, M. Bando, N. Kimura, K. Shimizu, K. Kadono, N. Umez, K. Miyahara, S. Hayazaki, S. Nagai, Y. Mizuguchi, Y. Murakami, and D. Hobara, “Production of a 100-m-long high-quality graphene transparent conductive film by roll-to-roll chemical vapor deposition and transfer process,” *Appl. Phys. Lett.*, vol. 102, no. 2, p. 023112, 2013.
- [29] P. N. First, W. A. De Heer, T. Seyller, C. Berger, J. A. Stroscio, and J. Moon, “Epitaxial Graphenes on Silicon Carbide,” *MRS Bull.*, vol. 35, pp. 296–305, 2010.
- [30] V. Panchal, A. Lartsev, A. Manzin, R. Yakimova, A. Tzalenchuk, and O. Kazakova, “Visualisation of edge effects in side-gated graphene nanodevices,” *Sci. Rep.*, vol. 4, p. 5881, Jul. 2014.
- [31] M. Ruan, Y. Hu, Z. Guo, R. Dong, J. Palmer, J. Hankinson, C. Berger, and W. a. de Heer, “Epitaxial graphene on silicon carbide: Introduction to structured graphene,” *MRS Bull.*, vol. 37, no. 12, pp. 1138–1147, Nov. 2012.
- [32] M. Suemitsu and H. Fukidome, “Epitaxial graphene on silicon substrates,” *J. Phys. D. Appl. Phys.*, vol. 43, p. 374012, Sep. 2010.
- [33] I. Gierz, C. Riedl, U. Starke, C. R. Ast, and K. Kern, “Atomic hole doping of graphene,” *Nano Lett.*, vol. 8, no. 12, pp. 4603–7, Dec. 2008.
- [34] J. Lin, Z. Peng, Y. Liu, F. Ruiz-Zepeda, R. Ye, E. L. G. Samuel, M. J. Yacaman, B. I. Yakobson, and J. M. Tour, “Laser-induced porous graphene films from commercial polymers,” *Nat Commun*, vol. 5, Dec. 2014.
- [35] J. Ma, D. Alfè, A. Michaelides, and E. Wang, “Stone-Wales defects in graphene and other planar sp<sup>2</sup>-bonded materials,” *Phys. Rev. B - Condens. Matter Mater. Phys.*, vol. 80, no. 3, pp. 1–4, 2009.
- [36] N. Tagmatarchis, Ed., *Advances in Carbon Nanomaterials Science and Applications*. Boca Raton Florida: CRC Press/Taylor and Francis, 2012.
- [37] A. C. Ferrari, F. Bonaccorso, V. Falco, K. S. Novoselov, S. Roche, P. Bøggild, S. Borini, F. Koppens, V. Palermo, N. Pugno, J. a. Garrido, R. Sordan, A. Bianco, L. Ballerini, M. Prato, E. Lidorikis, J. Kivioja, C. Marinelli, T. Ryhänen, A. Morpurgo, J. N. Coleman, V. Nicolosi, L. Colombo, A. Fert, M. Garcia-Hernandez, A. Bachtold, G. F. Schneider, F. Guinea, C. Dekker, M. Barbone, C. Galiotis, A. Grigorenko, G. Konstantatos, A. Kis, M. Katsnelson, C. W. J. Beenakker, L. Vandersypen, A. Loiseau, V. Morandi, D. Neumaier, E. Treossi, V. Pellegrini, M. Polini, A. Tredicucci, G. M. Williams, B. H. Hong, J. H. Ahn, J. M. Kim, H. Zirath, B. J. van Wees, H. van der Zant, L. Occhipinti, A. Di Matteo, I. a. Kinloch, T. Seyller, E. Quesnel, X. Feng, K. Teo, N. Rupesinghe, P.

- Hakonen, S. R. T. Neil, Q. Tannock, T. Löfwander, and J. Kinaret, “Science and technology roadmap for graphene, related two-dimensional crystals, and hybrid systems,” *Nanoscale*, vol. 7, no. 11, pp. 4598–4810, 2014.
- [38] S. K. Pati, T. Enoki, and C. N. R. Rao, Eds., *Graphene and Its Fascinating Attributes*. Singapore: World Scientific, 2011.
- [39] H. Brody, T. Scully, N. Haines, W. Fernandes, A. Duffy, K. Smart, P. Murphy, and Y. Smith, “Nature Outlook Graphene,” *Nature*, 2012.
- [40] V. Georgakilas, M. Otyepka, A. B. Bourlinos, V. Chandra, N. Kim, K. C. Kemp, P. Hobza, R. Zboril, and K. S. Kim, “Functionalization of graphene: covalent and non-covalent approaches, derivatives and applications.,” *Chem. Rev.*, vol. 112, no. 11, pp. 6156–214, Nov. 2012.
- [41] Q. Tang, Z. Zhou, and Z. Chen, “Graphene-related nanomaterials: tuning properties by functionalization,” *Nanoscale*, vol. 5, no. 11, pp. 4541–83, 2013.
- [42] B. Dume, “2D Materials: graphene and beyond,” *Physics World Focus on: Nanotechnology*, pp. 9–10, Jun-2014.
- [43] Z. Ao and S. Li, “Hydrogenation of Graphene and Hydrogen Diffusion Behavior on Graphene / Graphane Interface,” in *Graphene Simulation*, no. 111, J. Gong, Ed. Shanghai: InTech, 2011, pp. 53–73.
- [44] H. JONSSON, G. MILLS, and K. W. JACOBSEN, “Nudged elastic band method for finding minimum energy paths of transitions,” *Class. Quantum Dyn. Condens. Phase Simulations*, pp. 385–404, 1998.
- [45] K. Nakada and A. Ishii, “Migration of adatom adsorption on graphene using DFT calculation,” *Solid State Commun.*, vol. 151, pp. 13–6, Jan. 2011.
- [46] K. Nakada and A. Ishii, “DFT Calculation for Adatom Adsorption on Graphene,” in *Graphene Simulation*, J. Gong, Ed. Shanghai: InTech, 2011, pp. 3–20.
- [47] G. Kresse, M. Marsman, and J. Fürthmüller, *Vienna Ab-initio Simulation Package (VASP) the GUIDE*. 2014.
- [48] J. T. Robinson, J. S. Burgess, C. E. Junkermeier, S. C. Badescu, T. L. Reinecke, F. K. Perkins, M. K. Zalalutdniov, J. W. Baldwin, J. C. Culbertson, P. E. Sheehan, and E. S. Snow, “Properties of fluorinated graphene films.,” *Nano Lett.*, vol. 10, no. 8, pp. 3001–5, Aug. 2010.
- [49] H. Huang, Z. Li, J. She, and W. Wang, “Oxygen density dependent band gap of reduced graphene oxide,” *J. Appl. Phys.*, vol. 111, p. 054317, 2012.
- [50] H. Wang, Y. Wu, C. Cong, J. Shang, and T. Yu, “Hysteresis of Electronic Transport in Graphene Transistors,” *ACS Nano*, vol. 4, no. 12, p. 13, 2010.
- [51] K. Pi, K. M. McCreary, W. Bao, W. Han, Y. F. Chiang, Y. Li, S. W. Tsai, C. N. Lau, and R. K. Kawakami, “Electronic doping and scattering by transition metals on graphene,” *Phys. Rev. B - Condens. Matter Mater. Phys.*, vol. 80, no. 7, pp. 1–5, 2009.
- [52] H. Şahin, C. Ataca, and S. Ciraci, “Magnetization of graphane by dehydrogenation,” *Appl. Phys. Lett.*, vol. 95, no. 22, pp. 2–5, 2009.
- [53] L. Chen, H. Hu, Y. Ouyang, H. Z. Pan, Y. Y. Sun, and F. Liu, “Atomic chemisorption on graphene with Stone-Thrower-Wales defects,” *Carbon N. Y.*, vol. 49, no. 10, pp. 3356–3361, 2011.
- [54] H. Şahin and S. Ciraci, “Chlorine adsorption on graphene: Chlorographene,” *J. Phys. Chem. C*, vol. 116, no. 45, pp. 24075–24083, 2012.
- [55] X. Liu, C.-Z. Wang, M. Hupalo, H.-Q. Lin, K.-M. Ho, and M. Tringides, “Metals on Graphene: Interactions, Growth Morphology, and Thermal Stability,” *Crystals*, vol. 3, no. 1, pp. 79–111, Jan. 2013.
- [56] M. Farjam and H. Rafii-Tabar, “Energy gap opening in submonolayer lithium on graphene: Local density functional and tight-binding calculations,” *Phys. Rev. B -*

- Condens. Matter Mater. Phys.*, vol. 79, no. 4, pp. 1–7, 2009.
- [57] M. Wu, C. Cao, and J. Z. Jiang, “Light non-metallic atom (B, N, O and F)-doped graphene: a first-principles study,” *Nanotechnology*, vol. 21, no. 50, p. 505202, Dec. 2010.
- [58] J. Dai and J. Yuan, “Adsorption of molecular oxygen on doped graphene: atomic, electronic and magnetic properties,” *Phys. Rev. B*, vol. 81, no. November 2009, p. 165414, 2010.
- [59] P. Rani and V. K. Jindal, “Designing band gap of graphene by B and N dopant atoms,” *RSC Adv.*, vol. 3, no. 3, pp. 802–812, 2013.
- [60] Y. Tang, L. Yin, Y. Yang, X. Bo, Y. Cao, H. Wang, and W. Zhang, “Tunable Band Gaps and p-Type Transport Properties of Boron-Doped Graphenes by Controllable Ion Doping Using Reactive Microwave Plasma,” *ACS Nano*, vol. 6, pp. 1970–1978, 2012.
- [61] D. Usachov, O. Vilkov, A. Grüneis, D. Haberer, A. Fedorov, V. K. Adamchuk, a B. Preobrajenski, P. Dudin, A. Barinov, M. Oehzelt, C. Laubschat, and D. V Vyalikh, “Nitrogen-doped graphene: efficient growth, structure, and electronic properties.,” *Nano Lett.*, vol. 11, no. 12, pp. 5401–7, Dec. 2011.
- [62] G. Xiao-min, Z. Hong-Yu, Z. Meng, and L. You-Hua, “Opening Band Gap of Graphene by Chemical Doping : a First Principles Study,” *Chinese J. Struct. Chem.*, vol. 33, no. 4, pp. 513–8, 2014.
- [63] J. Ito, J. Nakamura, and A. Natori, “Semiconducting nature of the oxygen-adsorbed graphene sheet,” *J. Appl. Phys.*, vol. 103, p. 113712, 2008.
- [64] P. A. Denis, “Band gap opening of monolayer and bilayer graphene doped with aluminium, silicon, phosphorus, and sulfur,” *Chem. Phys. Lett.*, vol. 492, pp. 251–257, Jun. 2010.
- [65] E. Aktürk, C. Ataca, and S. Ciraci, “Effects of silicon and germanium adsorbed on graphene,” *Appl. Phys. Lett.*, vol. 96, p. 123112, 2010.
- [66] C. H. Hu, Y. Zheng, Y. Zhang, S. Q. Wu, Y. H. Wen, and Z. Z. Zhu, “Electronic and magnetic properties of silicon adsorption on graphene,” *Solid State Commun.*, vol. 151, pp. 1128–30, Sep. 2011.
- [67] M. C. Sison Escaño, T. Quang Nguyen, and H. Kasai, “Analysis of band gap formation in graphene by Si impurities: Local bonding interaction rules,” *Chem. Phys. Lett.*, vol. 515, pp. 85–90, Oct. 2011.
- [68] M. S. S. Azadeh, A. Kokabi, M. Hosseini, and M. Fardmanesh, “Tunable bandgap opening in the proposed structure of silicon-doped graphene,” *Micro Nano Lett.*, vol. 6, no. 8, p. 582, 2011.
- [69] D. Kaplan, V. Swaminathan, G. Recine, R. Balu, and S. Karna, “Bandgap tuning of mono- and bilayer graphene doped with group IV elements,” *J. Appl. Phys.*, vol. 113, no. 18, p. 183701, 2013.
- [70] P. A. Denis, “Concentration dependence of the band gaps of phosphorus and sulfur doped graphene,” *Comput. Mater. Sci.*, vol. 67, pp. 203–206, Feb. 2013.
- [71] P. V. C. Medeiros, A. J. S. Mascarenhas, F. de Brito Mota, and C. M. C. de Castilho, “A DFT study of halogen atoms adsorbed on graphene layers.,” *Nanotechnology*, vol. 21, no. 48, p. 485701, Dec. 2010.
- [72] L. Ma, J.-M. Zhang, K.-W. Xu, and V. Ji, “Hydrogen adsorption and storage of Ca-decorated graphene with topological defects: A first-principles study,” *Phys. E Low-dimensional Syst. Nanostructures*, vol. 63, pp. 45–51, 2014.
- [73] L. Hu, X. Hu, X. Wu, C. Du, Y. Dai, and J. Deng, “Density functional calculation of transition metal adatom adsorption on graphene,” *Phys. B Condens. Matter*, vol. 405, no. 16, pp. 3337–3341, 2010.
- [74] Y. Mao, J. Yuan, and J. Zhong, “Density functional calculation of transition metal

- adatom adsorption on graphene.,” *J. Phys. Condens. Matter*, vol. 20, no. 11, p. 115209, Mar. 2008.
- [75] M. Wu, E.-Z. Liu, M. Y. Ge, and J. Z. Jiang, “Stability, electronic, and magnetic behaviors of Cu adsorbed graphene: A first-principles study,” *Appl. Phys. Lett.*, vol. 94, no. 10, p. 102505, 2009.
- [76] X. Dai, Y. Li, M. Xie, G. Hu, J. Zhao, and B. Zhao, “Structural stability and electronic, magnetic properties of Ge adsorption on defected graphene: a first-principles study,” *Phys. E*, vol. 43, pp. 1461–4, Jun. 2011.
- [77] J. Kang, H.-X. Deng, S.-S. Li, and J. Li, “First-principles study of magnetic properties in Mo-doped graphene.,” *J. Phys. Condens. Matter*, vol. 23, no. 34, p. 346001, Aug. 2011.
- [78] X. Gonze, B. Amadon, P.-M. Anglade, J.-M. Beuken, F. Bottin, P. Boulanger, F. Bruneval, D. Caliste, R. Caracas, M. Côté, T. Deutsch, L. Genovese, P. Ghosez, M. Giantomassi, S. Goedecker, D. R. Hamann, P. Hermet, F. Jollet, G. Jomard, S. Leroux, M. Mancini, S. Mazevet, M. J. T. Oliveira, G. Onida, Y. Pouillon, T. Rangel, G.-M. Rignanese, D. Sangalli, R. Shaltaf, M. Torrent, M. J. Verstraete, G. Zerah, and J. W. Zwanziger, “ABINIT: First-principles approach to material and nanosystem properties,” *Comput. Phys. Commun.*, vol. 180, pp. 2582–615, Dec. 2009.
- [79] G. te Velde, F. M. Bickelhaupt, E. J. Baerends, C. Fonseca Guerra, S. J. a. van Gisbergen, J. G. Snijders, and T. Ziegler, “Chemistry with ADF,” *J. Comput. Chem.*, vol. 22, no. 9, pp. 931–967, Jul. 2001.
- [80] D. J. F. M. J. Frisch, G. W. Trucks, H. B. Schlegel, G. E. Scuseria, M. A. Robb, J. R. Cheeseman, G. Scalmani, V. Barone, B. Mennucci, G. A. Petersson, H. Nakatsuji, M. Caricato, X. Li, H. P. Hratchian, A. F. Izmaylov, J. Bloino, G. Zheng, J. L. Sonnenberg, M. Had, *Gaussian 09, Revision D.01*. Wallingford CT: Gaussian, Inc., 2009.
- [81] R. Dennington, T. Keith, and J. Millam, *GaussView, Version 5*. Shawnee Mission KS: Semichem Inc., 2009.
- [82] M. Valiev, E. J. Bylaska, N. Govind, K. Kowalski, T. P. Straatsma, H. J. J. Van Dam, D. Wang, J. Nieplocha, E. Apra, T. L. Windus, and W. a. de Jong, “NWChem: A comprehensive and scalable open-source solution for large scale molecular simulations,” *Comput. Phys. Commun.*, vol. 181, no. 9, pp. 1477–1489, Sep. 2010.
- [83] F. Neese, “The ORCA program system,” *Wiley Interdiscip. Rev. Comput. Mol. Sci.*, vol. 2, no. 1, pp. 73–78, Jan. 2012.
- [84] P. Giannozzi, S. Baroni, N. Bonini, M. Calandra, R. Car, C. Cavazzoni, D. Ceresoli, G. L. Chiarotti, M. Cococcioni, I. Dabo, A. D. Corso, G. Fratesi, S. De Gironcoli, R. Gebauer, U. Gerstmann, C. Gougoussis, A. Kokalj, L. Martin-samos, N. Marzari, F. Mauri, R. Mazzarello, S. Paolini, A. Pasquarello, L. Paulatto, C. Sbraccia, S. Scandolo, A. P. Seitsonen, A. Smogunov, P. Umari, and R. M. Wentzcovitch, “QUANTUM ESPRESSO : a modular and open-source software project for quantum simulations of materials,” *arXiv:0906.2569v2*, 2009.
- [85] M. J. Soler, E. Artacho, J. D. Gale, A. Garc, J. Junquera, P. Ordej, and S. Daniel, “The SIESTA method for ab initio order- N materials,” *J. Phys. Condens. Matter*, vol. 14, pp. 2745–2779, 2002.
- [86] D. Vanderbilt, “Soft self-consistent pseudopotentials in a generalized eigenvalue formalism,” *Phys. Rev. B*, vol. 41, no. 11, pp. 7892–7895, Apr. 1990.
- [87] P. E. Blöchl, “Projector augmented-wave method,” *Phys. Rev. B*, vol. 50, no. 24, pp. 17953–79, 1994.
- [88] S. Grimme, “Semiempirical GGA-type density functional constructed with a long-range dispersion correction.,” *J. Comput. Chem.*, vol. 27, no. 15, pp. 1787–1799, Nov. 2006.
- [89] J. P. Perdew, K. Burke, and Y. Wang, “Generalized gradient approximation for the



- exchange-correlation hole of a many electron system,” *Phys. Rev. B*, vol. 54, no. 23, pp. 16533–9, 1996.
- [90] M. A. Omar, *Elementary Solid State Physics: Principles and Applications*. Addison-Wesley Publishing Company, 1993.
- [91] W. Tang, E. Sanville, and G. Henkelman, “A grid-based Bader analysis algorithm without lattice bias.,” *J. Phys. Condens. Matter*, vol. 21, no. 8, p. 084204, Feb. 2009.
- [92] J. Wu, L. Xie, Y. Li, H. Wang, Y. Ouyang, J. Guo, and H. Dai, “Controlled chlorine plasma reaction for noninvasive graphene doping.,” *J. Am. Chem. Soc.*, vol. 133, pp. 19668–71, Dec. 2011.
- [93] Y. Ferro, N. Fernandez, A. Allouche, and C. Linsmeier, “Adsorption of beryllium atoms and clusters both on graphene and in a bilayer of graphite investigated by DFT,” *J. Phys. Condens. Matter*, vol. 25, p. 015002, Jan. 2013.
- [94] J.-A. Yan and M. Y. Chou, “Oxidation functional groups on graphene: Structural and electronic properties,” *Phys. Rev. B*, vol. 82, p. 125403, Sep. 2010.
- [95] A. Nourbakhsh, M. Cantoro, T. Vosch, G. Pourtois, F. Clemente, M. H. van der Veen, J. Hofkens, M. M. Heyns, S. De Gendt, and B. F. Sels, “Bandgap opening in oxygen plasma-treated graphene,” *Nanotechnology*, vol. 21, p. 435203, Oct. 2010.
- [96] P. Johari and V. B. Shenoy, “Modulating Optical Properties of Graphene Oxide : Role of Prominent Functional Groups,” *ACS Nano*, vol. 5, no. 9, pp. 7640–7, 2011.
- [97] W. H. Lee, J. W. Suk, H. Chou, J. Lee, Y. Hao, Y. Wu, R. Piner, D. Akinwande, K. S. Kim, and R. S. Ruoff, “Selective-area Fluorination of Graphene with Fluoropolymer and Laser Irradiation,” *Nano Lett.*, vol. 12, pp. 2374–8, May 2012.
- [98] S.-M. Choi and S.-H. Jhi, “Electronic property of Na-doped epitaxial graphenes on SiC,” *Appl. Phys. Lett.*, vol. 94, p. 153108, 2009.
- [99] H. Tachikawa, T. Iyama, and H. Kawabata, “MD simulation of the interaction of magnesium with graphene,” *Thin Solid Films*, vol. 518, pp. 877–9, Nov. 2009.
- [100] K. Kato, T. Iyama, and H. Tachikawa, “Density Functional Theory Study of the Interaction of Magnesium Ions with Graphene Chip,” *Jpn. J. Appl. Phys.*, vol. 50, p. 01BJ01, 2011.
- [101] E. Bichoutskaia and N. C. Pyper, “A theoretical study of the cohesion of noble gases on graphite,” *J. Chem. Phys.*, vol. 128, p. 024709, 2008.
- [102] V. A. Rigo, T. B. Martins, A. J. R. da Silva, A. Fazzio, and R. H. Miwa, “Electronic, structural, and transport properties of Ni-doped graphene nanoribbons,” *Phys. Rev. B*, vol. 79, p. 075435, Feb. 2009.
- [103] C. Gong, G. Lee, B. Shan, E. M. Vogel, R. M. Wallace, and K. Cho, “First-principles study of metal–graphene interfaces,” *J. Appl. Phys.*, vol. 108, p. 123711, 2010.
- [104] G. Giovannetti, P. Khomyakov, G. Brocks, V. Karpan, J. van den Brink, and P. Kelly, “Doping Graphene with Metal Contacts,” *Phys. Rev. Lett.*, vol. 101, p. 026803, Jul. 2008.
- [105] P. A. Khomyakov, G. Giovannetti, P. C. Rusu, G. Brocks, J. van den Brink, and P. J. Kelly, “First-principles study of the interaction and charge transfer between graphene and metals,” *Phys. Rev. B*, vol. 79, p. 195425, May 2009.
- [106] A. Antenucci, S. Guarino, V. Tagliaferri, and N. Ucciardello, “Electro-deposition of graphene on aluminium open cell metal foams,” *Mater. Des.*, vol. 71, pp. 78–84, 2015.
- [107] Z. Sun, Q. Xing, E. Axinte, W. Ge, J. Leng, and Y. Wang, “Formation of highly thermal stable Al<sub>88</sub>Ni<sub>6</sub>Y<sub>6</sub> amorphous composite by graphene addition design,” *Mater. Des.*, vol. 81, pp. 59–64, 2015.
- [108] C. Zhou, G. Ji, Z. Chen, M. Wang, A. Addad, D. Schryvers, and H. Wang, “Fabrication, interface characterization and modeling of oriented graphite flakes/Si/Al composites for thermal management applications,” *Mater. Des.*, vol. 63, pp. 719–728, 2014.
- [109] G. Kresse and J. Furthmüller, “Efficient iterative schemes for ab initio total-energy

- calculations using a plane-wave basis set,” *Phys. Rev. B*, vol. 54, no. 16, pp. 11169–86, 1996.
- [110] K. Momma and F. Izumi, “VESTA 3 for three-dimensional visualization of crystal , volumetric and morphology data,” *J. Appl. Crystallogr.*, vol. 44, pp. 1272–1276, 2011.
- [111] A. Bhattacharya, S. Bhattacharya, C. Majumder, and G. P. Das, “Transition-Metal Decoration Enhanced Room-Temperature Hydrogen Storage in a Defect-Modulated Graphene Sheet,” *J. Phys. Chem. C*, vol. 114, pp. 10297–301, Jun. 2010.
- [112] C. Tao, L. Jiao, O. V. Yazyev, Y.-C. Chen, J. Feng, X. Zhang, R. B. Capaz, J. M. Tour, A. Zettl, S. G. Louie, H. Dai, and M. F. Crommie, “Spatially Resolving Spin-split Edge States of Chiral Graphene Nanoribbons,” *Nat. Phys.*, vol. 7, no. 8, pp. 616–620, 2011.
- [113] F. Karlický, K. Kumara Ramanatha Datta, M. Otyepka, and R. Zbořil, “Halogenated graphenes: Rapidly growing family of graphene derivatives,” *ACS Nano*, vol. 7, no. 8, pp. 6434–6464, 2013.
- [114] Y.-C. Chen, T. Cao, C. Chen, Z. Pedramrazi, D. Haberer, de O. G., F. R. Fischer, S. G. Louie, M. F. Crommie, D. G. de Oteyza, F. R. Fischer, S. G. Louie, and M. F. Crommie, “Molecular bandgap engineering of bottom-up synthesized graphene nanoribbon heterojunctions,” *Nat Nano*, vol. advance on, Jan. 2015.
- [115] D. . Karki and N. . Adhikari, “First-principles study of the stability of graphene and adsorption of halogen atoms (F, Cl and Br) on hydrogen passivated graphene,” *Int. J. Mod. Phys. B*, vol. 28, no. 21, p. 1450141, 2014.
- [116] Z. Dai and Y. Zhao, “First-principles study of nitrobenzene adsorption on graphene,” *Appl. Surf. Sci.*, vol. 305, pp. 382–385, Jun. 2014.
- [117] J. H. Lee, S. G. Kang, H. S. Moon, H. Park, I. T. Kim, and S. G. Lee, “Adsorption mechanisms of lithium oxides (Li<sub>2</sub>O<sub>2</sub>) on a graphene-based electrode: A density functional theory approach,” *Appl. Surf. Sci.*, vol. 351, pp. 193–202, Oct. 2015.
- [118] F. Karlický, R. Zbořil, and M. Otyepka, “Band gaps and structural properties of graphene halides and their derivatives: a hybrid functional study with localized orbital basis sets,” *J. Chem. Phys.*, vol. 137, no. 3, p. 034709, Jul. 2012.
- [119] Z. Xu and K. Xue, “Engineering graphene by oxidation: a first-principles study,” *Nanotechnology*, vol. 21, no. 4, p. 045704, Jan. 2010.
- [120] M. Klintonberg, S. Lebègue, M. I. Katsnelson, and O. Eriksson, “Theoretical analysis of the chemical bonding and electronic structure of graphene interacting with Group IA and Group VIIA elements,” *Phys. Rev. B - Condens. Matter Mater. Phys.*, vol. 81, pp. 1–5, 2010.
- [121] H. Widjaja, Z.-T. Jiang, M. Altarawneh, C.-Y. Yin, B.-M. Goh, N. Mondinos, and B. Z. Dlugogorski, “Towards a better understanding of the geometrical and orientational aspects of the electronic structure of halogens (F–I) adsorption on graphene,” *Appl. Surf. Sci.*, vol. 356, pp. 370–377, 2015.
- [122] H. Y. Liu, Z. F. Hou, C. H. Hu, Y. Yang, and Z. Z. Zhu, “Electronic and magnetic properties of fluorinated graphene with different coverage of fluorine,” *J. Phys. Chem. C*, vol. 116, no. 34, pp. 18193–18201, 2012.
- [123] L. Fan, H. Zhang, P. Zhang, and X. Sun, “One-step synthesis of chlorinated graphene by plasma enhanced chemical vapor deposition,” *Appl. Surf. Sci.*, vol. 347, pp. 632–635, 2015.
- [124] S. Yuan, M. Rösner, A. Schulz, T. O. Wehling, and M. I. Katsnelson, “Electronic Structures and Optical Properties of Partially and Fully Fluorinated Graphene,” *Phys. Rev. Lett.*, vol. 114, no. 4, pp. 1–5, 2015.
- [125] B. Van Den Broek, M. Houssa, E. Scalise, G. Pourtois, V. V. Afanas’Ev, and a. Stesmans, “First-principles electronic functionalization of silicene and germanene by adatom chemisorption,” *Appl. Surf. Sci.*, vol. 291, pp. 104–108, 2014.

- [126] R. R. Nair, W. C. Ren, R. Jalil, I. Riaz, V. G. Kravets, L. Britnell, P. Blake, F. Schedin, a. S. Mayorov, S. Yuan, M. I. Katsnelson, H. M. Cheng, W. Strupinski, L. G. Bulusheva, a. V. Okotrub, I. V. Grigorieva, a. N. Grigorenko, K. S. Novoselov, and a. K. Geim, “Fluorographene: Two Dimensional Counterpart of Teflon,” *Small*, vol. 6, no. 24, pp. 2877–84, 2010.
- [127] K.-J. Jeon, Z. Lee, E. Pollak, L. Moreschini, A. Bostwick, C.-M. Park, R. Mendelsberg, V. Radmilovic, R. Kostecki, T. J. Richardson, and E. Rotenberg, “Fluorographene: A Wide Bandgap Semiconductor with Ultraviolet Luminescence,” *ACS Nano*, vol. 5, no. 2, pp. 1042–1046, Jan. 2011.
- [128] B. Wang, J. R. Sparks, H. R. Gutierrez, F. Okino, Q. Hao, Y. Tang, V. H. Crespi, J. O. Sofo, and J. Zhu, “Photoluminescence from nanocrystalline graphite monofluoride,” *Appl. Phys. Lett.*, vol. 97, no. 14, pp. 97–100, 2010.
- [129] D. K. Samarakoon, Z. Chen, C. Nicolas, and X.-Q. Wang, “Structural and electronic properties of fluorographene,” *Small*, vol. 7, no. 7, pp. 965–969, 2011.
- [130] F. Karlický and M. Otyepka, “Band Gaps and Optical Spectra of Chlorographene, Fluorographene and Graphane from G0W0, GW0 and GW Calculations on Top of PBE and HSE06 Orbitals,” *J. Chem. Theory Comput.*, vol. 9, no. 9, pp. 4155–64, 2013.
- [131] F. Karlický and M. Otyepka, “Band gaps and optical spectra from single- and double-layer fluorographene to graphite fluoride: many-body effects and excitonic states,” *Ann. Phys.*, vol. 526, no. 9–10, pp. 408–414, 2014.

# APPENDIX A

## FILES AND PARAMETERS IN VASP

---

This appendix: (1) explains VASP input and output files (appendix A.1); and (2) provides all non-default VASP parameters that were used during this research (appendix A.2). However, for comprehensive explanations, the VASP documentation[47] is the ultimate source to consult.

### A.1 Input and Output Files

Each job in VASP is bundled in a folder. There are minimum of five input files :

#### 1. job file

This file interfaces the VASP, the machine/supercomputer and the users. It defines the estimated computing time and resources allocations (*e.g.* number of processors, memory size, storage size). It sends notifications to the users about the status of the job (*e.g.* e-mail). It also can perform some algorithmic tasks, *e.g.* to run multi-stage jobs, to run jobs with a range of parameters.

#### 2. INCAR

This file stores all VASP parameters and tasks. All undefined parameters are set to default. Section 4.4 and chapter 5 to 9 share common VASP parameters that are described later in appendix A.2.

#### 3. POSCAR

This file defines the unit cell and the initial atomic configuration. In this thesis, upon convergence test, vacuum in *z*-direction is fixed to 15 Å. However, dipole correction is still applied to increase the accuracy of the calculations (see item 11 in appendix A.2).

#### 4. KPOINTS

This file determines the number of sampling points in the reciprocal coordinate. This thesis uses Monkhorst-Pack scheme, automatic  $k$ -mesh generation and gamma centred grid. Lower  $k$ -points is cheaper. There are two convergence tests against these  $k$ -points :

##### 4.1a $k$ -points for geometry optimisations

Rule of thumb in this thesis,  $k$ -points  $\approx 29.5 /$  lattice constant ( $\text{\AA}$ ) for  $x$  and  $y$  directions and  $k$ -point =1 for  $z$ -direction.

##### 4.1b $k$ -points for DOS calculations

Rule of thumb in this thesis,  $k$ -points  $\approx 4 \times 29.5 /$  lattice constant ( $\text{\AA}$ ) for  $x$  and  $y$  directions and  $k$ -point =1 for  $z$ -direction.

However, actual calculations were done in 3 stages :

4.2a geometry optimisation against the initial atomic positions at  $k$ -points  $\approx 29.5 /$  lattice constant ( $\text{\AA}$ ) for  $x$  and  $y$  directions and  $k$ -point =1 for  $z$ -direction.

4.2b geometry optimisation against the first optimised atomic positions (4.2a) at  $k$ -points  $\approx 2 \times 29.5 /$  lattice constant ( $\text{\AA}$ ) for  $x$  and  $y$  directions and  $k$ -point =1 for  $z$ -direction.

4.2c geometry optimisation against the second optimised atomic positions (4.2b) at  $k$ -points  $\approx 4 \times 29.5 /$  lattice constant ( $\text{\AA}$ ) for  $x$  and  $y$  directions and  $k$ -point =1 for  $z$ -direction.

#### 5. POTCAR

This file stores the potential of each atoms in the job. This thesis uses spin-polarized Perdew-Burke-Wang generalized gradient approximation (GGA) exchange-correlation functional [89] with projector augmented wave (PAW) pseudopotential[87].

Subsequent to running a job in supercomputer, output files are created, some of them are:

1. OUTCAR

This file stores the calculation outputs.

2. vasprun.xml

This file stores the calculation outputs in XML (Extensible Markup Language) format. XML is a text format that is interoperable across the internet.

3. DOSCAR

This file stores the density of states (DOS).

4. CONTCAR

This file stores the optimised unit cell and final atomic configuration. This file can be converted into the next POSCAR in the multi-stage calculation.

5. CHGCAR

This file stores the charge density, which can be used for multi-stage calculation or visualisation. This thesis uses the version 3.2.1 of Vesta software to visualise charge density[110].

## A.2 INCAR Parameters

This section explains the common non-default INCAR parameters that are used throughout this thesis :

1. ENCUT=500.0 or higher

Cut off energy for the plane wave basis set (eV). Lower cut off energy is cheaper. This parameter must be tuned as low as possible but still gives convergence calculation results.

2. NSW=300

Maximum number of steps in geometry optimisation.

3. EDIFF=1E-4 or smaller

This parameter sets the energy threshold (eV) to break the iteration in the DFT self-consistent calculation. If two consecutive iterations have energy change smaller than this parameter, the calculation ends.

4. IBRION=2

This parameter sets the conjugate-gradient algorithm to perform the geometry optimisation. This algorithm is recommended by VASP as the most reliable geometry optimisation routine and can handle most difficult situations.

5. ISTART=0

This parameter tells VASP to calculate the job from scratch.

6. IALGO=48 and ALGO=FAST

These combined parameters are suggested to be the most reliable and relatively economical algorithm by VASP. This is VASP's algorithm called residual minimization scheme, direct inversion in the iterative subspace (RMM-DIIS).

7. ISPIN=2

This parameter turns on the calculation with spin polarization. Spin polarization is important to obtain the true ground state energy and also to reveal the magnetic properties of the materials.

8. ISIF=2

This parameter tells VASP to optimise the atomic configuration inside a static unit cell. However, to optimise the unit cell, another approach is used, *i.e.* to calculate a range of lattice parameters and select the lowest energy.

9. ISMEAR=0

This parameter turns on the Gaussian smearing with the default broadening of 0.2 eV. This is to ensure convergence results in all calculations, especially for metallic elements.

10. IVDW=1

This parameter switches on the calculation with van der Waals correction using Grimme D2 method[88].

11. IDIPOL=3

This parameter turns on the dipole correction along the z-direction.

12. ALGO=DAMPED, LHFCALC=.TRUE., HFSCREEN=0.2 and PRECFOCK=F

These combined parameters select HSE06 functional for obtaining the electronic structures (*e.g.* density of states and energy band gap) more accurately.